PHYSICAL LIMITATIONS ON ANTENNAS

by

JOHN RUZE

B.S. College of the City of New York
(1938)

M.S. Columbia University
(1940)

SUBMITTED IN PARTIAL FULFILLMENT OF THE
REQUIREMENTS FOR THE DEGREE OF
DOCTOR OF SCIENCE

at the

MASSACHUSETTS INSTITUTE OF TECHNOLOGY
(1952)

Signature redacted

Signature of Author .....
Dept. of Elec. Engineering, May 9, 1952

Signature redacted

Certified by .....
Thesis Supervisor

Signature redacted

Chairman, Departmental Committee on Graduate Students

PHYSICAL LIMITATIONS ON ANTENNAS

John Ruze

Submitted to the Department of Electrical Engineering on May 9, 1952, in partial fulfillment of the requirements for the degree of Doctor of Science.

ABSTRACT

This thesis is concerned with physical limitations on the realizability of a given radiation polar diagram from an antenna aperture of a finite extent. It is convenient to divide the problem into three related parts; namely:

1). Limitations Imposed by Aperture Distribution Errors.

Inherent aperture illumination errors or deviations from the theoretical distribution cause corresponding deviations from the theoretical polar diagram. The nature of the illumination errors is examined and such errors are divided into systematic or "predictable" errors and "random" errors. Existing methods, available in the literature, for the treatment of systematic errors, are reviewed. Random errors form a statistical problem and have not been treated. A theory is formulated for their treatment, in both the discrete and continuous aperture cases. This theory indicates that the effect of random errors is first manifested in the minor lobe region where the errors tend to cancel the almost complete destructive interference from various elements of the aperture. Random errors therefore impose a physical limitation on the obtainable minimum side lobe level. It is shown that, in the discrete case where the current errors are assumed independent from element to element, the average spurious radiation of an ensemble of similar antennas is spatially constant and proportional to the mean squared error and inversely to the gain of the array. In the continuous aperture where independence of neighboring errors cannot be assumed, it is necessary to define a correlation interval beyond which the errors are essentially independent. It is shown that in this case the spurious radiation is now proportional not only to the mean squared error but also to the size of the correlated region in square wavelengths. The radiation is no longer spatially constant but directed along the axis of the aperture; the directivity increasing with the size of the correlated region. It is further shown that such spurious radiation is distributed in a modified Rayleigh manner with the Rayleigh and Gaussian distributions being the limiting cases of large and small errors respectively. Experimental work on a broadside array and on a "randomly" distorted parabolic mirror provide a verification of the theory.

2). Limitations Imposed by the Synthesis Procedure.

The antenna synthesis problem is one wherein we are given the shape of the desired polar diagram and we are required to find an aperture distribution of a given finite width whose radiation pattern approximates the desired one under some condition of optimization. The existing synthesis procedures are examined. These consist of the a) Fourier Series or Fourier Integral method where the function is approximated in a least square sense but the approximation exhibits a Gibb's phenomena at every point of discontinuity; b) the Levinson-Woodyard method wherein the pattern is fitted with $(\sin x)/x$ or cardinal functions.

The nature of the optimization condition is examined and two procedures are suggested for approximating a function in an approximate Tschebyscheff sense. In one of these use is made of the Tschebyscheff polynomials and an approximation is obtained wherein approximately equal deviations from the desired curve are obtained with the exception of points of discontinuity. The magnitude of the deviations or ripple may be adjusted to any desired value by the proper choice of the Tschebyscheff function. Although no rigorous condition of optimization is derived for approximating an arbitrary function the method of derivation suggests that the resulting approximation obtained yields at least approximately the greatest slope at discontinuities or rapid changes of the function for a given deviation or ripple. A number of worked out examples are included.

3). Limitations Imposed by the Aperture "Q"

It is shown by direct integration of the Poynting vector over the antenna aperture that those field components which possess spatial variation of a period smaller than a wavelength contribute essentially to reactive power. They therefore increase the "Q" of the aperture and impose a physical limitation on the synthesis procedure or on the possible polar diagrams.

Thesis Supervisor: L. J. Chu
Title: Professor of Electrical Engineering

ACKNOWLEDGEMENT

The writer wishes to express his gratitude to Professor L. J. Chu for his supervision of this thesis. In addition, he wishes to acknowledge the valuable suggestions made by the thesis readers, Prof. Y. W. Lee and Prof. S. J. Mason. The author would also like to thank the Air Force Cambridge Research Center for the use of the facilities of the Ipswich Antenna Test Station and the assistance of their personnel.

TABLE OF CONTENTS

		Page
I.	INTRODUCTION	1
	1). Limitations Imposed by Aperture Distribution Errors on the Radiation Pattern	1
	2). Limitations Imposed by the Synthesis Procedure..	2
	3). Limitations Imposed by the Aperture "Q"	3
II.	LIMITATIONS IMPOSED BY APERTURE DISTRIBUTION ERRORS..	5
	1). Introduction	5
	2). Nature of Aperture Distribution Errors	9
	3). Predictable Errors	11
	4). Statistical Introduction	15
	a. Gaussian Distribution	15
	b. Divers Non-Normal Distributions	22
	c. Rayleigh Distribution	26
	d. Modified Rayleigh Distribution	30
	5). Application to a Discrete Array	35
	a. Effect of Distribution Errors on the Antenna Pattern	35
	b. Effect of Distribution Errors on Antenna Gain	50
	6). Application to a Continuous Aperture	53
	a. Application to a Parabolic Mirror	53
	b. Effect of Distribution Errors on Antenna Gain	70
	7). Basic Assumptions in the Analysis	78
	a. Discrete Arrays	79
	b. Continuous Aperture	80
	8). Experimental Verification	81
	a. Evaluation of 25 Element Broadside Array ...	83a
	b. Slot Array Work at Hughes Aircraft Corp. ...	86
	c. Distorted Parabolic Mirror	91
	9). Application of Similar Techniques to Other Fields	101
	a. Application to the Theory of Aberrations of Optical Instruments	101
	b. Application to Electrical Filters	103

Table of Contents (Continued)

	page
III. LIMITATIONS IMPOSED BY THE SYNTHESIS PROCEDURE....	105
1). Fourier Series and Fourier Integral Method ..	107
2). Woodyard-Levinson Method	111
3). Some Remarks on Tschebyscheff and Gaussian Approximations	117
4). Pattern Synthesis in an Approximate Tschebyscheff Sense Using the Cardinal Functions ...	122
5). Pattern Synthesis in an Approximate Tschebyscheff Sense by the Use of the Tschebyscheff Polynomials	124
IV. LIMITATION IMPOSED BY THE APERTURE"Q"	145
1). Angular Spectrum of Plane Waves	146
2). Radiation Pattern and Radiated Power	155
3). "Q" of an Aperture	157
4). Complementary Case	158
V. APPENDIX	161
VI. BIBLIOGRAPHY	164

I. INTRODUCTION

This thesis is essentially concerned with the physical realizability of a given radiation polar diagram from an antenna system of finite extent. It has been found convenient to divide the problem into three related parts; namely:

1). Limitations Imposed by Aperture Distribution Errors on the Radiation Pattern

The antenna designer can readily compute by means of existing synthesis methods the aperture excitation necessary for a desired polar diagram. However, when he constructs his antenna and measures its performance he will find that his experimental pattern only approximates the theoretical one.

This is because he has not achieved the necessary theoretical aperture distribution in his model. The question naturally arises what aperture distribution tolerance is necessary to obtain a given approximation to the theoretical radiation pattern and conversely what pattern distortion and reduction in gain is obtained with given aperture excitation errors.

The problem has attracted considerable attention in the literature when the error is of a prescribed form; such as a periodic phase or amplitude error or when it is expandable in a power series such as a defocussing error in a parabolic mirror or coma in a metal plate lens. However, no work has been done on the case when the error is of a random nature. Such random

errors occur, for example, due to machining errors in a slot array or due to random distortions of a parabolic antenna.

Random errors form a statistical problem and we can speak only about the average behavior of a large number or "ensemble" of seemingly identical antennas and the liklihood or probability distribution of members of the ensemble about this average pattern.

In Section II of the thesis a theory is formulated for the treatment of random distribution errors for both a discrete array of elements and a continuous aperture.

2). Limitations Imposed by the Synthesis Procedure

The antenna synthesis problem is one wherein we are given the shape of the polar diagram and we are required to find an aperture distribution of a given finite width whose radiation pattern approximates the desired one under some condition of optimization.

The synthesis problem assumed importance during the last war when it was necessary to design antenna equipment with a prescribed radiation pattern for radar purposes. As a result a number of standard procedures are available in the literature.

As the radiation pattern and the aperture excitation form a Fourier Transform pair, the Fourier Integral method, and its counterpart for discrete arrays, the Fourier Series method, suggested itself early to investigators. This procedure yields an approximation which is optimum in the least square sense.

An alternate procedure was suggested by Levinson at the Radiation Laboratory and by Woodyard in England. This method approximates the desired function by sin x/x functions; functions which the finite aperture can readily generate. The approximation obtained by this procedure is no longer optimum in the least square or Gaussian sense but fits the desired function exactly in a number of equispaced points.

The various approximation procedures are examined in Section III of the thesis and a synthesis procedure is suggested which is optimum in a Tschybyscheff sense.

3). Limitations Imposed by Aperture "Q"

During the war years considerable speculation existed as to whether it was possible to construct an antenna with greater gain than that predicted by conventional theory. This problem of "supergain" antennas has only recently been settled by a series of papers. It is indeed possible, at least theoretically, to postulate an antenna of a given finite aperture with an arbitrarily large gain. However, such "supergain" antennas are characterized by extremely large and spatially rapidly varying currents. If it were possible to construct such antennas with conventionally available metallic materials they would possess prohibitive ohmic losses. Of greater theoretical difficulty is the fact that such radiators are associated with a very large reactive field. Supergain antennas are therefore inherently high Q devices. Unfortunately their "Q" increases at an astronomical rate as soon as we attempt to achieve gains

in excess of those predicted by the conventional analysis.

In Section IV of this thesis the limitations imposed by the antenna "Q" on the synthesis procedure is made evident. The complex power flow thru the antenna aperture for an arbitrary aperture excitation is determined and the antenna "Q" is defined as the ratio of reactive to radiated power. The antenna "Q" is shown to exert a physical limitation not only on available gain but also on the polar diagram, that is a limitation on the synthesis procedure.

II. LIMITATIONS IMPOSED BY APERTURE DISTRIBUTION ERRORS ON THE RADIATION PATTERN

1). Introduction

The radiation polar diagram of a specified current distribution may be obtained from the basic Maxwell's Equations. Two methods of doing this are available. In one, with the aid of auxiliary functions called potentials, Maxwell's Equations are put into a form involving only these potentials and the source functions. The resulting differential equation can be expressed as an integral solution involving the source Green's Function. The electromagnetic fields can be obtained from the potential defining equations. (Stratton, pg. 430 and 23.) An alternate procedure is that of direct integration of Maxwell's equations with the aid of the vector Green's theorem (Stratton and Chu). Both procedures give the same results.

For our application we are content with the far field of a current distribution of finite extent. The vector field components for an arbitrary electric current distribution may be written from the literature (Silver, pg. 89)

$$\mathcal{F}_\theta(\theta,\varphi) = \frac{-j\omega\mu}{4\pi R}\int_V \mathcal{J}\cdot i_\theta\, e^{jk\rho\cdot R}\, dv \qquad (1).$$

$$\mathcal{F}_\varphi(\theta,\varphi) = \frac{-j\omega\mu}{4\pi R}\int_V \mathcal{J}\cdot i_\varphi\, e^{jk\rho\cdot R}\, dv \qquad (2).$$

* Notation Note: $\mathcal{F}$ is a vector, F corresponding scalar magnitude.

In the far field approximation the radial electric component becomes negligibly small. The coordinate system is the standard one and is shown in Fig. No. 1. $\mathcal{R}$ is the unit vector in the direction of observation and ρ the source position vector.

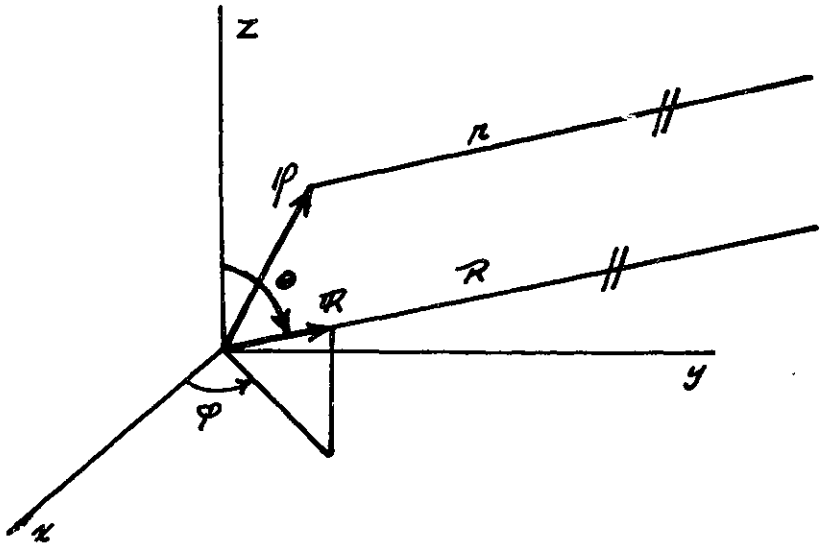

$$r = R - \rho \cdot R$$

$$k = \frac{2\pi}{\lambda}$$

Fig. No. 1

As we are interested primarily in the normalized polar diagram we need only consider the integral of (1) + (2) as that alone is angularly dependent. We further lose no generality if we consider only an electric current flowing in the x-direction - the effect of other current components may be taken into account by superposition.

With these simplifications our basic equations become

$$F_\theta(\theta,\varphi) = \cos\theta\cos\varphi \int_v J_x e^{jk\rho\cdot R}\, dv \qquad (1a)$$

$$F_\varphi(\theta,\varphi) = \sin\varphi \int_v J_x e^{jk\rho\cdot R}\, dv \qquad (2a)$$

If we are dealing with a surface current distribution, the above integration is restricted to this surface. In particular let us consider a plane aperture lying in the xy plane. Then since

$$\rho = x i' + y j'$$

$$R = \sin\theta\cos\varphi\, i' + \sin\theta\cos\varphi\, j' + \cos\theta\, k.$$

$$\rho \cdot R = \sin\theta[x\cos\varphi + y\sin\varphi].$$

and our formulas become

$$F_\theta(\theta,\varphi) = \cos\theta\cos\varphi \int_a J_x(x,y)\, e^{jk\sin\theta[x\cos\varphi + y\sin\varphi]}\, dx\,dy \qquad (16)$$

$$F_\varphi(\theta,\varphi) = \sin\varphi \int_a J_x(x,y)\, e^{jk\sin\theta[x\cos\varphi + y\sin\varphi]}\, dx\,dy \qquad (26).$$

We can obtain the equations for a discrete array such as an array of infinitesimal elements or dipoles located in the xy plane by letting

$$J_x(x,y) = \sum_m \sum_n \delta(x - md)\,\delta(y - nd)\, I_{mn} \qquad (3).$$

where, for simplicity, we have considered our elements equi-spaced. Inserting this delta function formulation into our basic equation we have

$$F_\theta(\theta,\varphi) = \cos\theta\cos\varphi \sum_m \sum_n I_{mn}\, e^{jkd\sin\theta[m\cos\varphi + n\sin\varphi]} \qquad (4)$$

$$F_\varphi(\theta,\varphi) = \sin\varphi \sum_m \sum_n I_{mn}\, e^{jkd\sin\theta[m\cos\varphi + n\sin\varphi]} \qquad (5).$$

Various types of polar diagrams can be obtained by a suitable choice of the current distribution. The determination of the necessary current distribution is the synthesis problem which is treated in Section III of this thesis.

As a means of introduction let us consider a uniform current distribution and obtain the polar diagram in the principal plane $\varphi = 90^{\circ}$. Applying (1b) we obtain

$$F_{\varphi}(\theta, 90^{\circ}) = \frac{\sin\left(\frac{\pi a}{\lambda}\sin\theta\right)}{\left(\frac{\pi a}{\lambda}\sin\theta\right)} \qquad (6).$$

This simple case yields the well known sin x/x pattern. It possesses a main beam of half-power width of 50.4° λ/a and decreasing minor lobes. The successive minor lobes have the intensity of 13.2 db, 17.8 db, 20.8 db, etc. The uniform discrete aperture has similar behavior. (Silver, pg. 180.)

Even in the early days of radio these minor lobes in discrete arrays proved troublesome and it was proposed that the individual elements have amplitudes proportional to the coefficients of the binomial series (Stone). Such an array has a radiation pattern with no side lobes; however this is achieved at the expense of approximately doubling the beamwidth and utilizing large current ratios in the array. Alternate less severe tapering schemes were usually employed and the resultant polar diagram was computed until a satisfactory arrangement was obtained.

Recently the use of the Tschbyscheff polynomials was proposed to obtain a current distribution for discrete arrays (Dolph). It has been shown that this arrangement yields an antenna of maximum gain and minimum beamwidth for a previously specified side lobe level. The minor lobes are all of equal amplitude and their magnitude may be chosen as low as desired. The limiting case of zero minor lobes reduces to the binomial distribution of Stone. (Kraus, pg. 109.)

With the advent of radar and the use of microwave frequencies similar tapering schemes were worked out for continuous apertures (Silver, pg. 187). Radar particularly required antennas with low minor lobes as targets in these directions would produce false indications. Theoretically at least, the side lobe level could be chosen as low as desired - greater side lobe suppression, in general, calling for a larger current taper and resulting in lower gain and wider beamwidth.

We inquire what is the effect of aperture distribution errors on the resulting polar diagram? We would expect that the effect of these errors is first manifested in the side lobe region where the radiation is low as the errors tend to destroy the almost complete destructive interference of the contributions from the different portions of the aperture.

Before we consider the effect of such aperture errors, let us first examine the types of possible antenna errors.

2). Nature of Aperture Distribution Errors

The aperture distribution errors or the deviation from the theoretical aperture excitation may be of many kinds and

due to many causes. Certain types of antenna systems may be prone to a particular error and that one may predominate. However in any case, we may divide the aperture errors into two general types; namely: (a) the first kind, which lacking a better name, we call "predictable" errors and (b) the second, called "random errors".

Predictable errors are those which occur due to the omission of some factor in the design or engineering analysis. In this classification we would include errors caused by such factors as (1) mutual impedance between elements, (2) diffraction at a lens antenna step, (3) termination mismatch of a broadside or slot array, (4) fixed error due to machining or faulty r.f. measurements, (5) incorrectly positioned feed in a parabolic mirror, etc. A number of antennas of the same type will have the same "predictable" error. Once this error is known, either from theory or experiment, its effect on the polar diagram can be computed by standard methods.

In contrast, "random errors" are caused by accidental and usually slight deviations of the antenna parameters from their design value. Examples of such random errors are (1) machining errors in a broadside or slot array - these may cause an error in the current delivered to an element or actually radiated from it, (2) r.f. measurement errors incurred in adjusting the array, (3) wall spacing errors in metal plate lenses, (4) random distortion of the surface of a parabolic mirror, etc. These "random" errors will vary from antenna to antenna among seemingly identical antennas. They create a statistical problem

and we can speak only about the average behavior of the "ensemble" and the probability distribution of its members.

In a constructed antenna it may be difficult to differentiate the two classes of errors - however, they can always be theoretically resolved for, if we designate by $J_o(x)$ the desired aperture distribution, by $J(x)$ the distribution of a given antenna and by $\overline{J(x)}$ the system average distribution, i.e. the average distribution of a large number of similar antennas, then the predictable error is given by

$$\overline{J(x)} - J_o(x) \tag{7}$$

and the random error by

$$J(x) - \overline{J(x)} \tag{8}$$

As mentioned, standard methods may be applied to determine the effect of the "predictable" errors once these errors are known. A brief review of this treatment and references to the literature will be presented in the next subsection. Random errors have not received treatment in the literature and a theory will be formulated for them in the remainder of this section.

3). Predictable Errors

To illustrate the methods of treating known aperture errors it is sufficient to consider the two dimensional problem - that is the pattern of a line source. Referring to equations (1a) and (2b) and changing our notation slightly to conform

with that usual in the literature for this analysis (Spencer - Austin) we have, outside of the obliquity factors,

$$g_o(u) = \int_{-w}^{w} f_o(x)\, e^{j 2\pi u x}\, dx \qquad (9)$$

where $g_0(u)$ is the field strength pattern, $f_0(x)$ the source distribution, "x" is measured in wavelengths and $u = \sin \theta$.

If we now consider the amplitude distribution to be in error by $f(x) - f_0(x)$, the new distribution can in general be expanded in a power series

$$f(x) = f_o(x)\left[a_0 + a_1 x + a_2 x + \cdots\right]. \qquad (10)$$

The resulting pattern can be written

$$g(u) = \sum_n \int_{-w}^{w} a_n x^n f_o(x)\, e^{j 2\pi u x}\, dx \qquad (11)$$

Now since

$$\frac{d^n}{du^n} \int_{-w}^{w} f_o(x)\, e^{j 2\pi u x}\, dx = (j 2\pi)^n \int_{-w}^{w} x^n f_o(x)\, e^{j 2\pi u x}\, dx.$$

we can write for the new pattern

$$g(u) = \sum_n \frac{a_n}{(j 2\pi)^n} \frac{d^n}{du^n} g_o(u) \qquad (12).$$

The modified pattern is therefore seen to be a linear sum of the original pattern and its derivatives.

A similar technique can be applied to a pure phase error, that is if

$$g(u) = \int_{-w}^{w} f_o(x)\, e^{j\varphi(x)}\, e^{j2\pi ux}\, dx \qquad (13)$$

However, only for small phase errors can the exponential be readily expanded and a result similar to (12) obtained. In addition, special cases may be worked out directly from (13) - for instance if we have only a linear phase error this produces a tilt of the beam or a square law phase error may be evaluated for uniform illumination in terms of the Fresnel integrals. (Friis and Lewis, pg. 243) For pencil beams several important cases of phase error are evaluated in the literature in the form of plotted curves, especially in (Spencer - Austin).

The above method of analysis of errors is especially useful for computation of defocussing errors and coma scanning errors in parabolas or lens antennas. An alternate analysis, more suitable for use in the case where the error is periodic as in slot or lens antennas, is found in (Brown). In this case the amplitude error is expanded in a Fourier Series instead of a power series.

$$f(x) = f_o(x)\left[1 + \sum_{-N}^{N} a_n e^{j\frac{2\pi n}{d}x}\right]. \qquad (14)$$

"d" may be any fundamental period, although the function will be used only in the interval $-W < x < W$; any convenient functional extension may be used outside this interval.

The radiation pattern due to (14) may be computed as

$$g(u) = \int_{-W}^{W} f_0(x)\, e^{j2\pi x u}\, dx + \sum_{-N}^{N} a_n \int_{-W}^{W} f_0(x)\, e^{j2\pi x (u + n/d)}\, dx \qquad (15)$$

$$g(u) = g_0(u) + \sum_{-N}^{N} a_n\, g_0(u + n/d) \qquad (16)$$

It is seen that the modified pattern now consists of the original pattern plus patterns of the same shape displaced from the origin by the amount n/d. This is illustrated in Fig. No. 2 for the first harmonic.

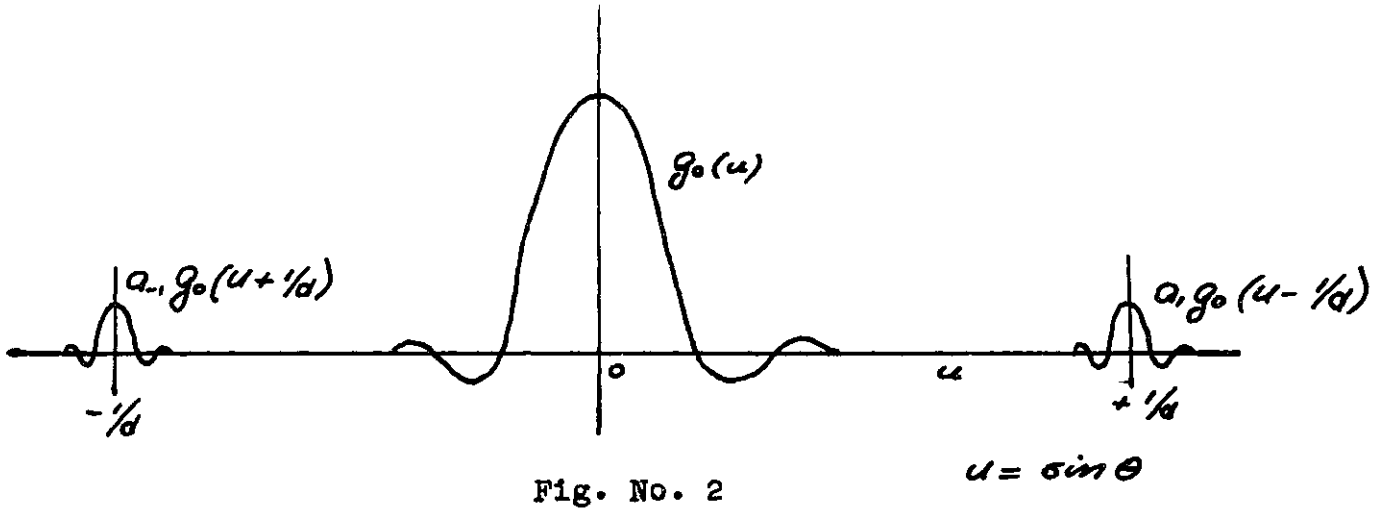

Fig. No. 2

Successive harmonics would create additional patterns at $\pm$ 2/d, $\pm$ 3/d, etc. For large periods the additional error lobe is not distinct from the main beam and serves largely in distorting the desired radiation. For smaller periodicities

the disturbing lobes become distinct and frequently the source of error may be located by computing its fundamental period.

It should be noted that for $n/d > 1$ or for periodicities less than a wavelength the spurious lobe occurs at $\sin \theta > 1$ and therefore does not appear in the actual pattern. A similar expansion can be made for an arbitrary phase error and for small errors the exponential can again be expanded yielding a similar pattern structure.

The power series and the Fourier series treatment of aperture errors will yield the same result provided a sufficient number of terms are taken in each case. However, in a particular problem one may be of considerable advantage over the other.

Having briefly considered "predictable" errors we turn our attention to "random" errors. The next subsection serves as a statistical introduction.

4). Statistical Introduction (Cramer, Chptrs. 15 to 20)

We can begin our study of "random" errors by first considering the simpler discrete array. In this case we assume that the individual elements of the array are independently in error. From eq. (4) and (5) we see that we are dealing with sums of quantities which have a random component. We first inquire what are the statistical properties of sums.

a). Gaussian Distribution

Let us consider the sum "S" of a large number of independent random scalar variables x_k:

$$S = \sum^{N} x_k \tag{17}$$

The x_k's are samples chosen at random from N distributions, not necessarily the same, and we inquire, what is the distribution or likelihood of their sum. The Central Limit Theorem of statistical theory, subject to rather general conditions, states that the sum will be distributed in an asymptotically Gaussian manner with a mean "m" and variance "σ^2" which are the sum of the individual N distributions, that is

$$m = \sum^{N} m_k \tag{18}$$

$$\sigma_x^2 = \sum^{N} \sigma_k^2 \tag{19}$$

and the distribution of "S" is (m, σ_x^2), or

$$w(S) = \frac{1}{\sqrt{2\pi}} \frac{1}{\sigma_x} e^{-(S-m)^2/2\sigma_x^2} \tag{20}$$

The theorem may be derived by the characteristic function method and for the case where the individual distributions are the same and normal the derivation is quite simple. However, for different and non-Gaussian distributions the derivation is mathematically more subtle and is obtained by a limiting process. It may be found in the literature (Cramer pg. 212).

Briefly the derivation assumes that the number of components "N" is large and that the third absolute moment of x_k about its mean

$$\rho_k^3 = E(|x_k - m_k|^3)^* = \int_{-\infty}^{\infty} |x_k - m_k|^3 w(x)\,dx \qquad (21)$$

is finite for every "k" and that the limit

$$\lim_{N\to\infty} \frac{\rho}{\sigma_x} \to 0 \qquad (22)$$

where

$$\rho^3 = \sum^N \rho_k^3 \qquad (23)$$

Eq. 21 and 22 are therefore the conditions of applicability of the Central Limit Theorem.

We note that the theorem requires only condition (21) when the "x_k" come from the same distribution, as then

$$\rho^3 = N\rho_k^3 \qquad (24)$$

and

$$\sigma^2 = N\sigma_k^2 \qquad (25)$$

so that

$$\lim \frac{\rho}{\sigma} = \lim_{N\to\infty} \frac{\rho_k}{\sigma_k} \frac{1}{\sqrt[6]{N}} \to 0 \qquad (26)$$

This less stringent condition is also sufficient when the individual components come from proportional distributions as then

$$\lim_{N\to\infty} \frac{\rho}{\sigma} = \lim \frac{\rho_k}{\sigma_k} \frac{[\Sigma |a_n|^3]^{1/3}}{[\Sigma |a_n|^2]^{1/2}} \to 0 \qquad (27)$$

* The symbol E( ) has the usual statistical significance of expected value.

Although the theorem is only asymptotically true, that is we only approach a Gaussian distribution, it has been found that if the number of components is above say six the resulting distribution is already closely Gaussian. In particular if the individual components originally come from a Gaussian distribution themselves no restriction need be placed on the number in the sum.

The Gaussian or normal distribution is shown in Fig. No. 3.

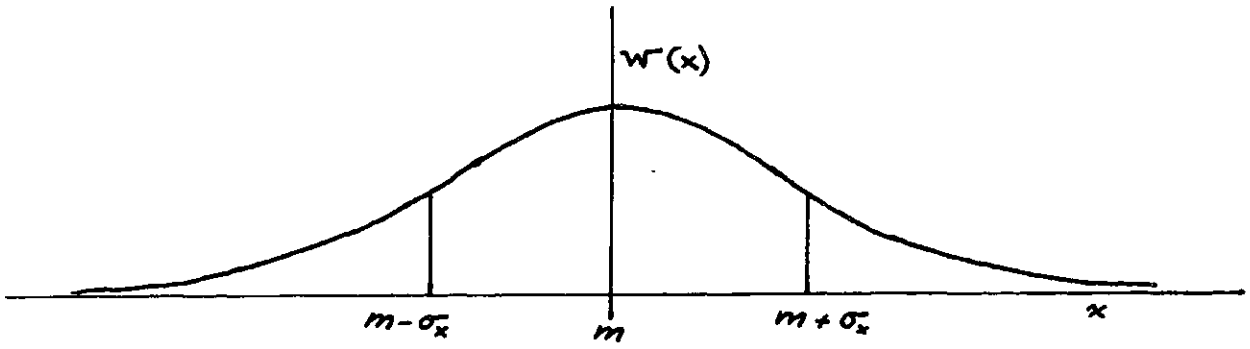

Fig. No. 3

It is characterized by a mean "m" and a variance σ^2 and it can be computed that approximately 68 percent of the sums lie within $m \pm \sigma$ and 95 percent between $m \pm 2\sigma$.

The Gaussian distribution may in a sense be termed the "natural" distribution in that it occurs in physical phenomena. As the deviation of a physical quantity from a theoretical value is generally due to a number of independent causes, the Central Limit Theorem informs us that the quantity will be distributed in an asymptotically Gaussian manner about its mean.

The normal distribution of the sum (17) can be applied to electrical problems as it may be interpreted as the sum of a large number of d.c. or in-phase voltages or vectors.

We next inquire what is the effect of adding a constant value to our (17), that is, what is the distribution of the sum

$$S = a + \sum^{N} x_k \tag{28}$$

We would expect that the distribution W(S) would still be Gaussian but now displaced by the amount "a", that is, it would be characterized by $(m+a, \sigma)$.

We can utilize this very simple example to introduce the characteristic function method and statistical manipulations in general.

Given a distribution function W(x), the characteristic or moment generating function is defined as

$$\varphi_x(t) = \int_{-\infty}^{\infty} e^{ixt} w(x)\, dx \tag{29}$$

This function is called the moment generating function as, if the exponential is expanded

$$\varphi_x(t) = \sum_{n=0}^{\infty} (it)^n \int_{-\infty}^{\infty} x^n w(x)\, dx \tag{30}$$

it is seen that the "nth" moment of W(x) can be obtained directly from the characteristic function by

$$\mathcal{E}(x^n) = (i^{-n}) \frac{d^n}{dt^n} \varphi_x(t)\Big|_{t=0} \tag{31}$$

Furthermore, by the Fourier Integral Theorem the probability distribution and the characteristic function (29) form a Fourier Transform pair, so that:

$$w_x(x) = \frac{1}{2\pi} \int_{-\infty}^{\infty} e^{-ixt} \varphi_x(t)\, dt \tag{32}$$

Now let us consider the sum, z, of two random and independent variables, x and y; then

$$\varphi_z(t) = \int_{-\infty}^{\infty} e^{izt} w_z(z)\, dz = \mathcal{E}(e^{izt})$$

but

$$\mathcal{E}(e^{izt}) = \mathcal{E}(e^{i(x+y)t}) = \mathcal{E}(e^{ixt} e^{iyt}).$$

As we are dealing with independent variables, the expected value or mean of a product is the product of the means, so that

$$\mathcal{E}(e^{izt}) = \mathcal{E}(e^{ixt})\,\mathcal{E}(e^{iyt}).$$

or

$$\varphi_z(t) = \varphi_x(t)\, \varphi_y(t) \tag{33}$$

We can extend this to any number of independent variables and have the important theorem on characteristic functions, namely that:

"The characteristic function of a sum of independent variables is equal to the product of the characteristic functions of the terms."

As we wish the distribution of "z" we must take the inverse transform of eq. (33). This can be readily done by the use of the convolution theorem and the desired distribution may be expressed in terms of the original component distributions

$$\left.\begin{aligned} w_z(z) &= \int_{-\infty}^{\infty} w_y(z-x)\, w_x(x)\, dx \\ \text{or} \\ w_z(z) &= \int_{-\infty}^{\infty} w_x(z-x)\, w_y(x)\, dx \end{aligned}\right\} \quad (34).$$

This same result could have been obtained directly by the consideration of the joint probability of independent events. The probability of a given value of "z" is

$$w_z(z) = \int_{-\infty}^{\infty} w_x(x)\, w_y(y)\, dx \qquad (35)$$

As we are subject to the restriction $z = x + y$, this becomes

$$w_z(z) = \int_{-\infty}^{\infty} w_x(x)\, w_y(z-x)\, dx$$

which is the same result as (34).

Returning now to our displacement problem as presented by eq. (28), by the Central Limit Theorem the sum is Gaussian

and the constant is distributed as a delta function $\delta(x - a)$. Applying eq. (34)

$$w(s) = \int_{-\infty}^{\infty} \delta(x-a) \frac{1}{\sqrt{2\pi}} \frac{1}{\sigma_x} e^{-(s-x-m)^2/2\sigma_x^2} dx$$

or

$$w(s) = \frac{1}{\sqrt{2\pi}} \frac{1}{\sigma_x} e^{-(s-m-a)^2/2\sigma_x^2} \qquad (36).$$

which is the expected result, that is, Gaussian with $(m+a, \sigma_x)$.

b). Diverse Non-normal Distributions

Due to the generality of the Central Limit Theorem, there is the danger of assuming that all sums of a large number of elements are distributed in a Gaussian manner and that therefore all physical quantities involving a number of additive components are at least asymptotically Gaussian.

This fallacy can be readily demonstrated by the consideration of some examples. Although $S = \Sigma x_k$ is normally distributed, the magnitude $M = |\Sigma x_k|$ is not. If S is normally distributed with zero mean, then the distribution of the magnitude

$$\left.\begin{aligned} w(M) &= \sqrt{\frac{2}{\pi}} \frac{1}{\sigma_x} e^{-M^2/2\sigma_x^2} \qquad M>0 \\ w(M) &= 0 \qquad\qquad\qquad\quad M<0 \end{aligned}\right\} \qquad (37).$$

will be of the form of a folded over normal curve (Fig. 4)

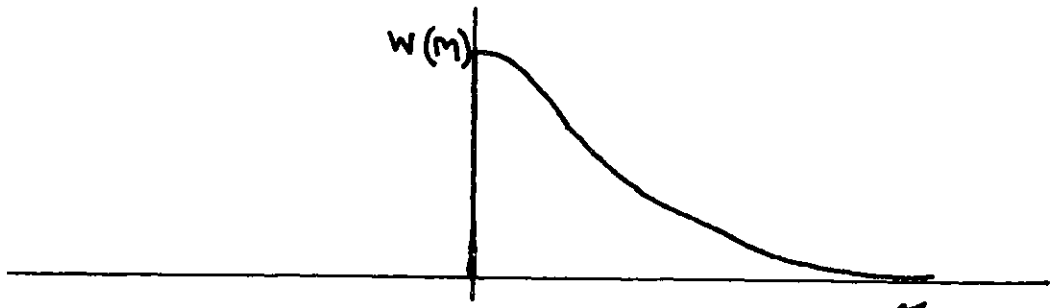

Fig. No. 4

Another non-Gaussian distribution of interest is the distribution of $p = (\Sigma x_k)^2$, which could be used to represent the distribution of the power in d.c. circuits when the individual voltages are random in magnitude.

To obtain the distribution of "p" we can make a change in variable in eq. (20) as the sum, by itself, is Gaussian; that is, we let

$$\rho = s^2 \qquad d\rho = 2s\,ds$$

and since

$$w(\rho)\,d\rho = 2w(s)\,ds \qquad \text{as} \quad \rho > 0$$

$$w(\rho) = 2w(s)\frac{ds}{d\rho} = \frac{1}{\sqrt{2\pi}}\frac{1}{\sigma_x}\frac{e^{-\rho/2\sigma_x^2}}{\sqrt{\rho}} \qquad \rho > 0$$

$$w(\rho) = 0 \qquad \rho < 0 \qquad \Big\} \quad (38).$$

where we have assumed that the original normal distribution

had zero mean. Fig. No. 5 shows this distribution.

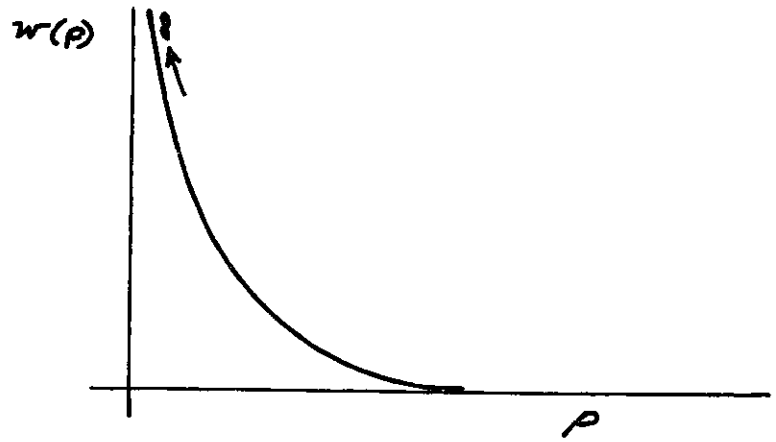

Fig. No. 5

A distribution of greater interest to our problem is that of

$$\rho = \left(\Sigma x_k\right)^2 + \left(\Sigma y_k\right)^2 = \eta + \zeta \qquad (39)$$

By the Central Limit Theorem the individual sums will be Gaussian. For our application we can assume that they have zero mean and both have the same variance. This distribution can be used to represent the distribution of power in an a.c. circuit where the individual a.c. voltages have random magnitudes and all phase angles equally likely. The zero mean and identical variance is statistically assured by the equally likely phase angle condition.

The distribution of "p", W(p) can readily be obtained by means of characteristic functions or by means of the convolution integral, eq. (34). The individual distributions $W(\eta)$ and $W(\zeta)$ are given by eq. (38), and

$$w(\rho) = \int_{-\infty}^{\infty} w_1(\rho-\eta)\, w_\eta(\eta)\, d\eta$$

$$w(\rho) = \frac{1}{2\pi} \int_0^{\rho} \frac{1}{\sigma_x^2} \frac{e^{-\rho/2\sigma_x^2}}{\sqrt{\eta}\sqrt{\rho-\eta}}\, d\eta$$

This can be readily integrated by the substitution

$$\alpha = \sqrt{\eta} \qquad \alpha^2 = \eta \qquad d\alpha = \frac{1}{2}\frac{d\eta}{\sqrt{\eta}}$$

with the result

$$w(\rho) = \frac{e^{-\rho/2\sigma_x^2}}{\pi\sigma_x^2} \int_0^{\sqrt{\rho}} \frac{d\alpha}{\sqrt{\rho-\alpha^2}} = \frac{e^{-\rho/2\sigma_x^2}}{2\sigma_x^2}$$

This can be put into a more convenient form as

$$\rho = \Gamma + \eta$$

$$\overline{\rho} = \overline{\Gamma} + \overline{\eta} = \sigma_x^2 + \sigma_y^2 = 2\sigma_x^2 = \sigma^2 \qquad (40)$$

hence

$$\left.\begin{aligned} w(\rho) &= \frac{e^{-\rho/\sigma^2}}{\sigma^2} \qquad \rho > 0 \\ w(\rho) &= 0 \qquad\qquad\quad \rho < 0 \end{aligned}\right\} \qquad (41)$$

This distribution is therefore characterized only by the mean power $\overline{\rho} = \sigma^2$ and it is shown graphically in Fig. No. 6.

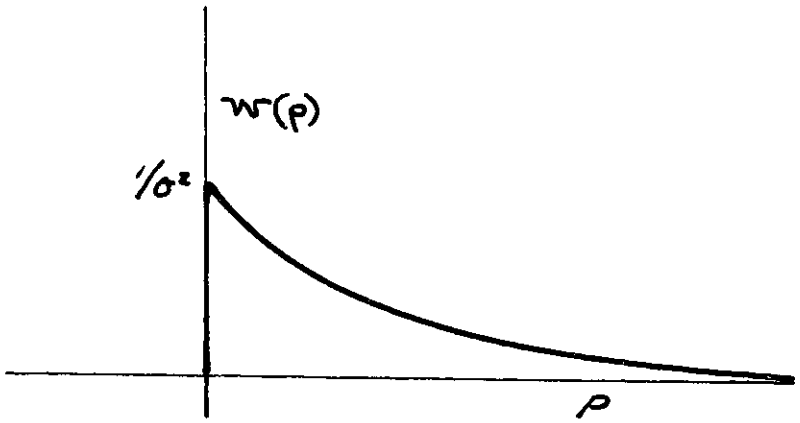

Fig. No. 6

c). Rayleigh Distribution

The Rayleigh distribution W(r), is the distribution of the magnitude

$$r = \sqrt{(\Sigma x_k)^2 + (\Sigma y_k)^2} \tag{42}$$

wherein the individual sums have zero mean and identical variance. It can be derived simply from the distribution W(p), Eq. (41), by the substitution $p = r^2$, $dp = 2rdr$ with the result

$$W(r) = \frac{2r}{\sigma^2} e^{-r^2/\sigma^2} \tag{43}$$

This distribution may be applied to a number of physical problems, that is, to those which satisfy eq. (42). This equation expresses the magnitude of a vector sum and the zero mean and identical variance conditions require having all directions equally likely.

This distribution was first investigated by (Rayleigh) in connection with the problem of the random walk and in the

incoherent addition of acoustic waves. In the random walk a particle suffers a large number of random displacements, with all directions equally likely, the magnitude and direction of each displacement being independent of all previous ones. We inquire about the probability that after "N" displacements the particle lies in the circular strip of "r" to "$r + dr$". As the particle's final position is given by (42), the probability distribution will be given by (43) with σ^2 equal to the mean square total displacement.

As the resultant voltage of a large number of random a.c. voltages of arbitrary phase can be represented by a vector sum, the resultant voltage magnitude will be Rayleigh distributed with σ^2 equal to the mean power. We can therefore apply this distribution to a number of electrical problems. These include the distribution or likelihood of a given: (1) voltage standing wave ratio on a transmission line caused by randomly located discontinuities, (2) the radar return from a group of random scatterers, (3) transmission in the rejection band of an electrical filter caused by errors in its circuit components, (4) side lobe level of an antenna caused by aperture excitation errors.

As an illustration of the Rayleigh distribution, consider 25 a.c. generators connected in series. The individual phases or shaft positions are at random and the generators may have either equal voltages of one volt or they may be taken from any population of unit variance. If this population were Gaussian then 68 percent of the generator voltages will be less than

one volt and 95 percent of them would be less than two. To apply eq. (43) we must evaluate the mean power

$$\overline{P} = \sigma^2 = \overline{(\Sigma x_k)^2} + \overline{(\Sigma y_k)^2} = \Sigma \overline{x_k^2} + \Sigma \overline{y_k^2}$$

$$\overline{P} = \Sigma \left(\overline{x_k^2} + \overline{y_k^2} \right) = n$$

where "n" is the number of voltages. This is the well known result that the intensity resulting from the superposition of "n" waves with random phases is just "n" times that due to a single wave. However, this is merely the expected or average value and if individual readings were obtained with different shaft positions we would obtain a distribution of values ranging from 0 to n^2. Fig. No. 7 shows this distribution for the case of $n = 9$ and $n = 25$.

To better illustrate the nature of the distribution we compute the cumulative probability, that is, the probability that the magnitude greater than a specified value will occur. This is equal to

$$P[>r] = \int_r^\infty w(r)\,dr = e^{-r^2/\sigma^2} \qquad (44).$$

which is plotted in Fig. No. 8.

As another illustration of the Rayleigh distribution, consider the light incident on this page. As it is due to a large number of incoherent atomic sources, its intensity will be distributed in a Rayleigh manner. We do not "see" this variation of intensity as our perception is too coarse and too slow.

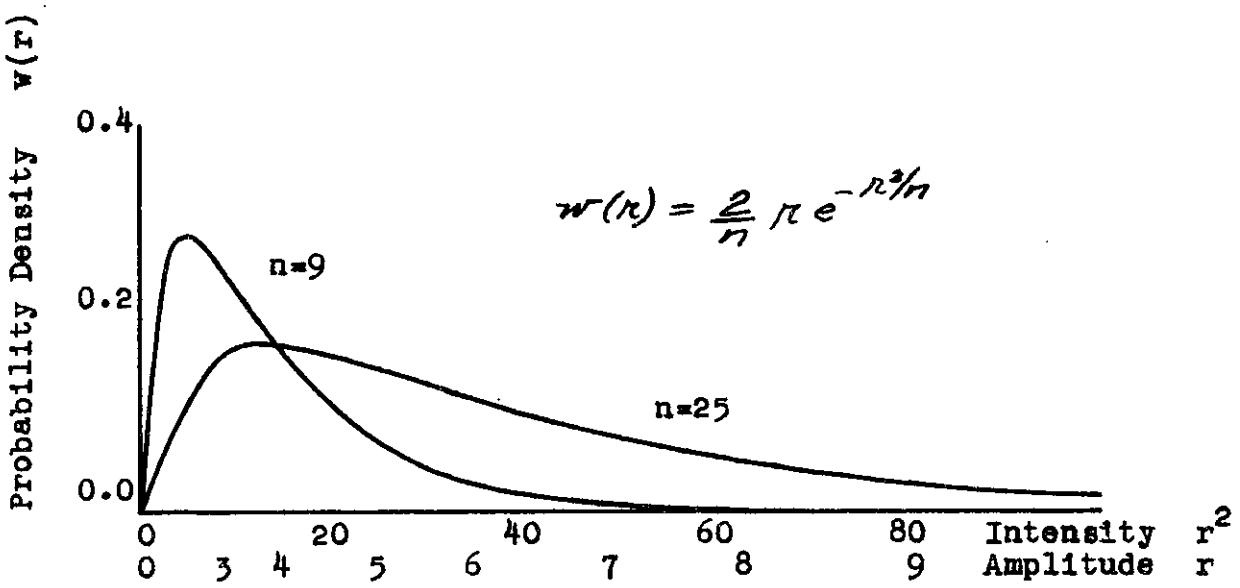

Fig. No. 7

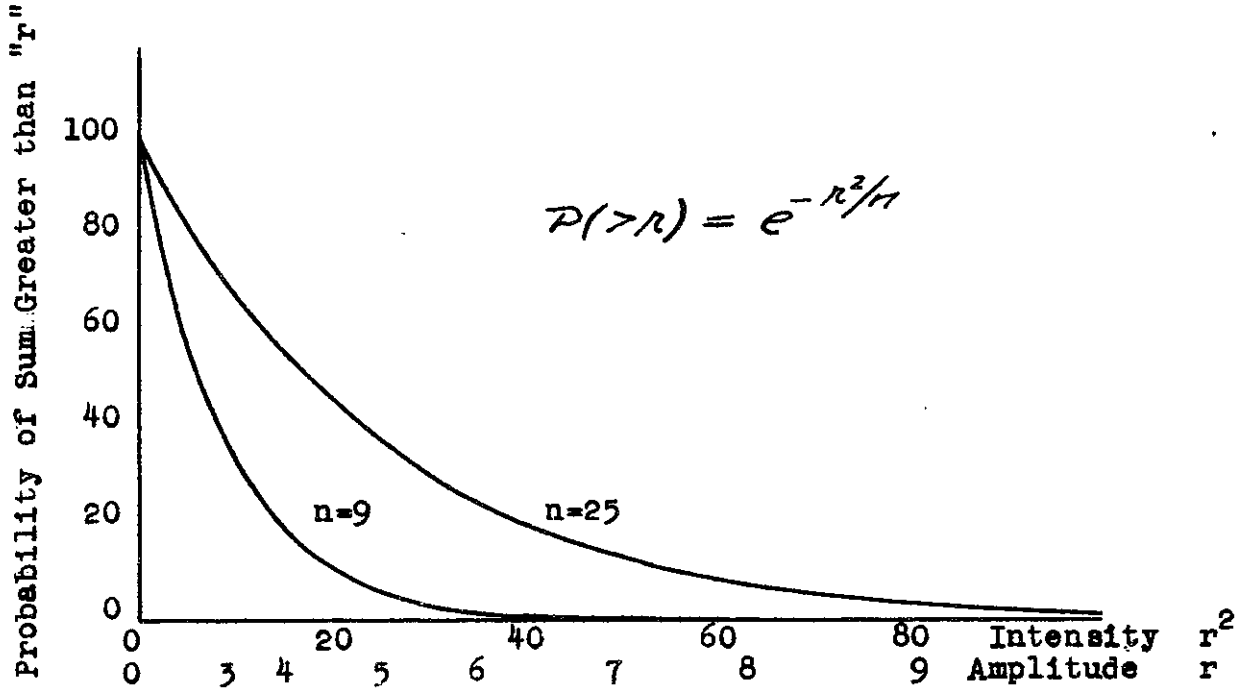

Fig. No. 8

However, our statistical analysis indicates that 13 percent of the area has an incident intensity greater than twice the mean and only 2 percent greater than four times the average. A photocell measures the average intensity as it performs an integration over its sensitive area.

Finally the Rayleigh distribution may be considered as being compounded from two perpendicular and independent Gaussian distributions. The probability density surface is shown in Fig. No. 9.

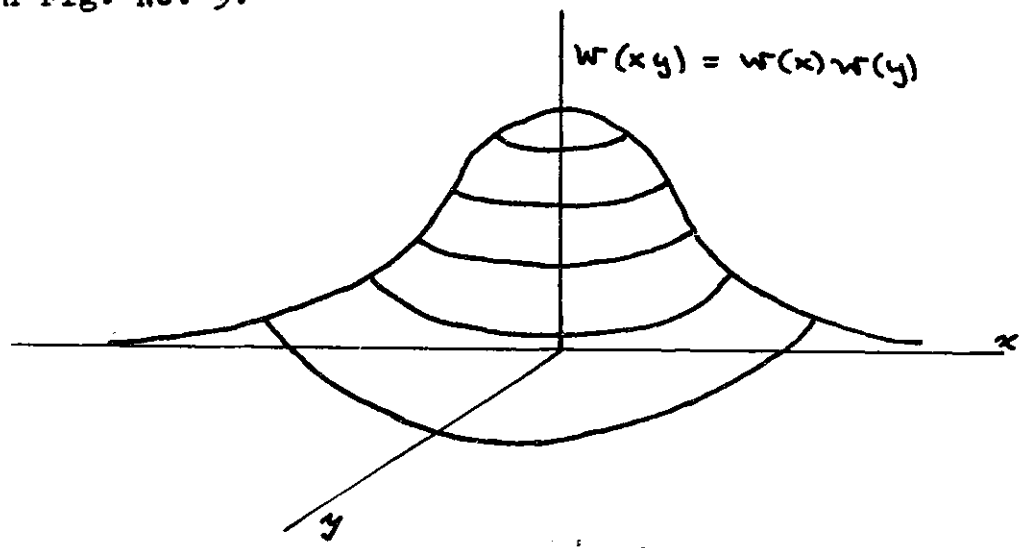

Fig. No. 9

The distribution of "r" could have been alternately derived by performing the "θ" integration. Another method of deriving the Rayleigh distribution is by the use of characteristic functions. This is done in (Chandrasekhar) and in (Uhlenbeck, pg. 50).

d). Modified Rayleigh Distribution

Let us now consider the addition of a constant displacement "a" to the Rayleigh distribution or the distribution

of "r" where

$$r = \left[(a + \Sigma x_k)^2 + (\Sigma y_k)^2\right]^{1/2} = \left[(a+\eta)^2 + \zeta^2\right]^{1/2} \qquad (45).$$

No generality is lost in adding the constant to only one of the sums as the axes can always be rotated so that the displacement coincides with the "x" axis. In the antenna problem the constant "a" would correspond to the signal present due to the existing or inherent side lobes of the zero error aperture.

To derive the modified distribution of eq. (45) we displace the two dimensional Gaussian distribution of Fig. No. 9 to the point (a,0). Fig. No. 10 indicates the result with the necessary coordinate system.

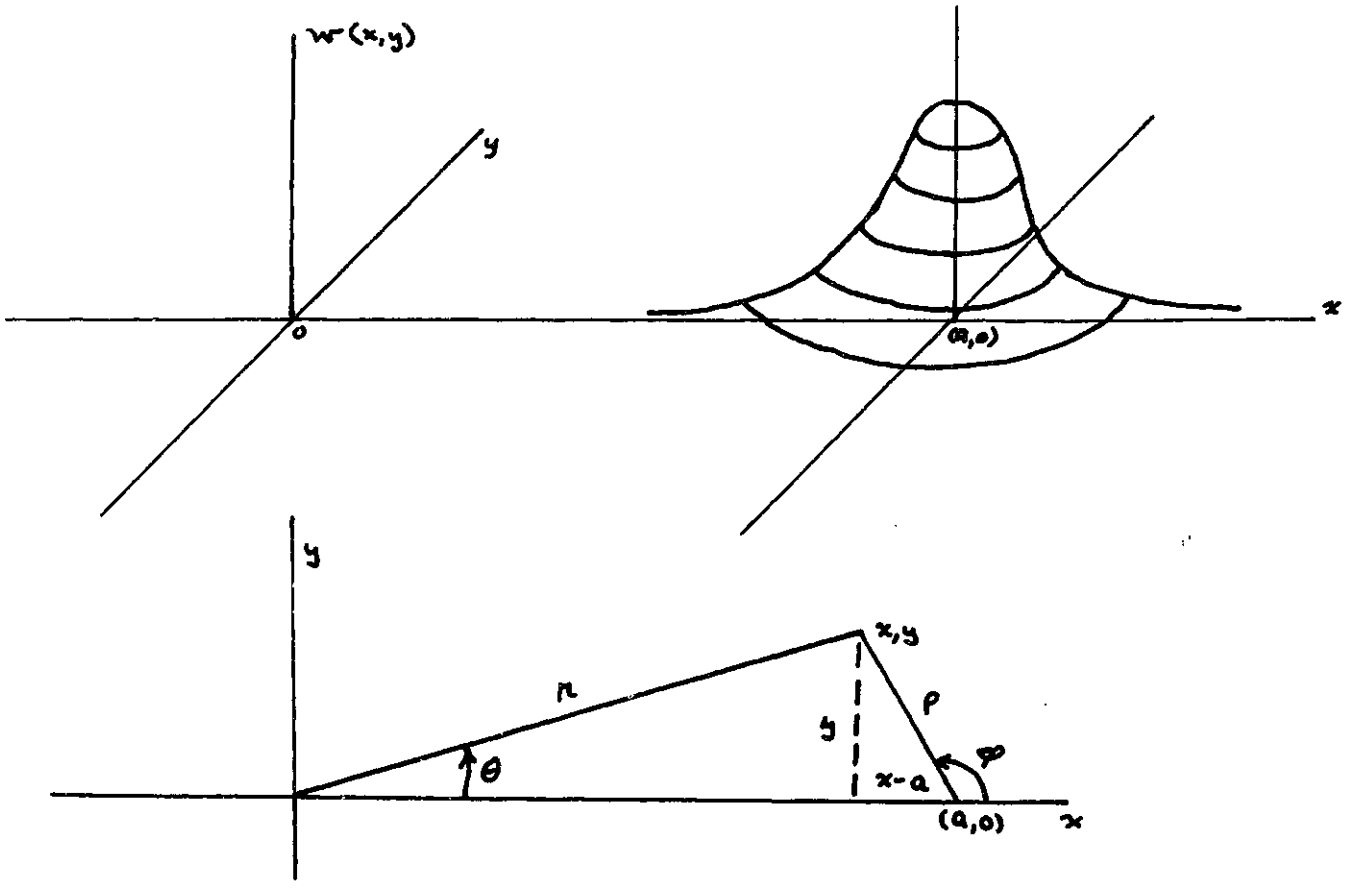

Fig. No. 10

Now

$$w(x,y) = w(x)w(y) = \frac{1}{\sqrt{2\pi}}\frac{1}{\sigma_x} e^{-(x-a)^2/2\sigma_x^2} \frac{1}{\sqrt{2\pi}}\frac{e^{-y^2/2\sigma_x^2}}{\sigma_x}$$

$$w(x)w(y) = \frac{1}{\pi}\frac{1}{\sigma^2} e^{-[r^2 + a^2 - 2ar\cos\theta]/\sigma^2}$$

$$w(r)\,dr = \int_{-\pi}^{\pi} w(x)w(y)\,r\,d\theta\,dr$$

$$w(r) = \frac{r}{\pi\sigma^2} e^{-(a^2+r^2)/\sigma^2} \int_{-\pi}^{\pi} e^{2ar\cos\theta/\sigma^2} d\theta.$$

$$w(r) = \frac{2r}{\sigma^2} e^{-(a^2+r^2)/\sigma^2} I_0\left[\frac{2ar}{\sigma^2}\right] \qquad (46).$$

The last integration may be found in (McLachlan, pg. 162). $I_0[z]$ is the modified Bessel Function of the First Kind.

We can call (46) a modified Rayleigh distribution. It was discussed by (Blake) in connection with the probable radar return from random sea clutter with a direct signal present.

Fig. No. 11 shows this modified Rayleigh distribution for various values of the displacement "a". Fig. No. 12 gives the cumulative probability. This was calculated by graphical integration of Fig. No. 11. For small values of "a" this modified distribution naturally approaches the Rayleigh curve and for large values of "a", due to the asymptotic behavior of the Bessel function, we obtain

Rayleigh and Modified Rayleigh Distribution

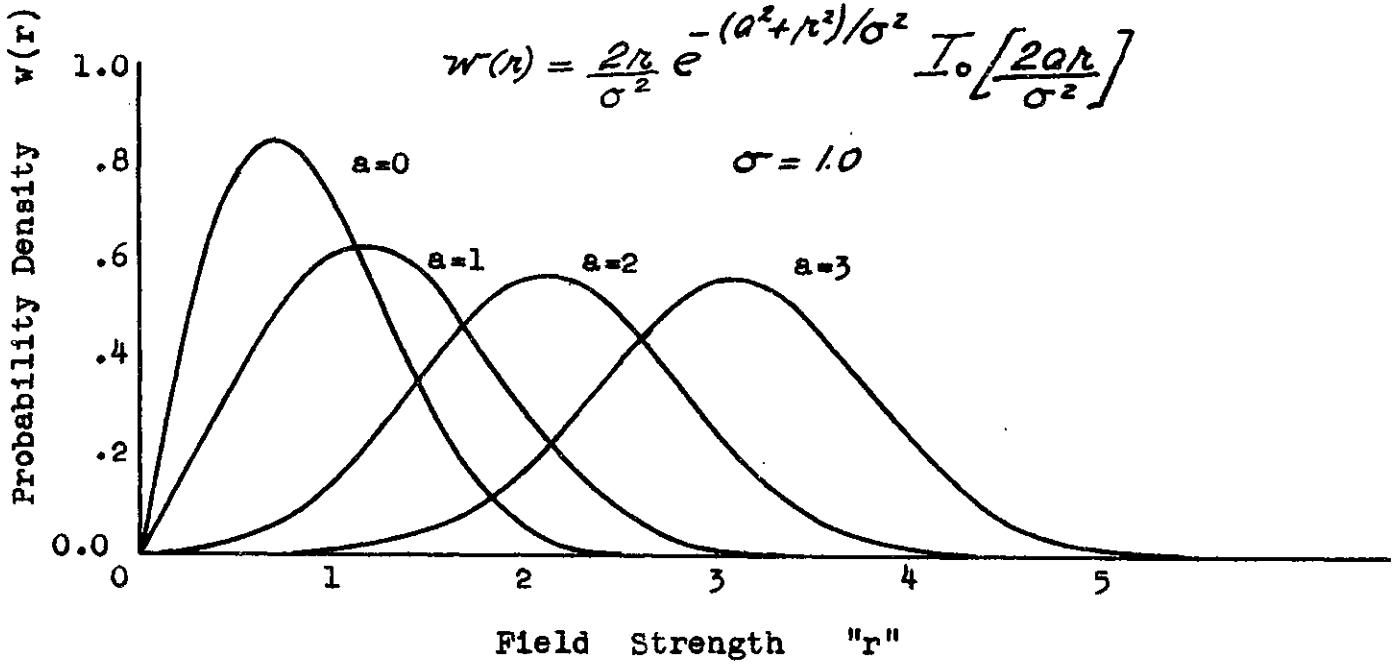

Fig. No. 11

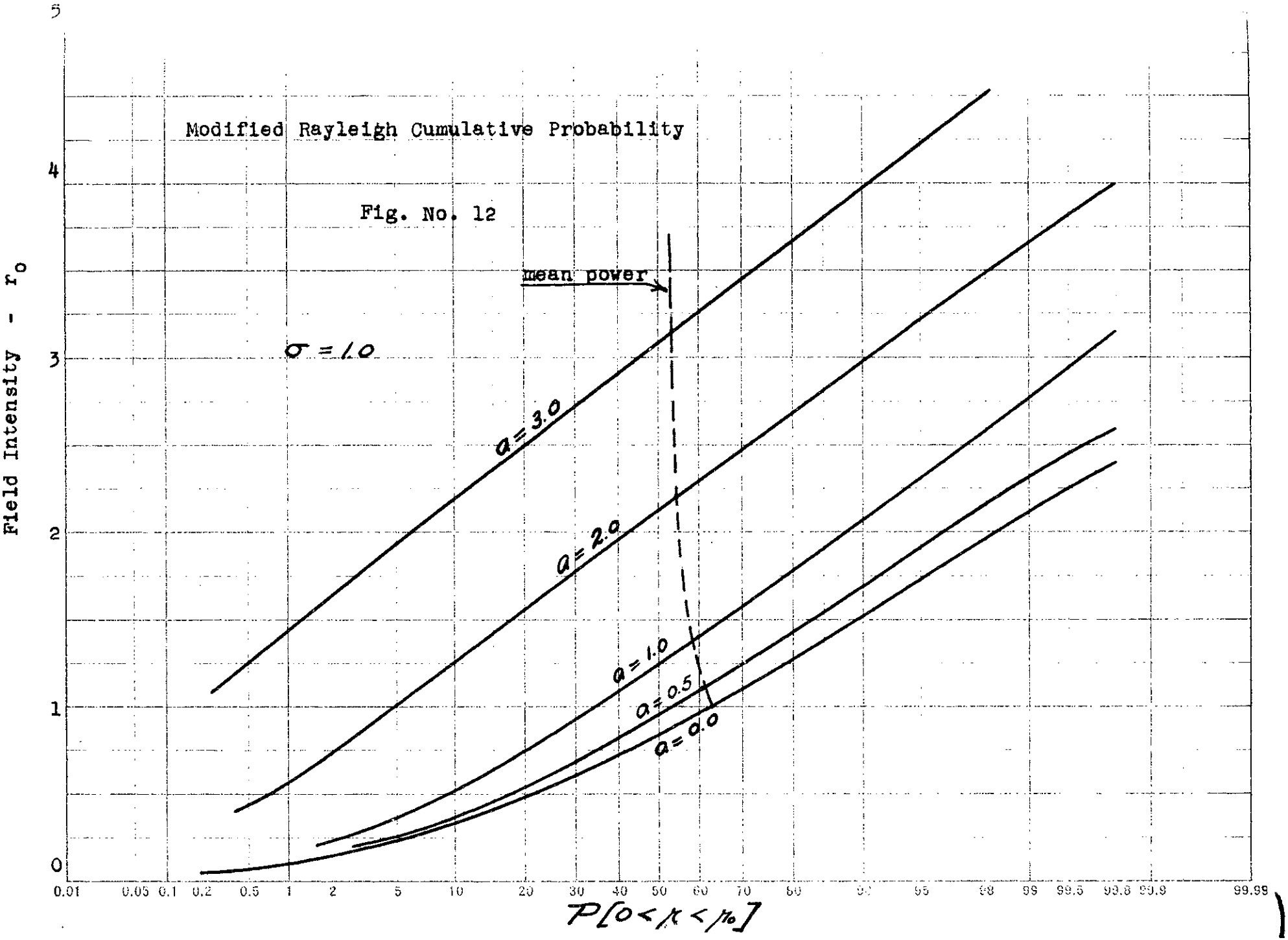
Modified Rayleigh Cumulative Probability
Fig. No. 12
mean power
σ = 1.0
a = 3.0
a = 2.0
a = 1.0
a = 0.5
a = 0.0
Field Intensity - r₀
0
1
2
3
4
0.01
0.05
0.1
0.2
0.5
1
2
5
10
20
30
40
50
60
70
80
90
95
98
99
99.5
99.8
99.9
99.99
P[0 < r < r₀]

$$W(r) \longrightarrow \frac{1}{\sqrt{\pi}} \frac{1}{\sigma} \sqrt{\frac{r}{a}}\, e^{-(a-r)^2/\sigma^2} \qquad (47).$$

or approximately Gaussian behavior with $(a, \sigma/\sqrt{2})$.

We still need to find the mean power of the modified distribution. This may be done by computing the expected value of "r^2" from W(r), eq. (46), or simply from eq. (45).

$$\overline{r^2} = \overline{(a+\eta)^2} + \overline{\zeta^2} = a^2 + \overline{\eta^2} + \overline{\zeta^2} = a^2 + \sigma^2 \qquad (48)$$

where we have realized that the mean of the sum of independent variables is the sum of the means and that $\overline{\zeta} = \overline{\eta} = 0$. The result is as we would expect from the incoherent addition of powers.

5). Application to a Discrete Array

a). Effect of Distribution Errors on Antenna Pattern

Having introduced the necessary statistical tools, we are in a position to analyse the effect of aperture distribution errors on the performance of a discrete array. We have mentioned that by the use of the (Dolph) distribution it is possible, at least theoretically, to obtain a side lobe level as low as desired. Fig. No. 13 shows the polar diagram of a broadside array of 25 elements designed for side lobe suppression of 29 db. We note that the radiation is practically confined to an angular width of "$2\alpha_0$". Outside of this

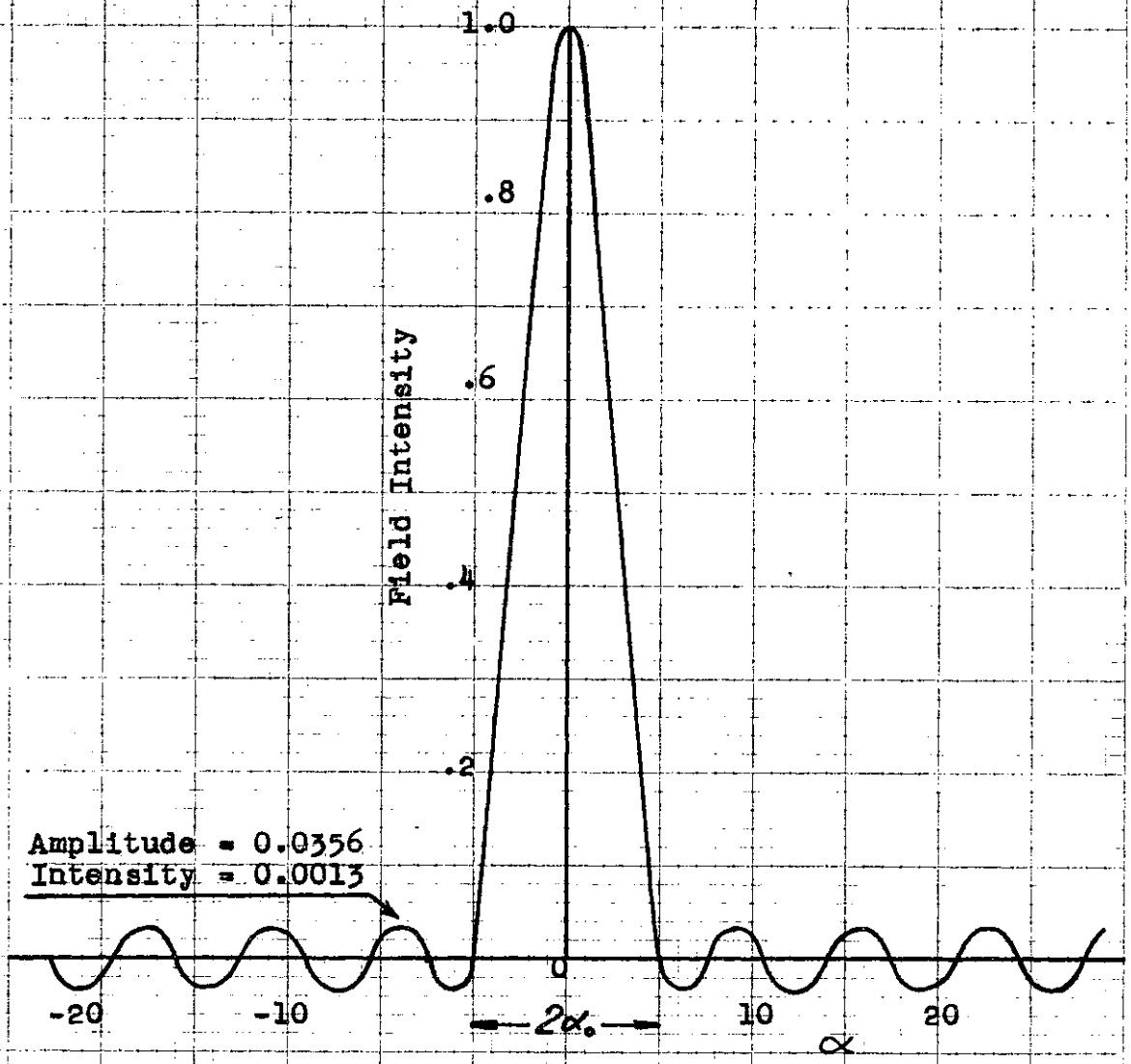

TYPICAL ANTENNA PATTERN

25 ELEMENTS

MAXIMUM SIDE LOBES - 29db

Fig. No. 13

region, due to almost complete destructive interference of the contributions from the various members of the array, the radiation magnitude does not exceed this previously specified small value.

Fig. No. 14 gives a physical explanation of the pattern formation. In the main beam direction the individual element contributions add up in phase creating a large amplitude. Whereas in the side lobe region the vectors spiral around many times but their resultant lies within the 29 db circle. It is evident that our individual vector magnitudes must be carefully chosen and precisely maintained so that no where does their sum exceed -29 db. Furthermore, we suspect that greater side lobe suppression requires not only a greater current taper but also a greater current accuracy.

The engineering question naturally arises as to what precision must the currents be maintained for a given side lobe suppression, or conversely what side lobes are caused by a given current error. It is suspected that if great side lobe suppression is utilized the side lobe level will be determined not by the current taper but by the error or deviation of the antenna currents from their theoretical values.

If the individual contributions are in error at random, say both in phase and magnitude, the resultant electric intensity would be of the form

$$g(u) = \sqrt{\left[g_0(u) + \Sigma x_k\right]^2 + \left[\Sigma y_n\right]^2} \qquad (49).$$

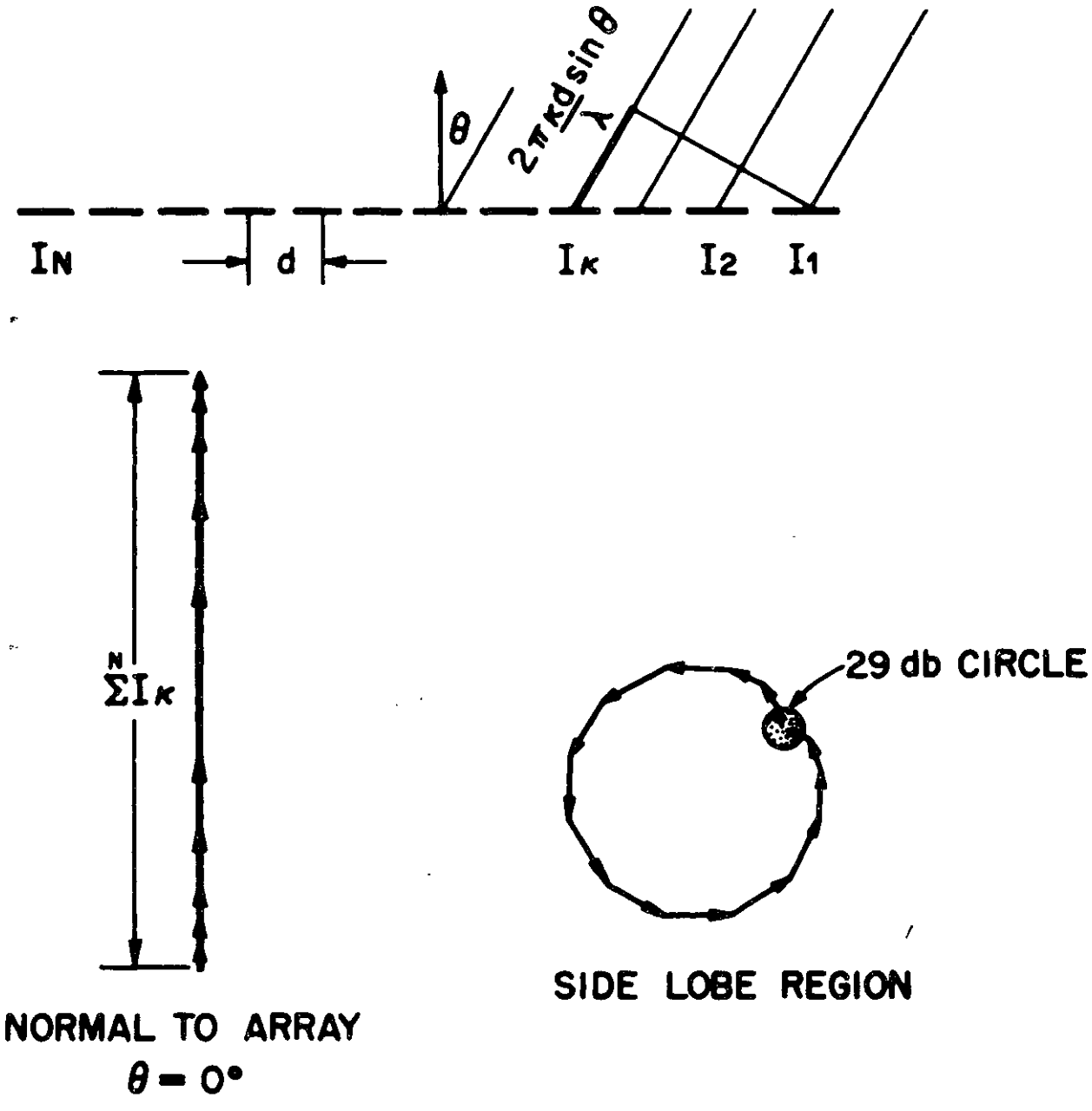
θ
2πκd sin θ / λ
IN
d
Iκ
I2
I1
N
ΣIκ
NORMAL TO ARRAY
θ = 0°
29 db CIRCLE
SIDE LOBE REGION

Figure No. 14

where $g_0(u)$ is the intensity with no error. In the side lobe region where the contributing vectors have spiraled around many times, the sums in (49) would have statistically zero mean and identical variance. Furthermore, as we are dealing with a large number of elements, at least greater than six, the individual sums would be asymptotically Gaussian according to the Central Limit Theorem. As Eq. (49) is of the form of eq. (45) and we have satisfied the necessary conditions, the resultant electric intensity will be distributed in a modified Rayleigh manner with $g_0(u)$ playing the role of the previously introduced displacement "a".

If we could now determine the mean power, our distribution would be completely specified. The mean power or the average power of a large "ensemble" of similar antennas can be found from the radiation patterns by standard statistical methods. Let us apply our analysis to the important case of a broadside array of MN elements spaced a distance "d" apart, quarter wave in front of a reflecting screen. The far-field field-component intensities are given, outside of distance and proportionality factors, by eq. (4) and (5), (Section II, 1)

$$F_\theta(\theta,\varphi) = \cos\theta\cos\varphi \sum_n^N \sum_m^M I_{nm}\, e^{jk\sin\theta[md\sin\theta + nd\sin\varphi]} \qquad (4)$$

$$F_\varphi(\theta,\varphi) = \sin\varphi \sum_n^N \sum_m^M I_{nm}\, e^{jk\sin\theta[md\cos\varphi + nd\sin\varphi]} \qquad (5).$$

The coordinates are the usual right-handed system, with the array in the xy plane and directed along the z or $\theta = 0$ axis. The current is assumed to flow in the x-direction. The above formulas should be multiplied by a screen factor of $\sin(\frac{\pi}{2}\cos\theta)$, however we shall use the closely related function $\sqrt{\cos\theta}$ to preclude later integration difficulties. The two functions are shown in Fig. No. 15. As we will be primarily concerned with highly directive arrays, the difference is not significant.

Now let us consider the individual element currents independently in error, both in phase and magnitude; that is, our currents become $I_{mn}(1+\Delta_{mn})e^{j\delta_{mn}}$, where the phase angle is measured in radians. The power patterns may be obtained from (4) and (5) by forming the complex conjugate. Writing the summation term only we have:

$$P(\theta,\varphi) \propto \sum_{m}^{M}\sum_{n}^{N}\sum_{p}^{M}\sum_{q}^{N} I_{mn} I_{pq}^{*}(1+\Delta_{mn})(1+\Delta_{pq}) \times e^{j k \sin\theta [(m-p)d\cos\varphi + (n-q)d\sin\varphi]} \times e^{j(\delta_{mn}-\delta_{pq})} \qquad (50)$$

The desired or no-error pattern is

$$P_o(\theta,\varphi) \propto \sum_{m}^{M}\sum_{n}^{N}\sum_{m}^{M}\sum_{n}^{N} I_{mn} I_{pq}^{*} e^{j k \sin\theta [(m-p)d\cos\varphi + (n-q)d\sin\varphi]}. \qquad (51)$$

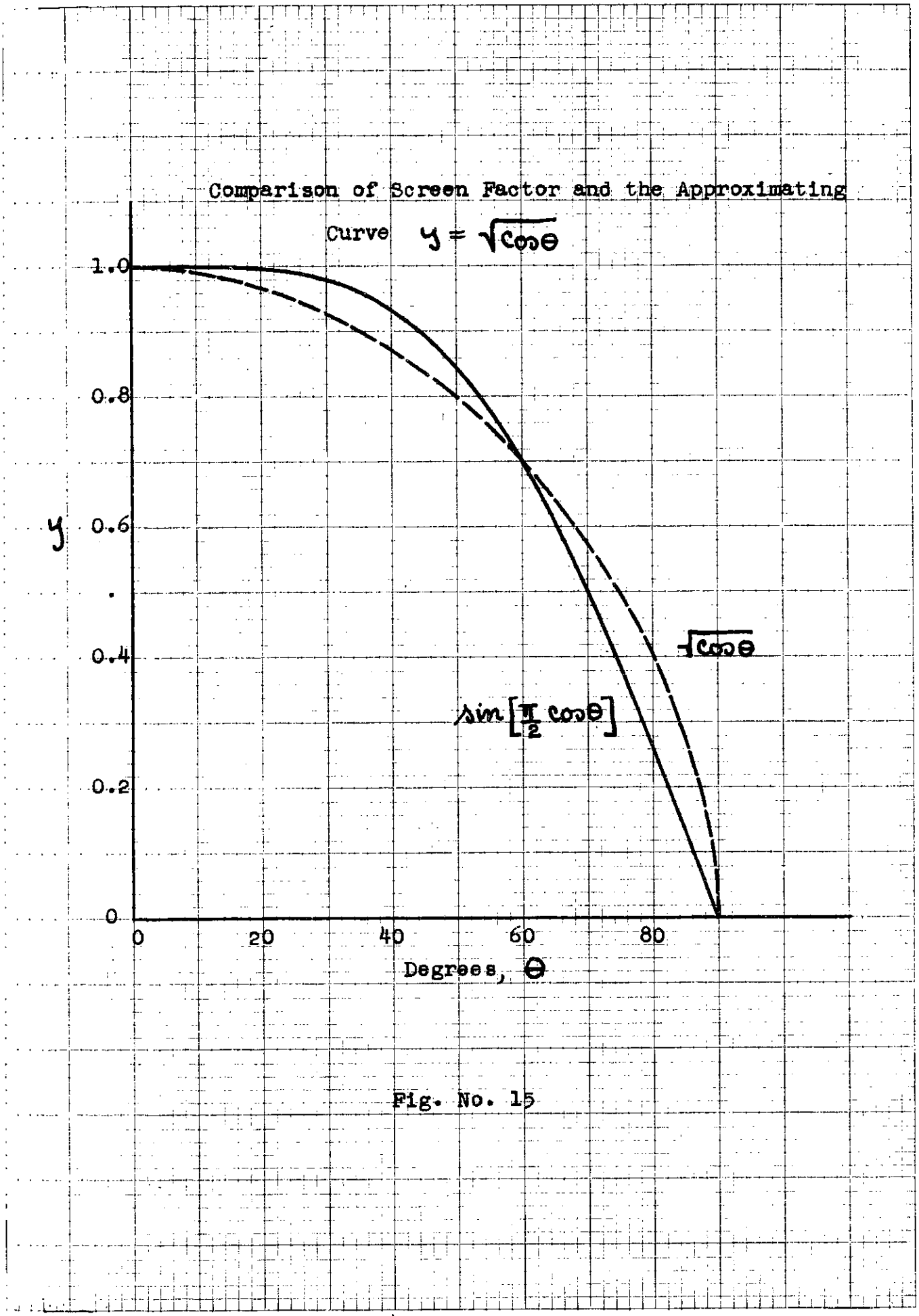
Comparison of Screen Factor and the Approximating Curve $y = \sqrt{\cos\theta}$
1.0
0.8
0.6
0.4
0.2
0
y
0
20
40
60
80
Degrees, θ
$\sqrt{\cos\theta}$
$\sin\left[\frac{\pi}{2}\cos\theta\right]$

Fig. No. 15

Let us now compute the "system average" pattern, that is, the average pattern of a large number of similar arrays. Designating this pattern by $\overline{P(\theta,\phi)}$ and assuming, as is likely, that the mean error is zero or that $\overline{\Delta_{mn}} = \overline{\delta_{mn}} = 0$, we have:

$$\overline{P(\theta,\varphi)} \propto \overline{\Delta^2} \sum_{m}^{M} \sum_{n}^{N} I_{mn}^2 + \sum_{m}^{M} \sum_{n}^{N} \sum_{m}^{M} \sum_{n}^{N} I_{mn} I_{pq}^{*} \left[\overline{\cos y} + j\overline{\sin y}\right] \times e^{jk \sin\theta \left[(m-p) d \cos\varphi + (n-q) d \sin\varphi\right]} \qquad (52)$$

where we have let $y = \delta_{mn} - \delta_{pq}$ and realized that the mean of the sum of independent variables is the sum of the means.

We must now evaluate the mean of cos y and sin y where our fundamental random variable is "δ". We may assume that "δ" is distributed in a normal manner. This will be asymptotically true if the phase error is due to a number of causes and such errors are small, so that a first order or linear relation exists between the cause of the phase error and the error itself.

"y" then becomes a random variable generated as the difference of two samples from a normal distribution. Fig. No. 16 shows the generation of this variable, commonly called the "range" in statistics.

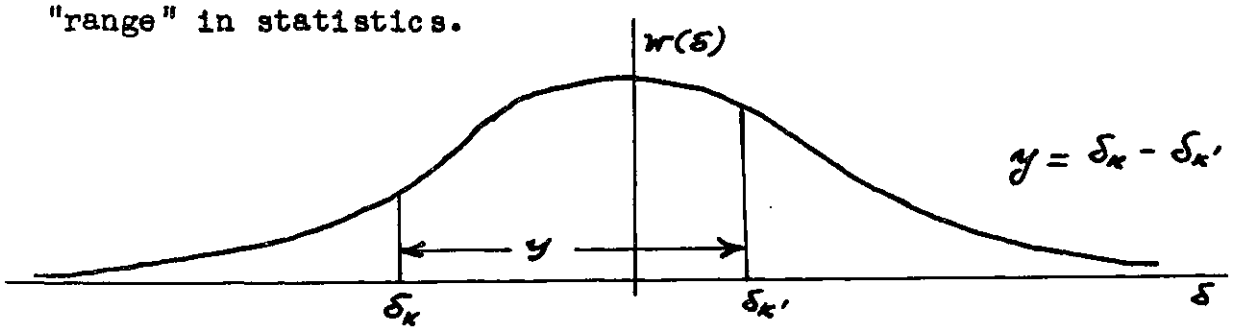

Fig. No. 16

The distribution "W(y)" is given by

$$w(y) = \int_{-\infty}^{\infty} w_1(\delta)\, w_1(\delta + y)\, d\delta \tag{53}$$

where

$$w_1(\delta) = \frac{1}{\sqrt{2\pi\,\overline{\delta^2}}}\, e^{-\delta^2/2\overline{\delta^2}} \tag{54}$$

and

$$w(y) = \frac{1}{2\pi\,\overline{\delta^2}} \int_{-\infty}^{\infty} e^{-\frac{1}{2\overline{\delta^2}}[2\delta^2 + 2\delta y + y^2]}\, d\delta$$

Performing the integration we obtain

$$w(y) = \frac{1}{\sqrt{4\pi\,\overline{\delta^2}}}\, e^{-y^2/4\overline{\delta^2}} \tag{55}$$

and

$$\overline{\cos y} = \int_{-\infty}^{\infty} \cos y\; w(y)\, dy = e^{-\overline{y^2}/2} = e^{-\overline{\delta^2}} \tag{56}$$

$$\overline{\sin y} = \int_{-\infty}^{\infty} \sin y\; w(y)\, dy = 0 \tag{57}$$

Applying these results to (52), making use of (51), and adding the two component powers (4) and (5)

$$P(\theta,\varphi) = P_0(\theta,\varphi)\, e^{-\overline{\delta^2}} + S(\theta,\varphi)\left[\overline{\Delta^2} + 1 - e^{-\overline{\delta^2}}\right] \sum_{m}^{M} \sum_{n}^{N} I_{mn}^2 \tag{58}$$

where the obliquity factor is reintroduced, being

$$s(\theta,\varphi) = \cos\theta\left[\cos^2\theta\cos^2\varphi + \sin^2\varphi\right] \qquad (59)$$

Normalizing our pattern and calling $\overline{\epsilon^2}$ the total mean square error

$$\overline{\epsilon^2} = \left[\Delta^2 + (1-e^{-\overline{\delta^2}})\right]e^{\overline{\delta^2}} \approx \Delta^2 + \overline{\delta^2} \qquad (60)$$

$$\overline{p(\theta,\varphi)} = p_0(\theta,\varphi) + s(\theta,\varphi)\,\overline{\epsilon^2}\,\frac{\sum^M\sum^N I_{mn}^2}{\left[\sum\sum I_{mn}\right]^2} \qquad (61)$$

Equation (61) gives the "average system" pattern. We note that the effect of the error distribution is to add a spatially constant (outside of an inherent obliquity and screen factor) power level proportional to the mean squared error. Individual arrays and particular spatial directions will show side lobe radiation differing from this constant value and distributed in a modified Rayleigh manner with the following constants

$$a^2 = p_0(\theta,\varphi) \qquad (62)$$

$$\sigma^2 = s(\theta,\varphi)\,\overline{\epsilon^2}\,\frac{\sum^M\sum^N I_{mn}^2}{\left[\sum^M\sum^N I_{mn}\right]^2} \qquad (63)$$

It should be noted that when the errors are small so that $a^2 \gg \sigma^2$, the field strength will be distributed approximately

Gaussian about the no-error pattern; whereas for large errors where $\sigma^2 >> a^2$ and the original minor lobe radiation may be neglected, we have Rayleigh behavior.

The formula also indicates that relatively smaller spurious radiation will occur for a larger number of elements, in fact the error contribution depends approximately on 1/NM. Hence, for a given current precision low side lobes are more readily realized with large antennas. This is not suprising physically as the main beam intensity increases as the square of the number of elements or as $(NM)^2$, whereas the spurious radiation, being incoherent, increases only as NM.

To illustrate the application of our result, eq. (61), we consider our 25 element array designed to suppress the minor lobes to 29 db. Following the Dolph procedure, we compute the current distribution to be

$I_0 = 1.00$ $\quad$ $I_7 = 0.627$

$I_1 = 1.00$ $\quad$ $I_8 = 0.535$

$I_2 = 0.970$ $\quad$ $I_9 = 0.445$

$I_3 = 0.923$ $\quad$ $I_{10} = 0.358$

$I_4 = 0.863$ $\quad$ $I_{11} = 0.278$

$I_5 = 0.795$ $\quad$ $I_{12} = 0.418$

$I_6 = 0.715$ $\quad$ and $\quad I_{-k} = I_k$

from which

$$\sum_{k}^{\pm 12} I_k = 16.85$$

$$\sum_{k}^{\pm 12} I_k^2 = 12.87$$

In Fig. No. 17 we plot, for those angular positions where the no-error minor lobes have maxima, the probability that the radiation will be below a specified number of db when a given mean error exists in the antenna currents. Fig. No. 12 is used to compute the necessary cumulative probability of the modified Rayleigh Distribution. A 50 element antenna with the same taper would have roughly 3 db lower spurious radiation.

Finally, we compute an actual pattern of our 29 db antenna with a specific set of error currents. The error chosen was one wherein each element was assumed to be in error by the addition of a current 40 percent in magnitude and at random phase. The random phases were obtained by drawing, at random, from a hat containing the numbers from 0 to 359. The random phases could preferably have been taken from a table of random angles (Morse - Table II). The author was unaware of the existence of these tables, which have been specifically checked for randomness, at the time this computation was made. Figure No. 18 shows both the no-error and the error pattern ($\overline{\epsilon^2} = 0.16$). Figure No. 19 plots the distribution of side lobe magnitudes as obtained from the error pattern and from the Rayleigh distribution. The limiting form of the Rayleigh case is used as the error currents are so large that the inherent no-error radiation is negligible.

It is worthwhile to point out that the actual computation of the error pattern is a very time consuming operation. At each angular position 25 inphase and phase quadrature terms must be summed and their magnitude obtained. The entire

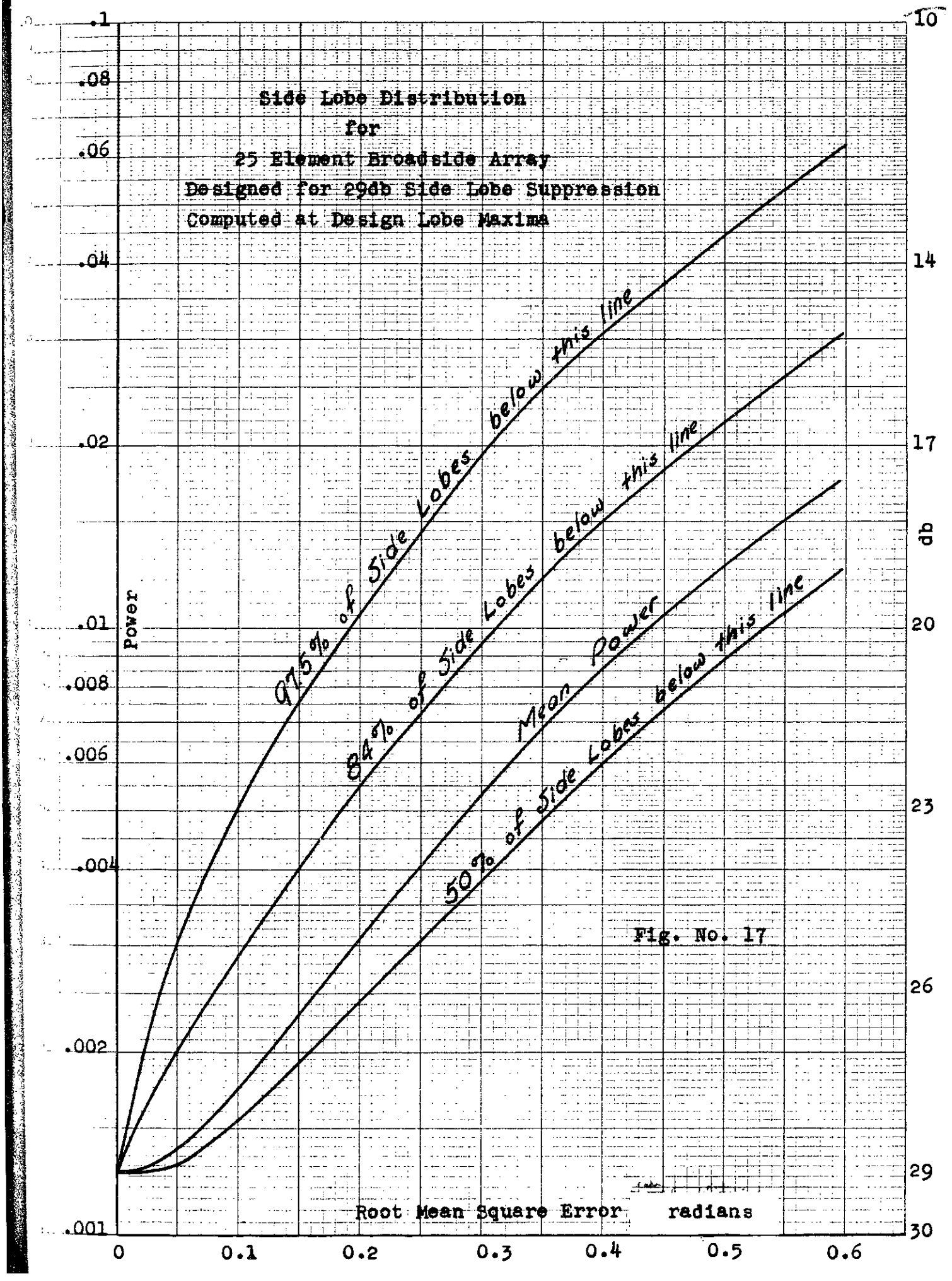
Side Lobe Distribution
for
25 Element Broadside Array
Designed for 29db Side Lobe Suppression
Computed at Design Lobe Maxima
97.5% of Side Lobes below this line
84% of Side Lobes below this line
Mean Power
50% of Side Lobes below this line
Power
db
Root Mean Square Error radians
.1
.08
.06
.04
.02
.01
.008
.006
.004
.002
.001
10
14
17
20
23
26
29
30
0
0.1
0.2
0.3
0.4
0.5
0.6

Fig. No. 17

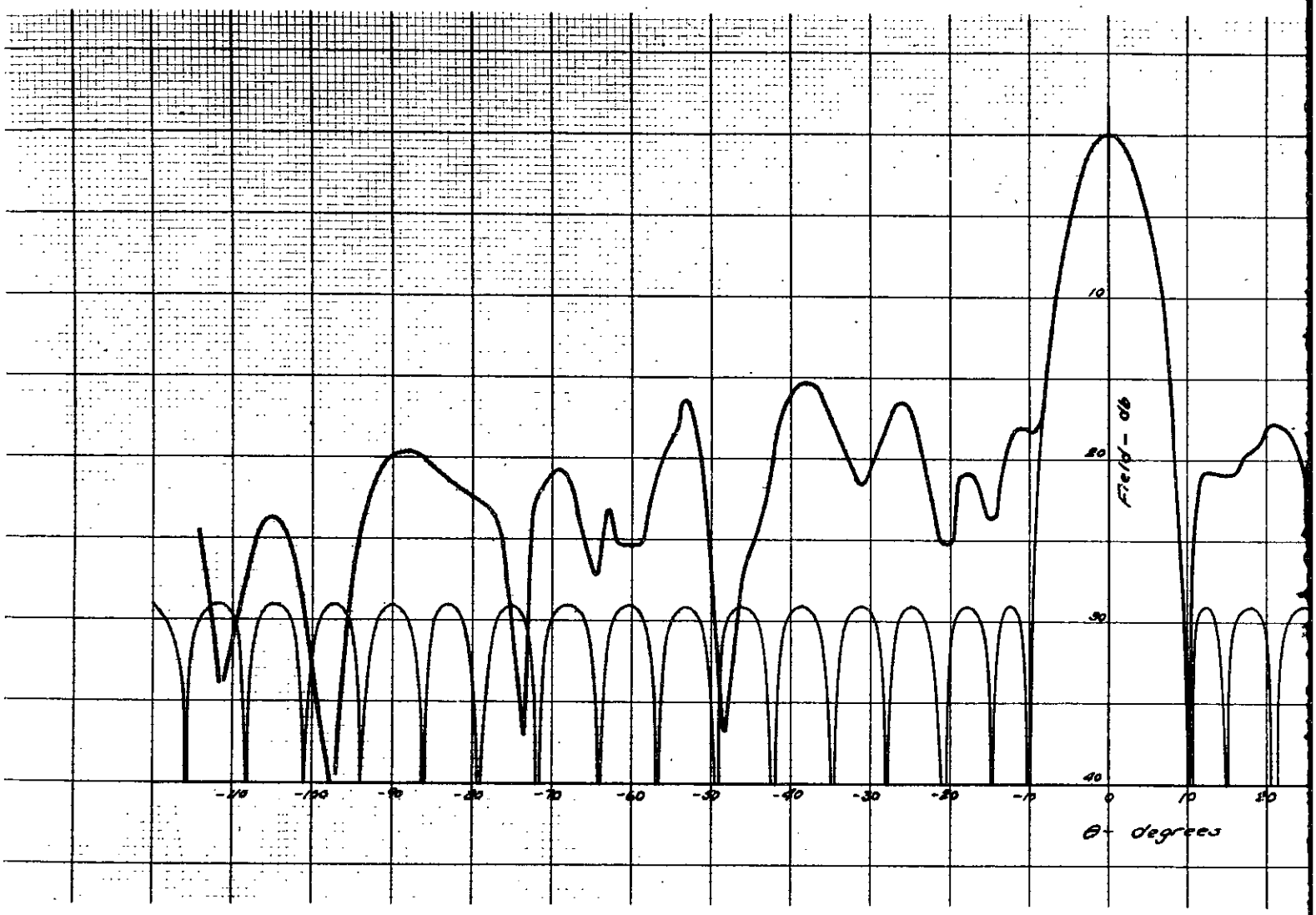
10
20
30
40
Field - db
-110
-100
-90
-80
-70
-60
-50
-40
-30
-20
-10
0
10
θ - degrees

Fig. No. 16

Theoretical Effect of Error Currents on Radiation Pattern

of

25 Element Broadside Array

designed for

29 db. Side Lobe Suppression

a). No Error

b). 0.40 r.m.s. error in each element at random phase.

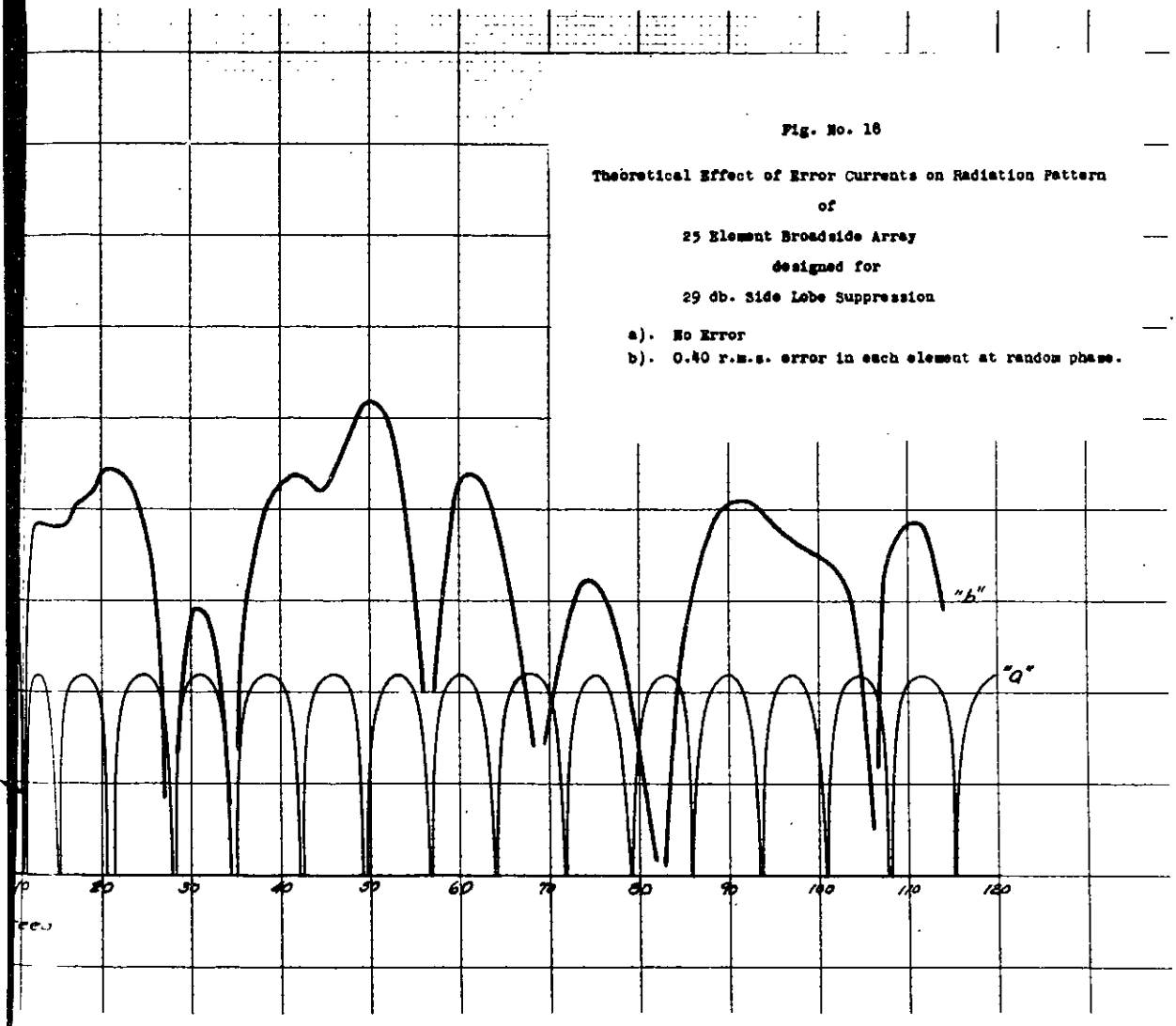

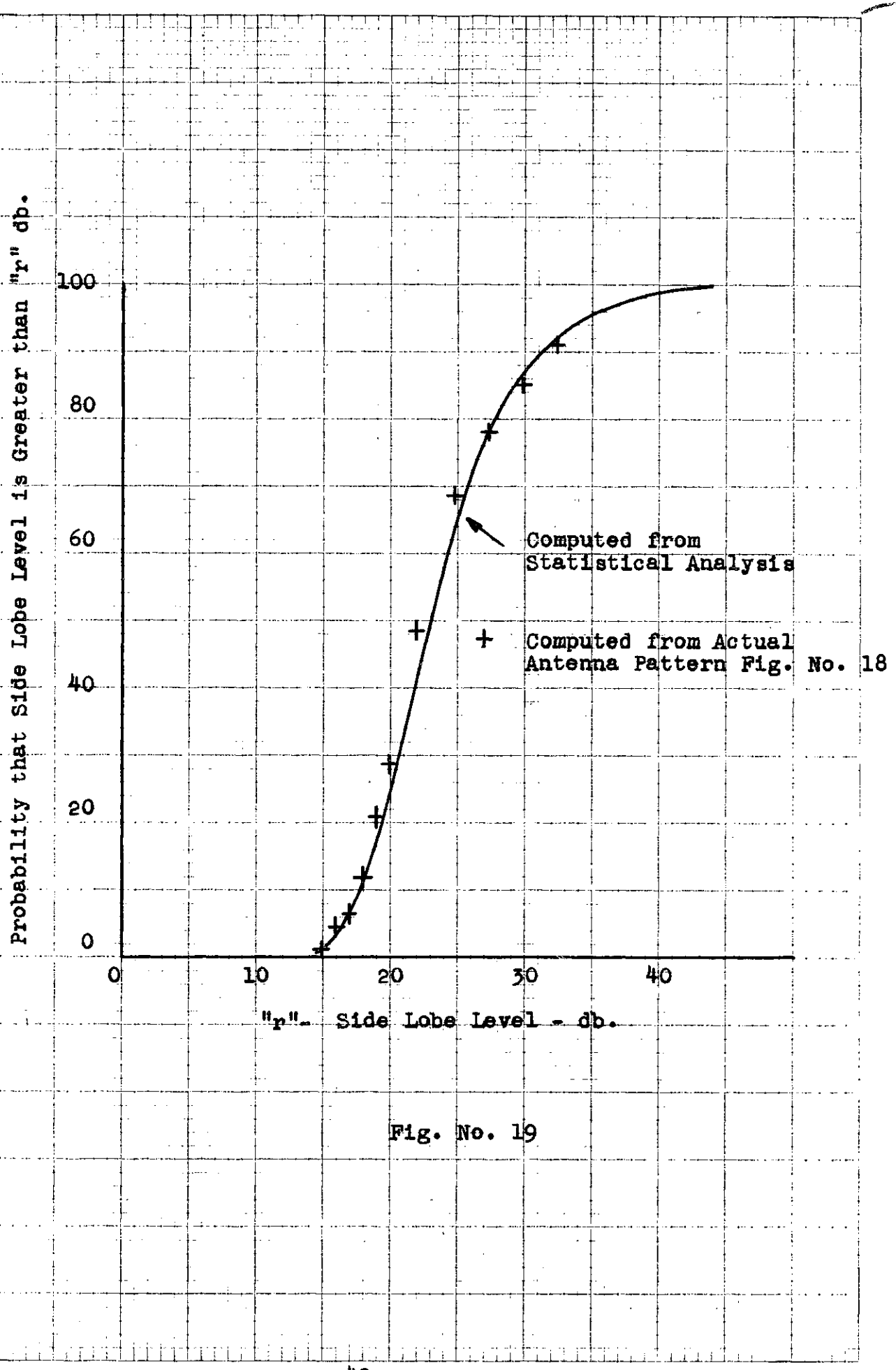
Probability that Side Lobe Level is Greater than "r" db.
100
80
60
40
20
0
0
10
20
30
40
"r" - Side Lobe Level - db.
Computed from Statistical Analysis
Computed from Actual Antenna Pattern Fig. No. 18

Fig. No. 19

operation must be performed with sufficient accuracy to reproduce the pattern in the side lobe region where almost complete cancellation exists under the no-error condition. The pattern drawn in Fig. No. 18 was actually computed by an electric analog antenna pattern calculator at the Naval Research Laboratory in Washington, D.C. Figure No. 19 indicates that our statistical theory gives our side lobe distribution without any tedious calculations.

The excellent agreement in Fig. No. 18 indicates that we can use the Rayleigh distribution in the case of a 25 element array, although it is only asymptotically applicable.

b). Effect of Distribution Errors on Antenna Gain

Let us now consider the effect of the current errors on the antenna gain. The gain G, over an isotropic radiator, may be written as the ratio of the radiated power of the isotropic radiator to that of the test antenna when both antennas create the same field strength. We therefore have the gain formula

$$G_0 = \frac{4\pi}{\int_{4\pi} p_0(\theta,\varphi)\, d\Omega} \qquad (64)$$

Letting G be the gain of the antenna with the error distribution and G_0 that of the no-error antenna, we have, upon inserting the average pattern (61) and performing the evident integrations

$$\frac{G}{G_0} = \frac{1 + \overline{\epsilon^2} \dfrac{\sum\sum I_{mn}^2}{\left[\sum\sum I_{mn}\right]^2} e^{\overline{\delta^2}}}{1 + \frac{3}{16} G_0 \overline{\epsilon^2} \dfrac{\sum\sum I_{mn}^2}{\left[\sum\sum I_{mn}\right]^2} e^{\overline{\delta^2}}} \qquad (65).$$

As G_0 is usually a large number, we can write approximately

$$\frac{G}{G_0} \cong \frac{1}{1 + \frac{3}{16} G_0 \overline{\epsilon^2} \dfrac{\sum\sum I_{mn}^2}{\left[\sum\sum I_{mn}\right]^2} e^{\overline{\delta^2}}} \qquad (66).$$

Into eq. (66) we can insert the value of G_0 as measured by experimental means or determined by graphical integration from the theoretical antenna patterns. It would be desirable to have a simple, even though approximate, expression for the gain of a braodside array that could be used to further simplify eq. (66). Search of the literature has failed in finding such a useful expression. We can, however, derive such an approximate value from its continuous aperture counterpart. The gain of a uniformly illuminated aperture of area at least one square wavelength is given by (Silver, pg. 177)

$$G_0 \cong \frac{4\pi A}{\lambda^2} \qquad (67).$$

If now the same aperture were to consist of discrete radiators with equal excitation, the radiation pattern would hardly change provided the elements are spaced closer than a wavelength so that the second order diffraction maximums do not occur. As the pattern has not changed, the gain is unaltered and may be written as

$$G_o \simeq \frac{4\pi}{\lambda^2} MN d^2 \qquad (68).$$

where "M" is the number of columns, "N" the number of rows, and "d" the spacing. If now the excitation be altered, so that the "mnth" element carries the current I_{mn}, then the "on-axis" radiation will become

$$\left[\frac{\Sigma\Sigma I_{mn}}{MN}\right]^2$$

and the input power becomes

$$\frac{\Sigma\Sigma I_{mn}^2}{MN}.$$

provided that we assume negligible coupling between elements. Inserting these modifications into (68) we have for the gain of a broadside array, quarterwave in front of a reflecting screen

$$G_o \equiv 4\pi \left(\frac{d}{\lambda}\right)^2 \frac{\left[\Sigma\Sigma I_{mn}\right]^2}{\Sigma\Sigma I_{mn}^2}. \qquad (69).$$

Using this useful though approximate expression in (66) we have for the reduction in gain due to errors

$$\frac{G}{G_0} = \frac{1}{1 + \frac{3}{4}\pi\left(\frac{\sigma}{\lambda}\right)^2 \overline{\epsilon^2}} \qquad (68)$$

A result independent of the current distribution and the size of the array.

6). Application to a Continuous Aperture

a). Effect of Distribution Errors on Antenna Pattern (Booker)

In general the same statistical considerations apply to the aperture antenna as to the discrete array. However, an additional factor is introduced which considerably alters the final result. In the discrete case we assumed that the error current in one element was independent of the error currents in adjacent elements. This assumption is untenable in an aperture antenna as if the error is large at one point it will probably be large in the immediate neighborhood. The size of the correlated region will be found to affect both the magnitude and the directional characteristics of the spurious radiation.

Let us begin our discussion by considering a circular aperture excited by an electric current in the x-direction. Fig. No. 20 shows the coordinate system. As we are interested primarily in parabolic mirrors we will consider only a pure phase error, "δ", expressed in radians.

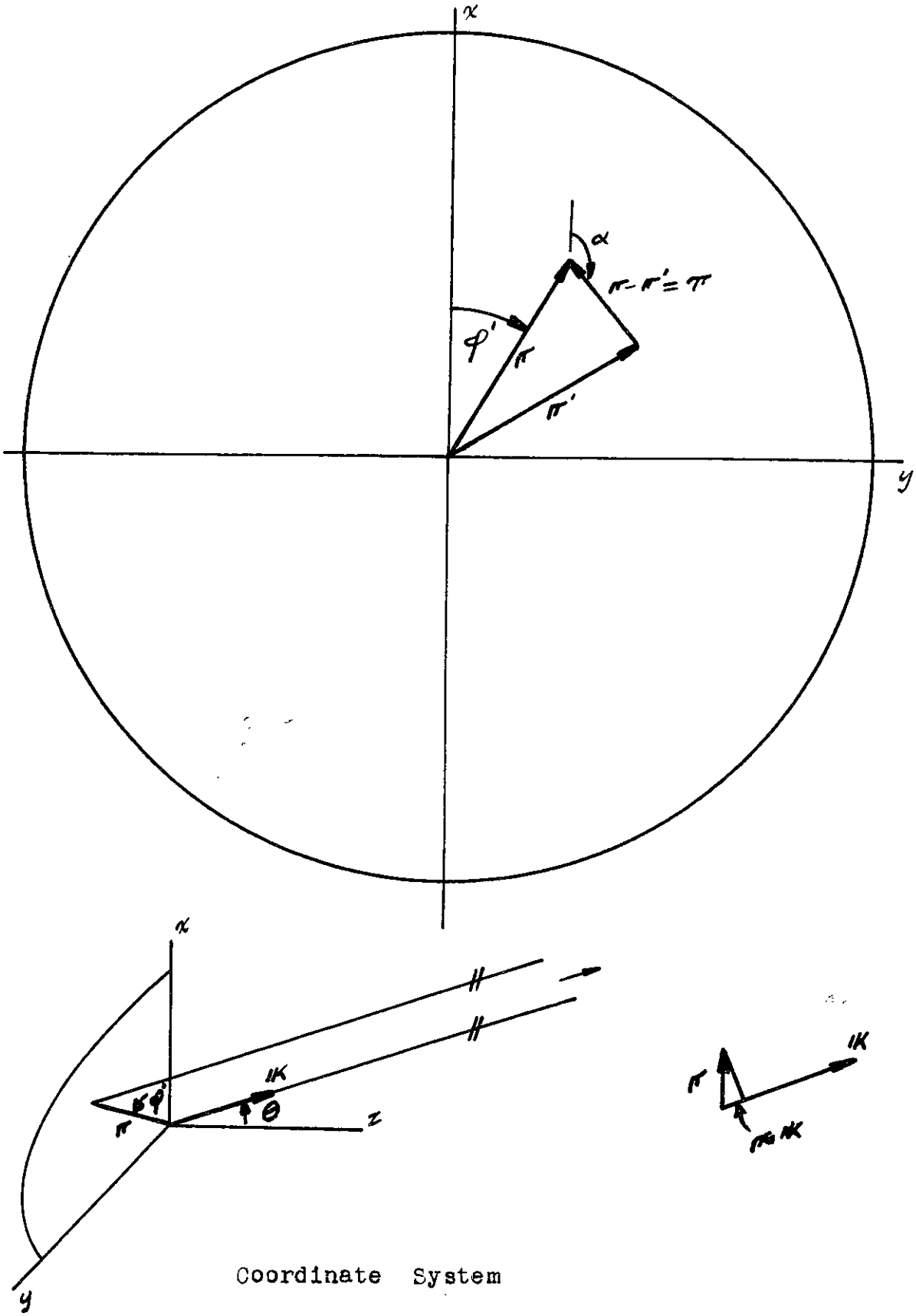

Coordinate System

Fig. No. 20

Following closely our discrete analysis and avoiding needless repetition, we write the far field, outside of the obliquity factor, from eq. (1a)

$$F(\theta,\varphi) = \int J_x(\pi)\, e^{j k \hat{\varphi}\cdot \mathbf{R}}\, dS_r$$

For a paraboloid the integration is performed over the mirror surface and the current is equal to the tangential magnetic component of the incident field. With a position dependent phase error the far field becomes

$$F(\theta,\varphi) = \int J_x(\pi)\, e^{j k \hat{\varphi}\cdot \mathbf{R}}\, e^{j\,\delta(\pi)}\, dS_r \qquad (69)$$

and the power pattern (corresponding to eq. (50) in the discrete case) formed by multiplication by means of the complex conjugate becomes

$$P(\theta,\varphi) = \iint J_x(\pi)\, J_x^*(\pi')\, e^{j k\cdot(\pi-\pi')}\, e^{j[\delta(\pi)-\delta(\pi')]}\, dS_r\, dS_{r'} \qquad (70)$$

changing the vector position variable, so that $(\pi - \pi') = \tau$,

$$P(\theta,\varphi) = \iint J_x(\pi+\tau)\, J_x^*(\pi)\, e^{j k\cdot\tau}\, e^{j[\delta(\pi+\tau)-\delta(\pi)]}\, dS_r\, dS_\tau \qquad (71)$$

and with the same notation as previously, we obtain for the mean pattern

$$\overline{\rho(\theta,\varphi)} = \iint \overline{J(r+\pi)\,J^{*}(r)\left[\cos y + i \sin y\right]}\, dS_r\, dS_\tau \qquad (72)$$

Now "y", the phase difference of two points on the aperture spaced a distance π apart, has zero mean as positive and negative errors are equally likely. For large values of τ the phase errors are uncorrelated and the mean square has the same value as previously, namely $\overline{y^2} = 2\overline{\delta^2}$. For $\tau = 0$, the mean square phase difference is obviously zero. The mean square value therefore depends on π and we have only its limiting values. We must assume some functional form to fit these two conditions. Assuming that:

$$\overline{y^2(\tau)} = 2\overline{\delta^2}\left[1 - e^{-\tau^2/c^2}\right] \qquad (73)$$

where "C" may be defined as a "correlation interval", that is, that distance "on average" where the errors become essentially independent. Equation (73) has the form indicated in Figure No. 21.

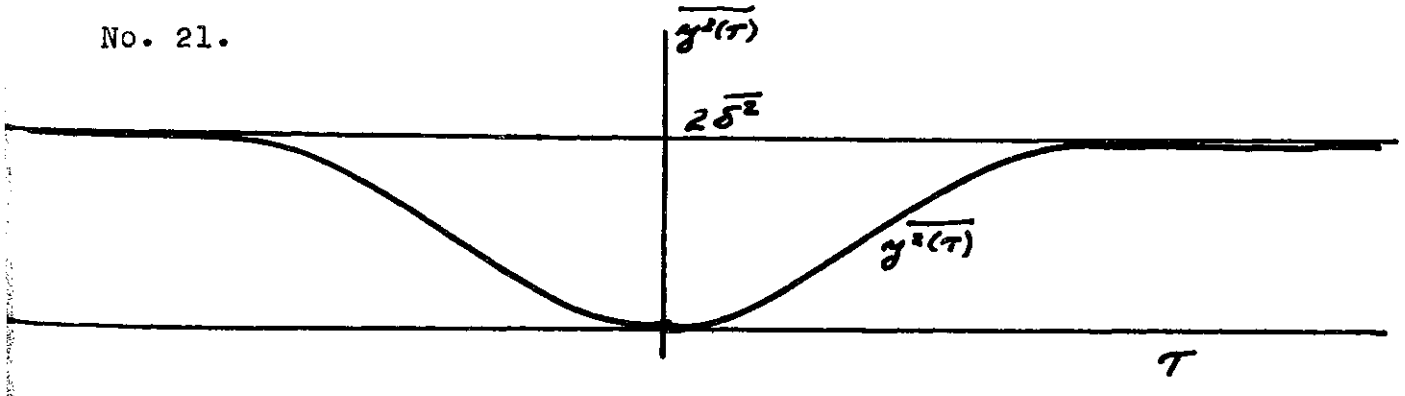

Fig. No. 21

In equation (73) we have purposely neglected the vector character of τ ; this means that we are assuming that the mean square phase difference between two points spaced a distance τ apart is independent of the direction in which we choose the second point. This is a good assumption if the errors are uniformly distributed over the aperture.

Inserting (73) into (56) and defining the aperture autocorrelation function

$$\varphi(\pi) = \frac{\int J(r+\pi)\, J^{*}(r)\, dS_r}{\int J^{2}(r)\, dS_r} .$$

eq. (72) becomes

$$P(\theta,\phi) = e^{-\overline{\delta^2}} \int J^{2}(r)\, dS_r \int \varphi(\pi)\, e^{j k\cdot\pi}\, e^{\overline{\delta^2} e^{-\tau^2/c^2}}\, dS_T \qquad (75).$$

Expanding the exponential and realizing that the undistorted pattern is

$$P_0(\theta,\phi) = \int J^{2}(r)\, dS_r \int \varphi(\pi)\, e^{j k\cdot\pi}\, dS_T \qquad (76).$$

we have

$$\overline{P(\theta,\phi)} = P_0(\theta,\phi)\, e^{-\overline{\delta^2}} + e^{-\overline{\delta^2}} \int J^{2}(r)\, dS \sum_{n=1}^{\infty} \int \varphi(\pi)\, e^{j k\cdot\pi} \frac{[\overline{\delta^2}]^{n}}{n!} e^{-n\tau^2/c^2}\, \tau\, d\tau\, d\alpha \qquad (77).$$

Now $\phi(\tau)$, the no-error aperture auto-correlation function, is a slowly varying function, with $\phi(0) = 1$ and decreasing to zero at twice the aperture diameter. Whereas the exponential essentially vanishes beyond the error correlation interval, that is for $\tau >> c$. This is illustrated in Fig. No. 22.

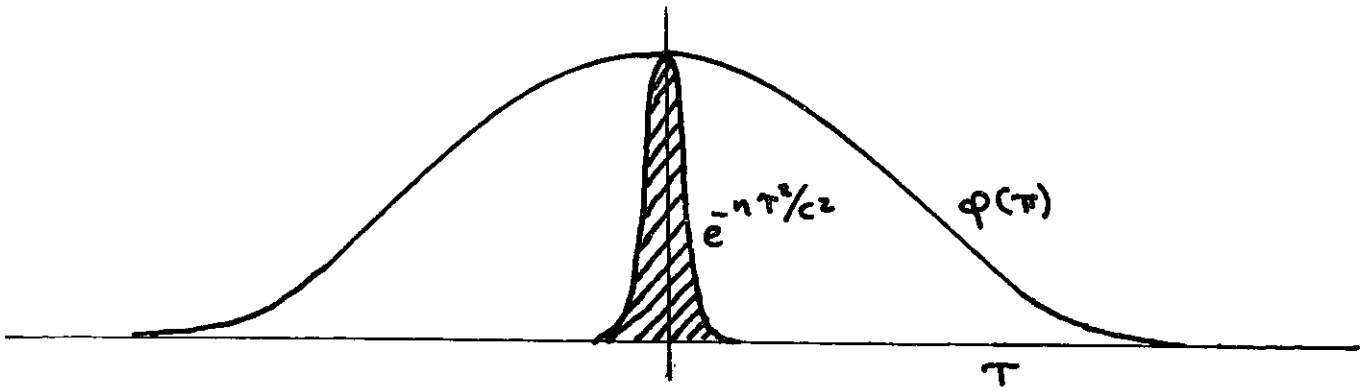

Fig. No. 22

We make little error in taking $\phi(\tau)$ as unity as the contribution to the integral for $\tau >> c$ where $\phi(\tau)$ differs from one is negligible.

Now

$$k\rho\cdot\tau = \frac{2\pi}{\lambda}\tau \sin\theta\left[\cos\varphi\cos\alpha + \sin\varphi\sin\alpha\right]$$

$$\therefore \quad k\rho\cdot\tau = \frac{2\pi\tau}{\lambda}\sin\theta\left[\cos(\varphi-\alpha)\right] \qquad (78)$$

inserting and performing the "α" integration (McLachlin, pg. 157), we obtain with the notation, $u = \sin\theta$:

$$P(\theta,\varphi) = P_0(\theta,\varphi)\, e^{-\overline{\delta^2}} + \int_S J^2(\pi)\, dS \cdot \sum \frac{[\overline{\delta^2}]^n}{n!} \int_0^\infty J_0\left(\frac{2\pi u \tau}{\lambda}\right) e^{-n\tau^2/c^2}\, \tau\, d\tau \qquad (79)$$

We are now faced with the evaluation of the integral

$$I = \int_0^\infty \tau e^{-n\tau^2/c^2} J_0\left(\frac{2\pi}{\lambda} u\tau\right) d\tau \qquad (80)$$

This integral is of some interest as the identical form would occur for the polar diagram of a circular aperture excited with a Gaussian taper (Silver, pg. 194). To evaluate we insert for the Bessel function Schlafli's contour integral form (Copson, pg. 319)

$$J_0(z) = \frac{1}{2\pi i} \int_C \frac{e^{t - z^2/4t}}{t}\, dt$$

The integration contour runs as indicated in Fig. No. 23

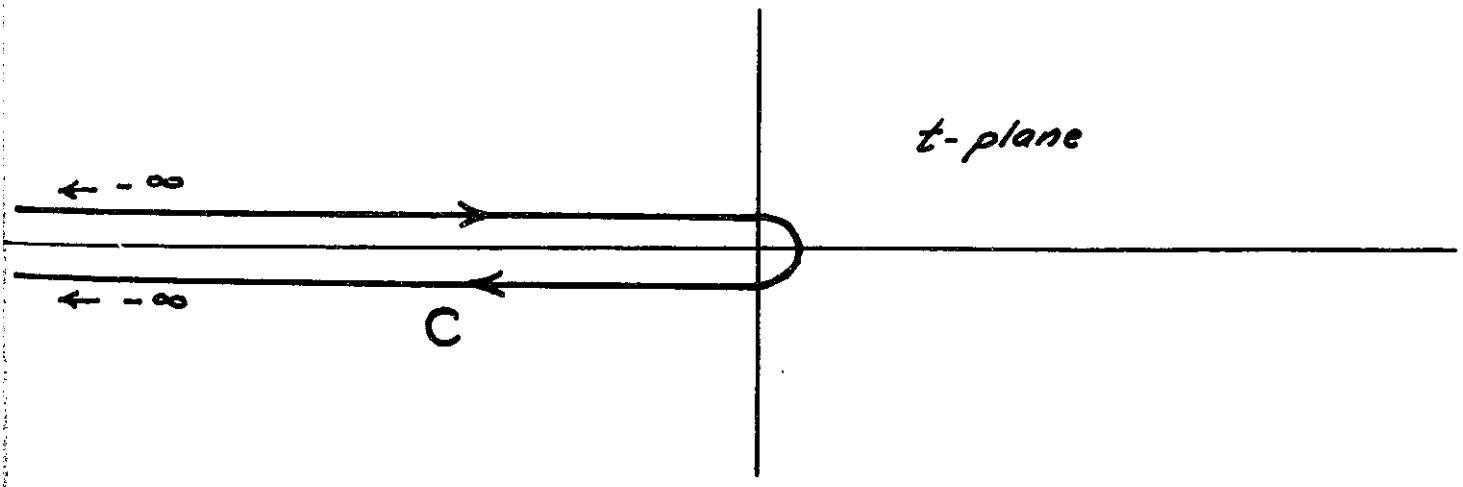

Fig. No. 23

We have now

$$I = \frac{1}{2\pi i} \int_c \frac{e^t}{t} \int_0^\infty \tau e^{-\frac{t + c^2 b^2/4n}{t c^2/n}} \tau^2 \, d\tau \, dt$$

where $b = \frac{2\pi}{\lambda} u$. The integration over τ can be readily evaluated leading to the form

$$I = \frac{1}{4\pi i n} \int_c \frac{c^2 e^t \, dt}{t + \frac{c^2 b^2}{4n}}$$

This last integration can be performed by the method of residues as it has a simple pole at $t = -\frac{c^2 b^2}{4n}$. We obtain

$$I = \frac{c^2}{2n} e^{-\frac{c^2 \pi^2 u^2}{\lambda^2 n}}. \qquad (81)$$

This is a rather interesting result as, since (80) could be interpreted as the polar diagram of a circular aperture with a Gaussian taper, the polar diagram is again Gaussian. This is rather suprising as circular apertures normally have Bessel functions for their radiation patterns.

Inserting (81) into (79)

$$\overline{P(\theta,\varphi)} = P_0(\theta,\varphi) e^{-\overline{\delta^2}} + \overline{\delta^2} c^2 \pi^2 e^{-\overline{\delta^2}} \left[\sum_{n=1}^{\infty} \frac{[\overline{\delta^2}]^{2(n-1)}}{n! \, n} e^{-\frac{\pi^2 u^2 c^2}{n \lambda^2}} \right] \int J^2(c) \, dS \qquad (82)$$

normalizing by dividing by the factor $\left[\int J(r)\,dS\right]^2$ and using the approximate though generally accepted formula for the gain of equiphase aperture (Silver, pg. 177)

$$G_0 = \frac{4\pi}{\lambda^2}\,\frac{\left|\int J(r)\,dS\right|^2}{\int J(r)\,J^*(r)\,dS} \tag{83}$$

we obtain

$$\overline{p(\theta,\varphi)} = p_0(\theta,\varphi) + 4\frac{c^2\pi\,\overline{\delta^2}}{\lambda^2 G_0}\,s(\theta,\varphi)\left[\sum_{n=1}^{\infty}\frac{\left[\overline{\delta^2}\right]^{n-1}}{n!\,n}\,e^{-\pi^2 c^2 u^2/n\lambda^2}\right] \tag{84}$$

where we have further summed the two component powers and introduced our obliquity and screen factors.

Equation (84) is comparable to eq. (61) and gives the average system pattern. For small phase errors we need to consider only the first term of the summation - the distrubing pattern then is

$$s(\theta,\varphi)\,\frac{4c^2\pi^2\,\overline{\delta^2}}{\lambda^2 G_0}\,e^{-\pi^2 u^2 c^2/\lambda^2} \tag{85}$$

We note that the spurious radiation is again proportional to the mean squared error but in addition is proportional to the square of the correlation interval in wavelengths. Furthermore, this radiation is no longer essentially uniformly spatially

distributed but becomes, on the average, directionally directed along the axis of the aperture. The directivity increases with the size of the correlated region, so that for "rough" reflectors, where the correlation interval is small, energy is scattered uniformly. This is not at all suprising physically, for regions large compared to a wavelength (which are at the same phase) will scatter more strongly and more directively. As we have many such regions randomly located and oriented, there will be a concentration of the "average ensemble" radiation along the axis of the reflector.

The importance of the accuracy of the reflector shape is well known in antenna design. A thirty-second of a wavelength tolerance on the reflector surface (sixteenth on the resulting phase front) is a common criteria. Our analysis introduces the like importance of the size or extent of the distortion. If errors are unavoidable in a reflecting surface, one should endeavor that they be small in extent - furthermore, small disturbances such as heads of screws and rivets holding the reflector in place will have but a small deleterious effect on the antenna performance.

The theory reveals that if we consider two reflectors of the same mechanical tolerance but of different values of "c", that is, the mechanical errors in one, although having the same average magnitude, have a larger period (Fig. No. 24), then the "rougher" reflector (smaller "c") will have lower side lobes and they will be more uniformly distributed in angular direction.

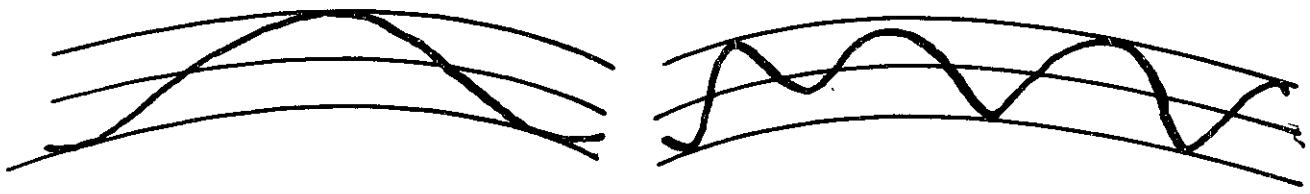

Smooth Reflector
Large "c"

"Rough" Reflector
Small "c"

Fig. No. 24

Unfortunately the analysis indicates that a reflector of given gain will degenerate much more rapidly than had been previously expected as the frequency is raised. Increasing the frequency increases the scattered energy both due to the increase in the correlation interval and due to the increase in the phase error. For reflectors of the same gain (same diameter in wavelengths) the relative side lobe level will increase as the fourth power of the frequency or 12 db per octave.

As the factor "c" occurs directly in our basic formula, it is of interest to speculate on its probable value in a typical reflector. The constant appears in relation to the wavelength so that for antennas in the "L" band (25 cm.) "c" may be quite small, say of the order of a tenth or a fifth, whereas in the "K" band (1.25 cm) values of "c" of the order of two or four would not be uncommon. Very large values of "c" would occur if the reflector is subjected to random warping

as would be caused by temperature changes or mechanical stress. Furthermore, if the reflector is carefully made so that many mechanical check points exist, then "c" would also be small whereas if great care is not utilized so that large mechanical errors occur they most likely would extend over quite a region making "c" large.

The higher order terms of eq. (84) are of lower directivity and hence have the same effect as a smaller correlation interval. This again has physical basis due to the periodic nature of the trigonometric functions; wherein a phase error of 360° represents no error at all but merely an effect similar to a reduction in the correlation interval. It should be noted that the correlation interval is not cut in half due to the Gaussian distribution of phase errors or in other words there will not be many places where the error exceeds 360°.

(1) Application to a Parabolic Mirror

We began the discussion of the continuous aperture by considering a plane circular aperture with an electric current flowing in the "x" direction. The result obtained, eq. (84), is of considerable greater generality. By the introduction of the concept of the correlated region and the assumption that the errors are uniformly distributed over the aperture, we have separated the error integration over essentially only the correlated region, eq. (77). The coherent term or the no-error pattern appeared as the first term of our expansion. This term contained the integration over the entire aperture.

If the aperture had a different cross-section, say elliptical or the integration were to be performed over a different surface, say parabolic or specially shaped, the no-error pattern would require modification. The effect on the scattered radiation would only be in relative level as expressed by the no-error gain of the antenna. Our result, therefore, holds for any continuous aperture provided we use the appropriate pattern and gain. Further, current separability is not required.

By this dodge we have circumvented the difficult electromagnetic theory problem of determining the complex currents on a shaped reflector when fed by a directive feed. Our result merely gives the spurious radiation that results when these currents are in error. The actual coherent or no-error pattern can be determined by existing approximate means or measured experimentally.

To apply our result to a parabolic reflector we need to determine the relation between the reflector error in wavelengths and the corresponding phase error of this contribution in the far field. For shallow reflectors this relation is

$$\delta \simeq 2\left(\frac{2\pi}{\lambda}\right)d \qquad \text{or} \qquad \overline{\delta^2} = 4\left(\frac{2\pi}{\lambda}\right)^2\overline{d^2}$$

where "d" is the mechanical distortion measured in the same units of length as the wavelength.

A number of graphs were prepared to illustrate the effect of the reflector error and correlation interval on the

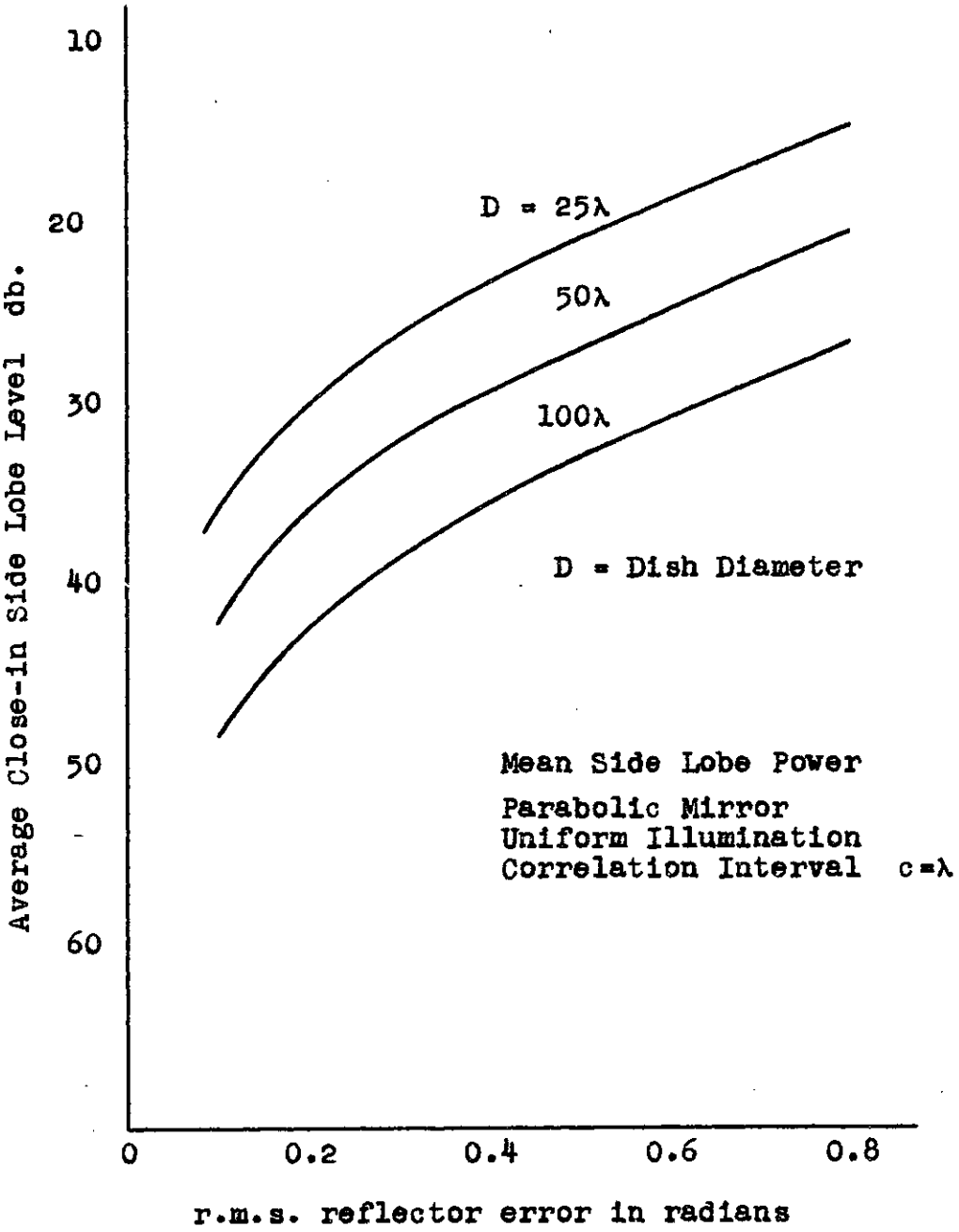
10
20
30
40
50
60
Average Close-in Side Lobe Level db.
D = 25λ
50λ
100λ
D = Dish Diameter
Mean Side Lobe Power
Parabolic Mirror
Uniform Illumination
Correlation Interval c=λ
0
0.2
0.4
0.6
0.8
r.m.s. reflector error in radians

Fig. No. 25

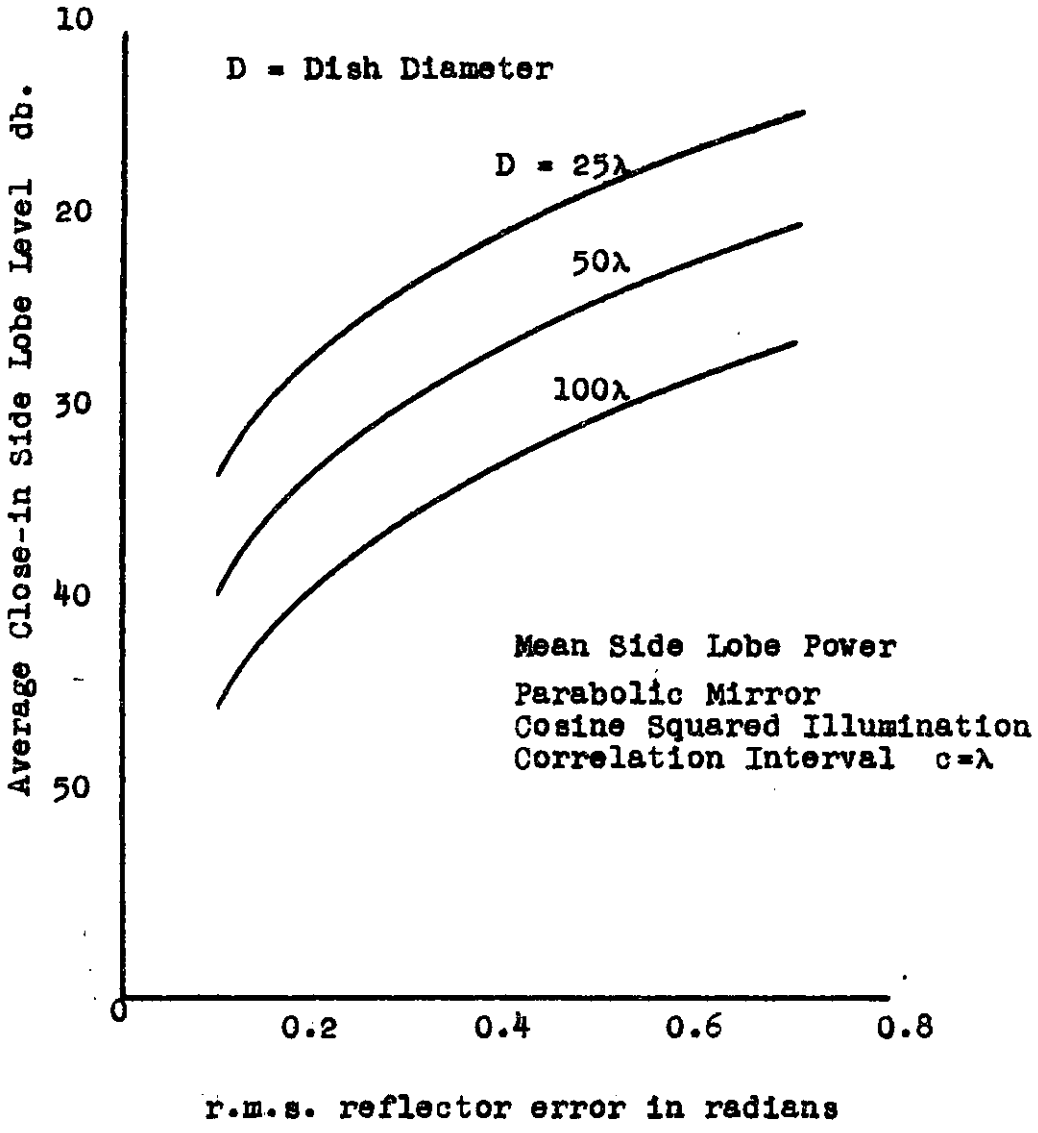
10
20
30
40
50
0
0.2
0.4
0.6
0.8
Average Close-in Side Lobe Level db.
D = Dish Diameter
D = 25λ
50λ
100λ
Mean Side Lobe Power
Parabolic Mirror
Cosine Squared Illumination
Correlation Interval c=λ
r.m.s. reflector error in radians

Fig. No. 26

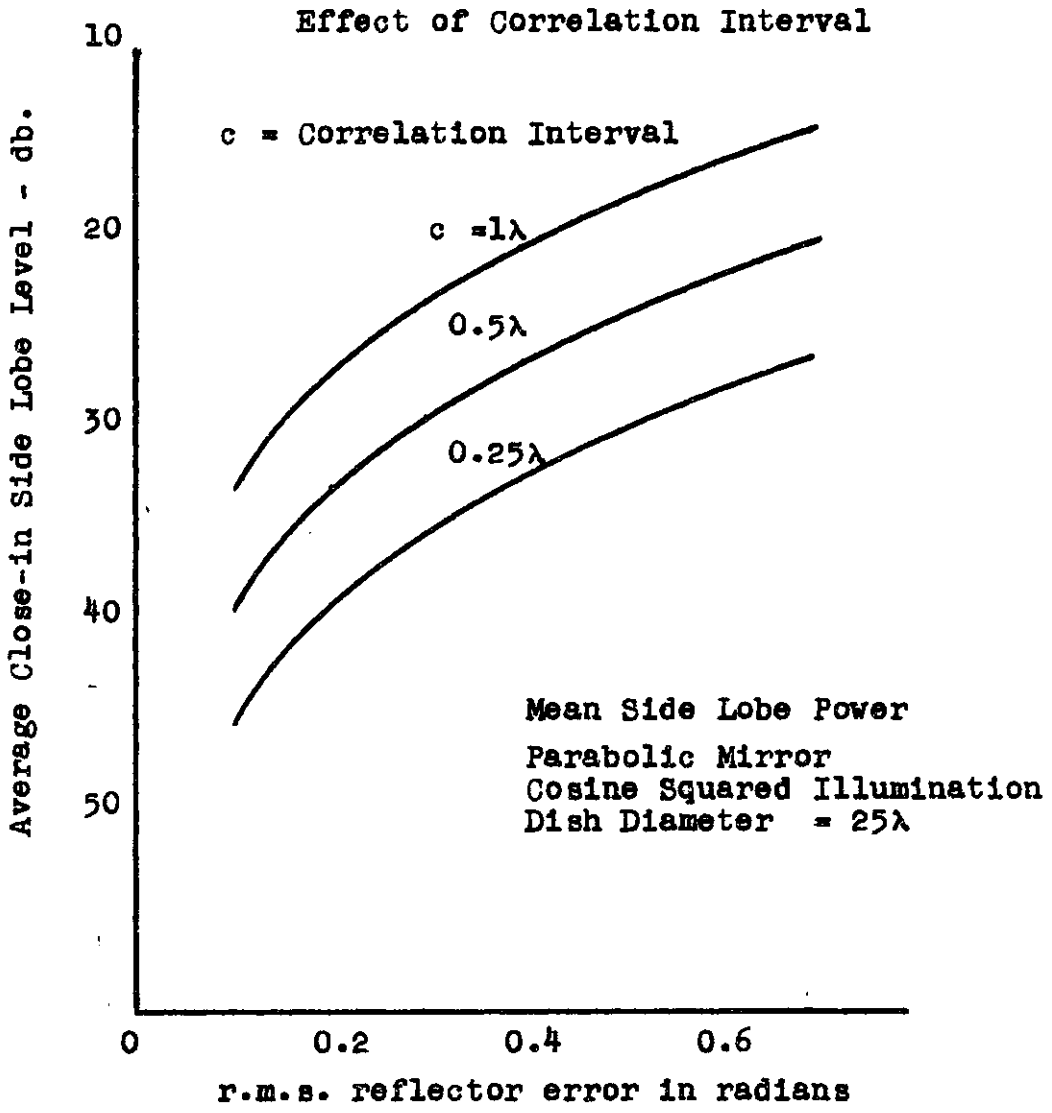
Effect of Correlation Interval
c = Correlation Interval
c =1λ
0.5λ
0.25λ
Mean Side Lobe Power
Parabolic Mirror
Cosine Squared Illumination
Dish Diameter = 25λ
Average Close-in Side Lobe Level - db.
10
20
30
40
50
0
0.2
0.4
0.6
r.m.s. reflector error in radians

Fig. No. 27

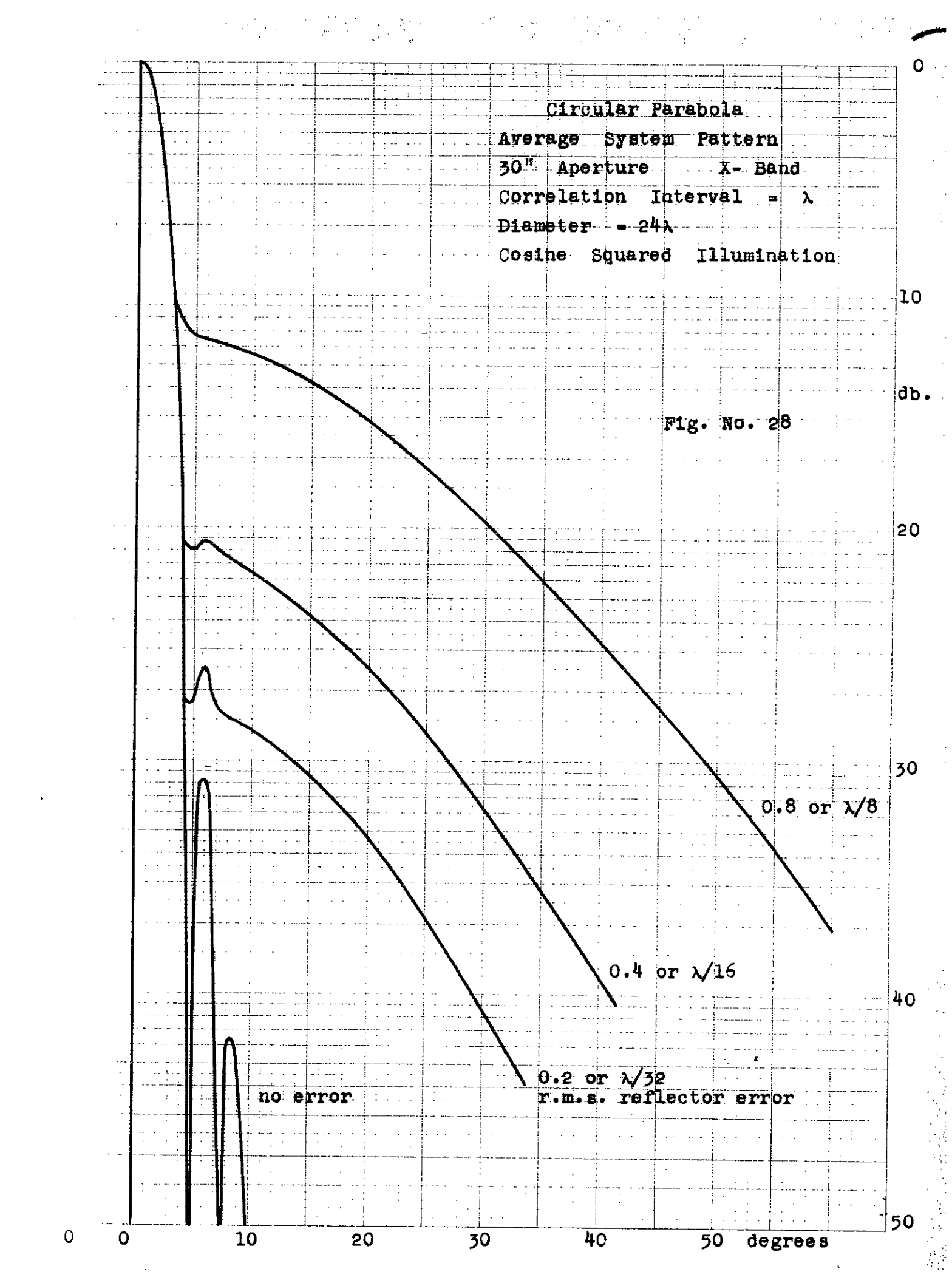
Circular Parabola
Average System Pattern
30" Aperture X- Band
Correlation Interval = λ
Diameter = 24λ
Cosine Squared Illumination
Fig. No. 28
0.8 or λ/8
0.4 or λ/16
0.2 or λ/32
r.m.s. reflector error
no error
0
10
20
30
40
50
db.
0
10
20
30
40
50 degrees

spurious side lobe level. The inherent coherent level is to be added to these curves. Although the "average" side lobe magnitude is spatially directive, we plot only the close-in lobes, that is, we set $u = 0$ in eq. (84). As we are dealing with highly directive systems these close-in lobes are of primary interest. Figure No. 25 plots the expected minor lobe level as a function of the r.m.s. reflector error for uniformly illuminated apertures of various diameters. Again we see the lower spurious radiation obtainable with the larger diameters for the same tolerance. Figure No. 26 is a similar plot for a cosine squared illumination which illumination yields an antenna of lower gain. This illumination is typical of current practice. Figure No. 27 shows the effect of the correlation interval. Finally, Fig. No. 28 shows the angular pattern of our system average pattern as it is affected by various amounts of phase error.

b).- Effect of Distribution Errors on Antenna Gain

The average reduction in gain can be obtained as in the discrete case by inserting into eq. (64) which is the exact expression for antenna gain, eq. (84). This yields for the ratio of the gains

$$\frac{G}{G_0} = \frac{1}{1 + \frac{c^2\pi^2\overline{\delta^2}}{\lambda^2} \sum_{n=1}^{\infty} \frac{[\overline{\delta^2}]^{n-1}}{n!\,n} \int [\cos^3\theta\cos^2\varphi + \cos\theta\sin^2\varphi] e^{-\pi^2 u^2 c^2/n\lambda^2} \sin\theta\, d\theta\, d\varphi} \qquad (86)$$

Confining our attention to the integral, performing the "ø" integration and writing $\frac{\pi^2 c^2}{\lambda^2} = a^2$

$$I = \int_0^{\pi/2} \left[\cos^3\theta \sin\theta + \cos\theta \sin\theta\right] e^{-\frac{a^2 \sin^2\theta}{n}} d\theta.$$

Expanding the exponential

$$e^{-\frac{a^2 \sin^2\theta}{n}} = \sum_{m=0}^{\infty} (-1)^m \frac{a^{2m}}{n^m} \sin^{2m}\theta.$$

and

$$I = \sum_{m=0}^{\infty} \frac{(-1)^m a^{2m}}{m!\, n^m} \left[\int_0^{\pi/2} \cos^3\theta \sin^{2m+1}\theta \, d\theta + \int_0^{\pi/2} \cos\theta \sin^{2m+1}\theta \, d\theta\right].$$

the integrals can be evaluated (Gröbner, pg. 95) so that the bracketed term becomes

$$\left[\frac{\Gamma\left(\frac{3+1}{2}\right)\Gamma(m+1)}{2\Gamma(m+3)} + \frac{\Gamma\left(\frac{1+1}{2}\right)\Gamma(m+1)}{2\Gamma(m+2)}\right]$$

Inserting and simplifying

$$I = \sum_{m=0}^{\infty} \frac{(-1)^m}{n^m} \frac{a^{2m}}{2} \frac{(m+3)}{(m+2)!}$$

so that we have finally a rather complex expression for the gain ratio

$$\frac{G}{G_0} = \frac{1}{1 + \frac{c^2\pi^2}{\lambda^2}\frac{\overline{\delta^2}}{2}\sum_{n=1}^{\infty}\sum_{m=0}^{\infty}\frac{[\overline{\delta^2}]^{n-1}}{n!\,n}\frac{(-1)^m}{n^m}a^{2m}\frac{(m+3)}{(m+2)!}} \qquad (87)$$

The above formula was used in the preparation of Fig. No. 29 giving the reduction in gain of a parabolic mirror for a given reflector mean deviation. It is possible to obtain simpler formulas than (87) for the limiting cases of small and large correlation intervals.

(a) Small correlation interval, $c/\lambda \ll 1$ - the exponential in eq. (86) is essentially constant and the reduction in gain approaches

$$\frac{G}{G_0} \longrightarrow \frac{1}{1 + \frac{3}{4}\overline{\delta^2}\frac{c^2\pi^2}{\lambda^2}\sum_{n=1}^{\infty}\frac{[\overline{\delta^2}]^{n-1}}{n!\,n}} \qquad (88)$$

Further, for small reflector errors

$$\frac{G}{G_0} \approx 1 - \frac{3}{4}\overline{\delta^2}\frac{c^2\pi^2}{\lambda^2} \qquad (89)$$

(b) Large correlation interval, $c/\lambda \gg 1$ - the exponential dies down rapidly and the integral in (86) can be written as (we need concern ourselves only for

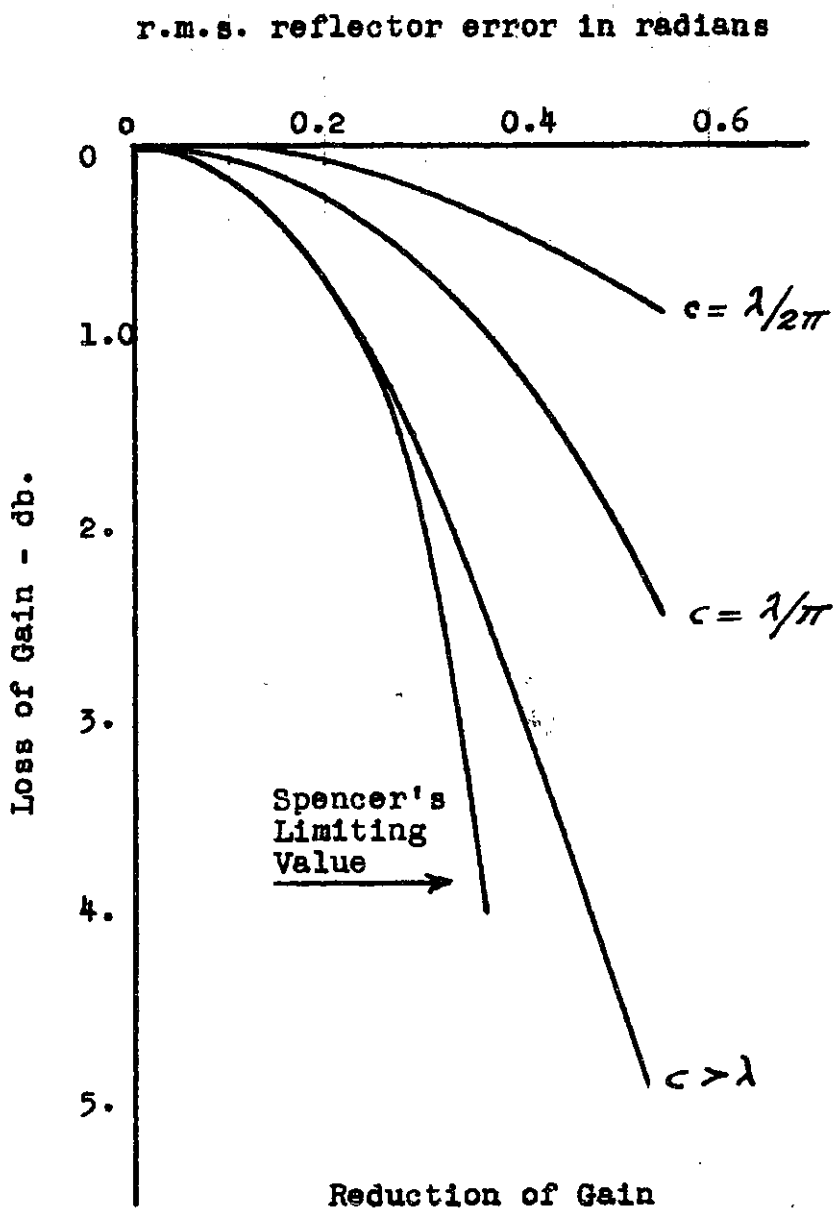

Reduction of Gain
of
Parabolic Mirror

Fig. No. 29

small values of θ as for appreciable values the exponential has vanished)

$$I \cong 2\int_0^{\pi/2} e^{-\pi^2 c^2 \theta / n\lambda^2} \theta\, d\theta \longrightarrow \frac{n\lambda^2}{\pi^2 c^2}$$

Therefore

$$\frac{G}{G_0} \approx \frac{1}{1 + \sum_{n=1}^{\infty} \frac{[\overline{\delta^2}]^n}{n!}} = e^{-\overline{\delta^2}} \qquad (90)$$

and for small reflector errors

$$\frac{G}{G_0} \approx 1 - \overline{\delta^2} \qquad (91)$$

In Fig. No. 29 we have also drawn a curve marked "Spencer's Limiting Value". This is based on an analysis of (Spencer, II) wherein he shows that the fractional loss of gain of an aperture is equal to the mean square phase error weighted according to the excitation amplitude. A similar expression is obtained by (Marechal) in the optical theory of aberrations. These results are derived by means of a much simpler analysis that that presented in this thesis. As the connection is of some interest it will be presented here.

The analysis is not statistical but it may readily be modified for our random error problem. The analysis is essentially based on the on-axis gain formula, eq. (83)

$$G_0 = \frac{4\pi \left| \int J(r)\, dS \right|^2}{\lambda^2 \int J(r)\, J^*(r)\, dS} \tag{83}$$

It is argued that if the distribution possesses a phase error then the gain is

$$G_0 = \frac{4\pi}{\lambda^2} \frac{\left| \int J(r)\, e^{j\cdot \delta(r)}\, dS \right|^2}{\int J(r)\, J^*(r)\, dS} \tag{91}$$

for small phase errors the exponential is expanded so that

$$\frac{G}{G_0} = \frac{\left| \int J(r)\, dS + j \int \delta(r)\, J(r)\, dS - \frac{1}{2} \int \delta^2(r)\, J(r)\, dS + \cdots \right|^2}{\left| \int J(r)\, dS \right|^2}.$$

Desiring only the first order effect we retain the first three terms in the numerator and performing the ensemble average with the mean phase error equal to zero we can write

$$\frac{G}{G_0} = 1 - \frac{1}{2} \frac{\int \overline{\delta^2(r)}\, J(r)\, dS \int J^*(r')\, dS' + \int \overline{\delta^2(r')}\, J^*(r')\, dS' \int J(r)\, dS}{\int J(r)\, dS \int J^*(r')\, dS'}$$

If now the ensemble mean square error is constant over the aperture, this becomes

$$\frac{\overline{G}}{G_0} = 1 - \overline{\delta_0^2}$$

a result identical to our eq. (91).

The question naturally arises why doesn't the correlation interval appear in this analysis. The reason lies in the applicability of eq. (83). This equation is frequently used for the gain of an aperture; however, it is based on the plane wave assumption. As the denominator represents the power transferred by a plane wave it gives the gain only for the limiting case of an aperture large in wavelengths and of uniform phase. When the aperture excitation has errors and thereby departs from a plane wave, then the denominator no longer represents the power transferred through the aperture. If the correlation interval is small this departure becomes marked. We would expect, therefore, that the approximate formula would agree with our analysis for large correlation intervals and small phase errors, as indeed it does.

Before we leave the subject of antenna gain, it is necessary to discuss the distribution of gain of the various members of the ensemble. The loss of gain which we have plotted in Fig. No. 29 is the average loss of a large number of seemingly identical antennas. Particular members will have gains both above and below this value. In fact, due to the strong coherent signal in the main beam direction, the field strength distribution will be asymptotically Gaussian and very closely 50 percent of the antennas will have gains greater than that indicated by Fig. No. 29.

The distributions of the major lobe field intensities will follow the Gaussian limit of the Modified Rayleigh distribution, eq. (47), with

$$a^2 = 1 + \frac{4c^2\pi^2\overline{\delta^2}}{\lambda^2 G_0} \approx 1 \qquad (92)$$

$$\sigma^2 = \frac{4c^2\pi^2\overline{\delta^2}}{\lambda^2 G_0} \qquad (93)$$

where we have used only the first term of the summation in eq. (84), and thereby confined our attention to small errors (a good approximation as the next term adds only 25 percent for an r.m.s. error of one radian). From eq. (47), the characteristics of this Gaussian distribution are $(1, \sigma/\sqrt{2})$.

To illustrate the distribution of gains we employ an example which we shall later use for experimental work. Consider a 30 inch parabolic dish at X-band (3.2 cm. wavelength), with a focal length of 10 inches. This antenna will have a power gain of 3340 or 35.2 db. Let us now randomly distort the reflecting surface so that it has a r.m.s. error of 0.39 radians. The resulting phase front will have an error of 0.78 radians. If the dents of the surface are uncorrelated beyond a wavelength, ($c \approx \lambda$), then from Fig. No. 29 we would expect a loss of 2.75 db.

Knowing the variance we can compute the probability of a given dish lying between given gain limits. With the use of a table of normal probability functions, we have that 68 percent of the dishes will have gain reductions in the interval 2.27 - 3.23 db and 95 percent in the interval 1.81 - 3.69 db.

It is also of interest to compute the probability of obtaining a gain with this battered dish at least as great as a perfect dish. This works out to be the infinitesimal likelihood of 0.15×10^{-8} percent.

The distribution of gains, according to eq. (93), depends on the correlation interval, the mean square error and the normal gain. Curves could be computed for a particular size and estimated machining tolerances. It should be noted that the gain distributions become more peaked as the gain increases and the errors become smaller, so that large dishes with moderate errors would cluster around our mean gain curve, Fig. No. 29, very closely.

7). Basic Assumptions in the Analysis

A number of assumptions have been made in the here developed theory of antenna errors. It is desirable to make them evident. The assumptions naturally stem from our application of statistical theory to our antenna problem. Similar assumptions invariably occur whenever statistics is applied to small sample physical phenomena.

In noting these assumptions, it should be borne in mind that in the application of the theory to an actual antenna it is necessary to make rather rough estimates of the error magnitudes. Our result cannot be better than the estimate of its cause and for this reason we would expect only an order of magnitude accuracy unless special means are taken to determine the error magnitudes.

The discussion is facilitated by again separating the discrete and continuous apertures.

a). Discrete Arrays

To derive our mean pattern eq. (61), it was necessary to assume:

(1) That the relative error was uniformly distributed over the aperture. This does not mean that in a given antenna the error need be the same for each element but merely "on the average". Actually it is probable that the strongly fed elements will have relatively smaller error due to more accurate adjustment and lower mutual effects.

(2) That the error currents were independent from element to element. This will be only approximately the case as we have interaction due to mutual coupling and internal circuitry. Furthermore, the cause of the error may be of a type wherein it affects several elements, for example, plate spacing error in a metal plate lens.

(3) That the phase error was distributed in a Gaussian manner. This will be approximately true for small errors on the basis of the Central Limit Theorem. This assumption was necessary to evaluate integral (56). Actually any distribution could have been assumed and the integral evaluated by graphical means.

It should be noted that taking the errors to have zero mean is really not an assumption as the non-mean error really forms a part of the "predictable" error problem, as such errors exist in the average ensemble antenna.

To apply our Modified Rayleigh distribution, it is necessary to assume that our error vectors have all directions equally likely and that there are a large number of elements. This condition is fulfilled for large arrays and in the side lobe region of the antenna pattern where the component vectors have spiraled around many times.

b). Continuous Aperture

The derivation of the mean pattern, eq. (84), required the assumption:

(1) That the errors be uniformly distributed over the aperture. In this connection it should be noted that if the aperture errors are caused by a shaped reflector such as a parabolic morror, the distribution of phase errors is no longer uniform unless larger distortions exist around the edges which contribute smaller phase errors. This effect is small for shallow reflectors and can be taken care of very closely by using a smaller r.m.s. error when the reflector has uniform tolerance. This uniform error assumption was necessary in order to neglect the vector character of $\mathcal{T}$ and the dependence of the mean square error, $\overline{\delta^2}$, on relative position in the aperture, both in eq. (73).

(2) That the various correlated error regions in the aperture are independent. Although we have taken care of the fact that error correlation exists in the immediate neighborhood we still assume that independence exists among the correlated regions themselves. This assumption is necessary to perform the averaging process indicated by eq. (72).

(3) That the phase error was distributed in a Gaussian manner and that the mean square phase correlation is expressed by the functional form (73). Actually any form could have been chosen if we resorted to graphical integration. However, the form chosen is reasonable. This assumption is identical to that made in turbulence or radio scattering theory as to the shape of the correlation curve. Actually, as we shall see, in subsection 8c, this assumption has considerable theoretical justification.

(4) That the size of the error correlated region is small compared to the average distance on the aperture over which we have an appreciable change in illumination. This assumption was necessary to extract the aperture illumination auto-correlation function from behind the integral (77). The assumption is well justified for moderate or large apertures with slowly varying illumination tapers where the aperture size is large compared to the correlation interval.

There further exists a physical limitation to the application of our analysis to correlation intervals which are much smaller than a wavelength. This is not really an assumption as the formal mathematics leading to eq. (84) is valid for any value of "c" and the final result would be valid if the aperture currents actually were in error over this small correlation interval. However, a small correlation region indicates a rapid spatial variation of field. In our parabolic application we are inherently assuming that the correlation interval is not much smaller than a wavelength as we are using

the geometrical optical approximation that the reflector surface current is equal in magnitude to the tangential magnetic field impinging from the feed. The geometrical optical approximation implies that the radii of curvation of the equiphase surfaces are large compared to a wavelength (Silver, pg. 116).

8). Experimental Verification

The verification of a statistical theory involves some difficulty as, in general, a large number of samples must be examined. In this problem, we are faced further with the fact that many-element antennas, to which the theory applies, are expensive and, furthermore, the determination of the actual antenna currents with sufficient accuracy for theoretical verification is a difficult task.

Realizing the need of some experimental justification, the author proceeded: firstly, to examine an already constructed antenna, estimate its errors and predict its performance on the basis of this thesis and compare this prediction with the experimental polar diagram; and secondly, to eliminate the necessary estimates in the first procedure, to construct an antenna with a built-in "random" error and measure its performance, in comparison to a "no-error" antenna. As an almost perfect "no-error" antenna is necessary, a parabolic mirror was chosen for this purpose. The introduced "random" error was made large enough to cause a measurable effect.

a). Evaluation of 25 Element Broadside Array*

The U. S. Air Force Cambridge Research Center has constructed and tested a 25 element broadside array. Provisions are incorporated for slewing the beam by means of phasing rings. The technique is identical to that described by (Bacon) and illustrated by Fig. No. 30. The beam direction is determined by the position of the phasing arm. The diameters of the various rings are proportional to the distance of the corresponding elements from the center of the array. The antenna is fed so that the various elements have a Tschbyscheff - Dolph taper to yield a side lobe suppression of 29 db. The theoretical pattern is that shown in Fig. No. 18.

A broadside array of this type has a number of possibilities of error:

(1) Mutual effect between elements, which occurs by two means; namely, by coupling between dipole elements and by coupling between phasing rings. The currents induced in an element when the adjacent one is excited were measured by the author. These measurements indicated a 10 percent excitation due to the element coupling and a 5 percent excitation between adjacent rings. Smaller couplings existed between more distant elements. Although this is actually a "predictable" error, its determination for a given phasing ring arm position is a hopeless task, especially when we consider 25 elements and

* Security restrictions prohibit giving detail information on this equipment and its purpose.

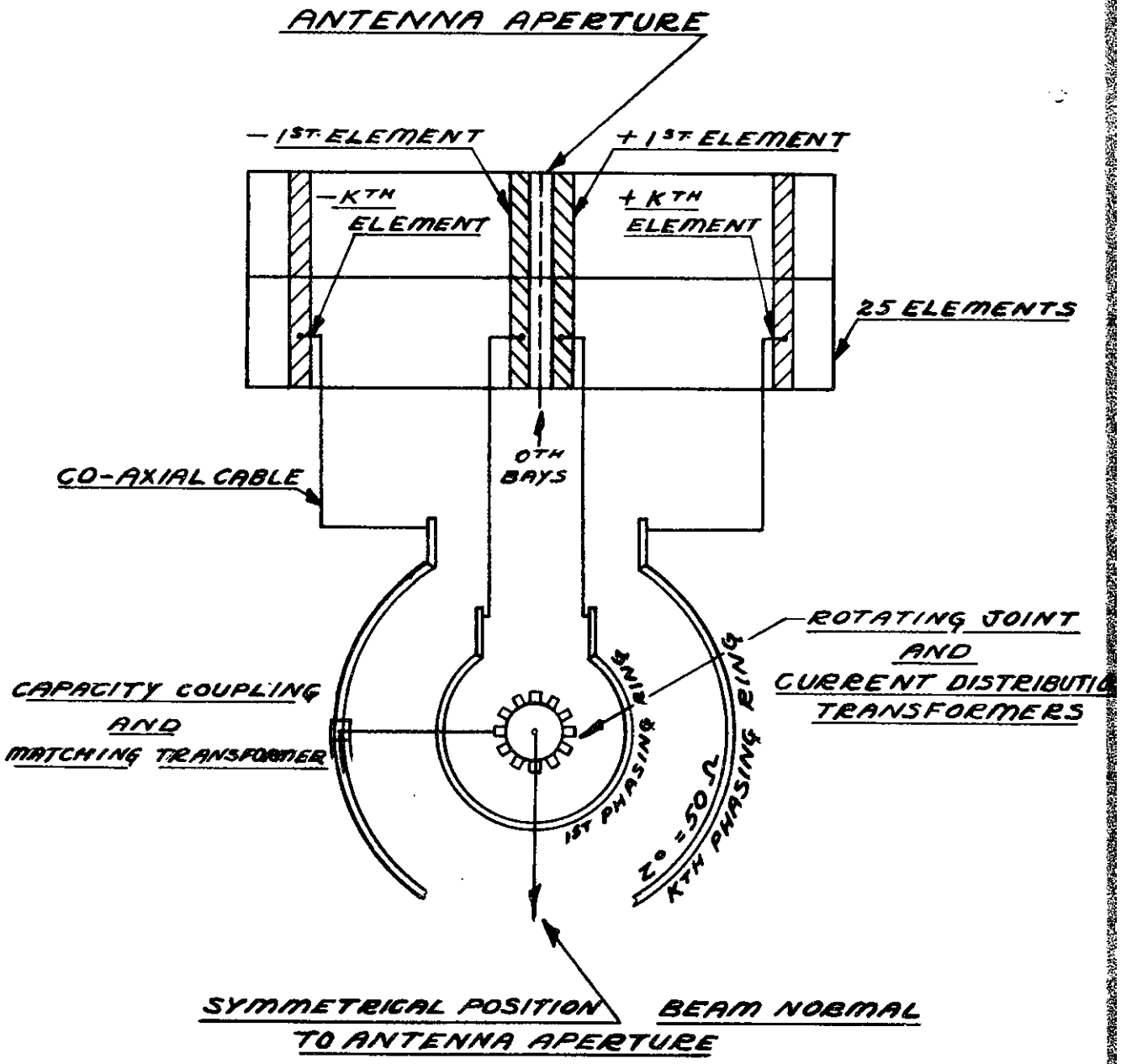
ANTENNA APERTURE
— 1ST. ELEMENT
+ 1ST. ELEMENT
— KTH ELEMENT
+ KTH ELEMENT
25 ELEMENTS
0TH BAYS
CO-AXIAL CABLE
ROTATING JOINT AND CURRENT DISTRIBUTIO TRANSFORMERS
CAPACITY COUPLING AND MATCHING TRANSFORMER
1ST PHASING RING
KTH PHASING RING
Z0 = 50 Ω
SYMMETRICAL POSITION TO ANTENNA APERTURE
BEAM NORMAL

Fig. No. 30

12 phasing rings whose mutual couplings depend not on free space conditions but on a resonant supporting framework. In statistical analysis, where we are interested in order of magnitude, we may take this error as equal to a mean deviation of the order of 10 percent.

(2) Pure phase errors occur at a number of places in the system. The various elements are connected by means of solid dielectric cable. It was found that such cable with attached connector could not be cut and assembled to better than two electrical degrees. Considering shop production, temperature changes and aging, and the use of a number of cable elements in series, it is felt that 6 degrees is not an excessive estimate for this cable length error. Another 6 degrees can be added due to machining and assembly errors in the phasing rings and various matching transformers.

(3) The operation of the current distribution and phasing arrangement, Fig. No. 30, depends on maintaining matched conditions in the entire system. Standing waves will alter the distribution of power. In addition, since the phase shift of a mismatched line is not equal to its electrical length, standing waves will create phase errors. The situation is especially complex as the phasing arm, during the scanning operation, feeds the different elements at different impedance levels depending on the relative standing wave positions on the phasing rings. This error in matching is essentially a random error as the various components were designed to be matched and they are connected by cables which are of

unequal length due to the necessity of making up the required electrical distance lost by the smaller diameter rings. Impedance measurements indicated an average VSWR of 1.25. Element impedance, connector discontinuity, phasing ring characteristic impedance variation, and impedance transformer errors contribute to this figure. This mismatch will cause approximately a 25 percent current error.

(4) R.F. measurement errors occur in the design of each component. It is estimated that such errors are equivalent to a current error of 15 percent. This figure may at first seem high as only relative measurements are made and these with skilled personnel. However, we are dealing with r.f. measurements where, with the presence of stray currents, it is a question of exactly "what" we measure.

The individual errors, being incoherent, are not summed directly but as their squares, with the result that the actual antenna currents are in error with a mean deviation of about 37 percent. Fig. No. 17 indicates that for a r.m.s. error of 0.37 we would expect a side lobe level of about 18 db for 84 percent of the time and occasionally lobes as high as 16 db. Various spatial directions, different scan angles and different frequencies in the operating band serve as statistical samples. Actual pattern measurement verified this prediction.

The practical result of this application is that the original equipment specification of 29 db was unrealistic. Furthermore, as the side lobe level was determined by the

current errors and not the current distribution, there was no advantage in using so heavy a taper. A more efficient utilization of the antenna aperture would have resulted if only a 20 db Tschbyscheff taper had been used.

b). Slot Array Work at Hughes Aircraft Co.

The author presented the material in subsection 5 at the National Convention of the Institute of Radio Engineers in New York in March 1951. The material aroused some interest as low side lobe antennas are required for many applications and this paper presented a physical limitation imposed by the accuracy of the techniques employed. It developed that the engineers of the Hughes Aircraft Company have been thinking along similar lines. In particular, they were concerned about the effects of machining tolerance on microwave slot arrays. They considered only small errors in discrete arrays and their theory is the Gaussian limiting case of this more general analysis. The Hughes Company constructed a number of arrays with a machining tolerance of 0.002". Their report (Bailin and Ehrlich) indicates agreement with the theory.

As the effect of errors on a slot array can be readily computed, it is worthwhile to determine the side lobe level for a given machining tolerance. Considering as the major sources of error: (1) the variation in the amplitude of excitation due to randomness in the transverse displacement of the slot "x", (2) the variation in phase due to randomness in the longitudinal distance "d", (3) the variation in phase due to randomness in slot length "l". Mutual effects and wall spacing errors are neglected.

Considering these errors in order:

(1) A change in the transverse position of the slot will cause an amplitude change due to a change in slot excitation. (Stevenson) has shown that the conductance of a slot in the broad face of a rectangular guide is

$$G = 2.09 \frac{\lambda_g}{\lambda} \frac{a}{b} \cos^2\left(\frac{\pi \lambda_0}{2\lambda_g}\right) \sin^2\left(\frac{\pi x}{a}\right) \qquad (94)$$

The radiated power is proportional to GV^2 and consequently the radiated field to G. The relative change in field due to a change in "x" may be written

$$\frac{\Delta\sqrt{G}}{\sqrt{G}} = \frac{\frac{\pi}{a}\cos\frac{\pi x}{a}\,\Delta x}{\sin\frac{\pi x}{a}} = \frac{\pi}{2}\cot\frac{\pi x}{a}\,\Delta x \qquad (95)$$

The mean square amplitude error becomes

$$\sigma_x^2\left(\frac{\pi}{2}\right)^2 \cot^2\frac{\pi x}{a} \qquad (96)$$

(2) The phase of the contribution from an element a distance "d" may be written (see Fig. No. 31)

$$\phi_d = \frac{2\pi d}{\lambda_0}\sin\theta - \frac{2\pi d}{\lambda_g} \qquad (97)$$

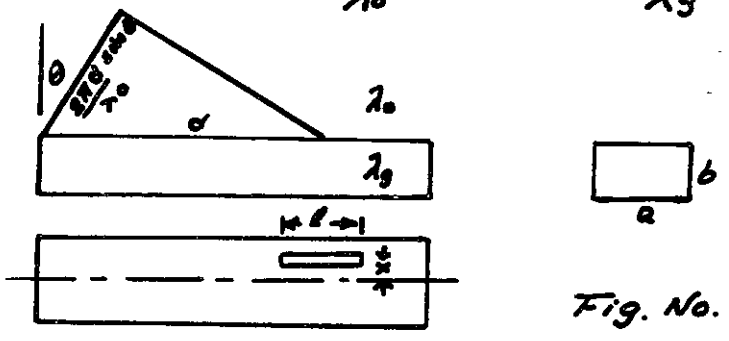

Fig. No. 31

Making the assumption that the slot spacing is not measured serially and, consequently, the errors in spacing do not accumulate, the mean square phase error is

$$\overline{\delta^2} = (2\pi)^2 \left[\frac{\sin\theta}{\lambda_0} - \frac{1}{\lambda_g} \right]^2 \sigma_d^2 \qquad (98).$$

(3) An error in the length of the slot will alter the phase of the field radiated from it. This effect can most readily be determined by measurement of the phase change. Such data is shown in Fig. No. 32. This curve can be approximated for small errors by

$$\phi_e = 4.55\pi \frac{\Delta \ell}{\ell} \text{ radians} \qquad (99).$$

with the resulting mean square error of

$$\overline{\phi_e^2} = (4.55\pi)^2 \overline{\left(\frac{\Delta \ell}{\ell}\right)^2} \qquad (100).$$

The error contribution represented by (96), (98), (100) are assumed independent so that their square values may be added. Their relative magnitudes are computed for X-band guide as 1.15, 1.18 and 54.3 respectively, bringing us to the conclusion that tolerance on slot length is most critical. Fig. No. 33 gives the predicted performance of a 25 element slot array as a function of machining tolerance.

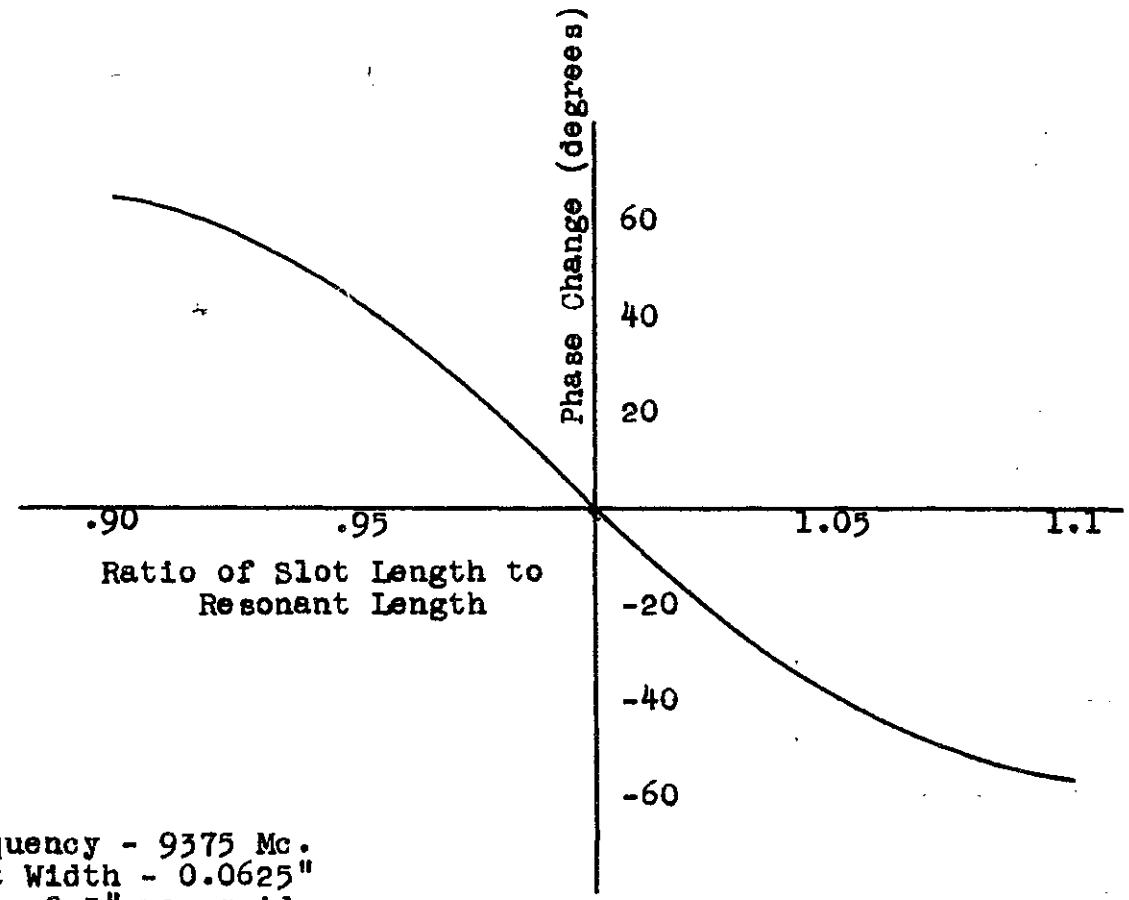

Frequency - 9375 Mc.
Slot Width - 0.0625"
1.0 x 0.5" wavequide
Resonant slot length - 0.617"

Experimental Data
Hughes Aircraft Co.,

Fig. No. 32

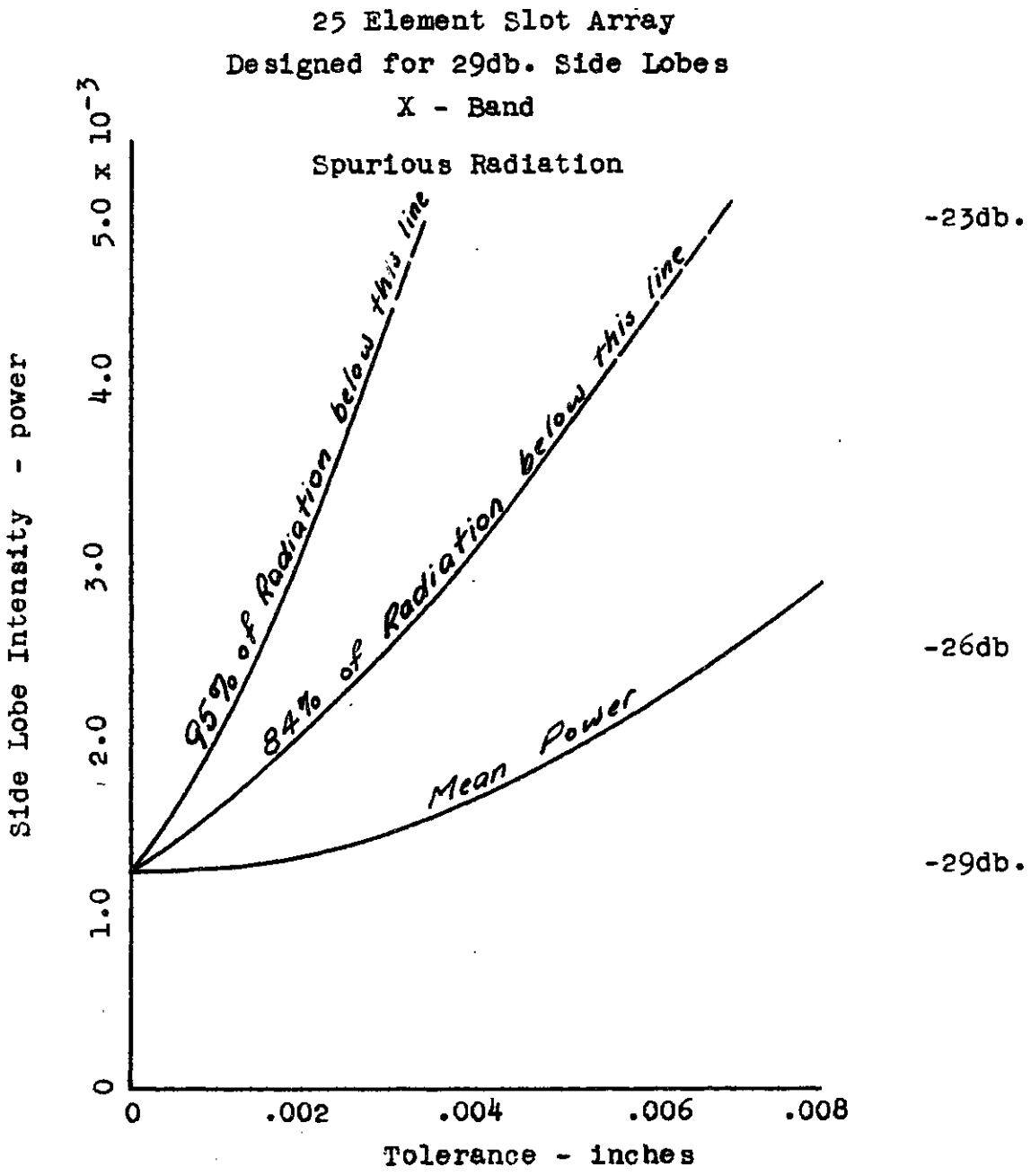
25 Element Slot Array
Designed for 29db. Side Lobes
X - Band
Spurious Radiation
Side Lobe Intensity - power
5.0 x 10⁻³
4.0
3.0
2.0
1.0
0
95% of Radiation below this line
84% of Radiation below this line
Mean Power
-23db.
-26db
-29db.
0
.002
.004
.006
.008
Tolerance - inches

Fig. No. 33

c). Distorted Parabolic Mirror

Although our theoretical analysis was useful in predicting the performance of the broadside and slot arrays, it cannot be considered as an experimental check of the theory. In the first case we made estimates of the various errors and in the slot array the assumption was made that an 0.002" machine shop tolerance actually resulted in the array. In neither case can we state with definiteness what the error is and how it is distributed.

To provide a more convincing check it was decided to take two commercial parabolic mirrors, distort one in a "random" and prescribed manner consistent with the theoretical assumptions and compare its performance with the undistorted mirror. Deliberate distortion was resorted to, instead of using a poorly made dish or one that was battered in use, due to the difficulty of accurately measuring the mechanical deviations of the reflector surface. Comparatively large distortions were used so that a measurable effect could be observed.

The dish chosen was a 30" diameter, 10" focal length paraboloid fed by a double dipole waveguide feed (Sichak). The frequency used was 9380 Mc (3.2 cm). The experimental work was performed at the Ipswich Field Station of the Air Force Cambridge Research Center. This antenna measuring installation was originally set up by the Radiation Laboratory at M.I.T. and is described in (Hiatt).

In order to find the necessary distortions, we consider an indentation on the parabolic surface of the form

$$\sigma = k e^{-r^2/m^2} \tag{101}$$

Such an indentation is characterized by the constants (k,m) and will create a phase front error of approximately

$$\delta(r) = 2k e^{-r^2/m^2} \tag{102}$$

Our analysis requires knowledge of the mean square of "y", eq. (74)

$$y(r,\tau) = \delta(r) - \delta(r+\tau) = 2k\left[e^{-r^2/m^2} - e^{-(r+\tau)^2/m^2}\right]$$

forming the mean square

$$\overline{y^2(\tau)} = \int_{-\infty}^{\infty} \left[\delta(r) - \delta(r+\tau)\right]^2 dr$$

Substituting and performing the integration

$$\overline{y^2(\tau)} = k^2\sqrt{2\pi}\, m\left[1 - e^{-\tau^2/2m^2}\right] \tag{103}$$

Comparing with eq. (73) we see that the constant "m" is related to the correlation interval by

$$2m^2 = c^2 \tag{104}$$

We have yet to find the mean square indentation. If the indentation, eq. (101) extends over the area "S", then the mean square indentation is

$$\overline{\sigma^2} = \frac{K^2}{S}\int_S e^{-4r^2/c^2}\, r\,dr\,d\theta \qquad (105)$$

As the indentations are well separated so that there is negligible overlap, the integration may be extended to infinity with little error and

$$\overline{\sigma^2} \simeq \pi \frac{K^2}{S}\frac{c^2}{4} \qquad (106)$$

If we now consider "N" such indentations and if these indentations are independent with values of indentation depth "k_n" coming from some population, we have

$$\overline{\sigma^2} = \frac{\pi c^2}{4S}\frac{1}{N}\sum^{N} K_n^2 = \frac{\pi c^2}{4S}\overline{K^2} \qquad (107)$$

We are now in a position to design our "randomly" distorted reflector. If we make our r.m.s. reflector deviation, $\sqrt{\overline{\sigma^2}}$, equal to 0.39 radians and our correlation interval equal to a wavelength, we have from Fig. No. 29 a mean reduction of gain of 2.75 db. If further we space our indentations on centers 4" apart, we compute that the mean indentation depth is 0.282" at x-band. The various independent indentation depths may be chosen from a Gaussian population. Table III in (Morse) may be used for this purpose with the result for a set of

indentations in inches:

.225	-.195	.107	.037	.488
-.152	-.059	-.169	-.450	-.169
.118	.470	.189	.017	.386
-.135	-.320	.141	-.054	.333
.045	-.172	.208	.327	.105

The values of the above table are still to be corrected for the effect of the reflector curvature, that is a given reflector error will cause a smaller phase error when this reflector deviation is located at the reflector edge than in the center. The correction formula is given by (Cutler, eq. 5) as

$$\frac{2}{1+\cos\theta} \qquad (108)$$

where θ is the angle between the reflector axis and the reflector indentation. This correction amounts to 50 percent at the reflector edge.

The reflector was distorted by forcing into the parabolic surface a metal die shaped according to eq. (101). The depth of penetration was adjusted according to the above table corrected by eq. (108). The completed reflector is shown in Fig. No. 34, with the indentation depths marked in inches. This reflector fulfills our conditions that a) the errors are "on the average" uniformly distributed over the aperture, b) the mean square phase error is such as to cause a mean loss of gain of 2.75 db, c) the correlation interval is one wavelength.

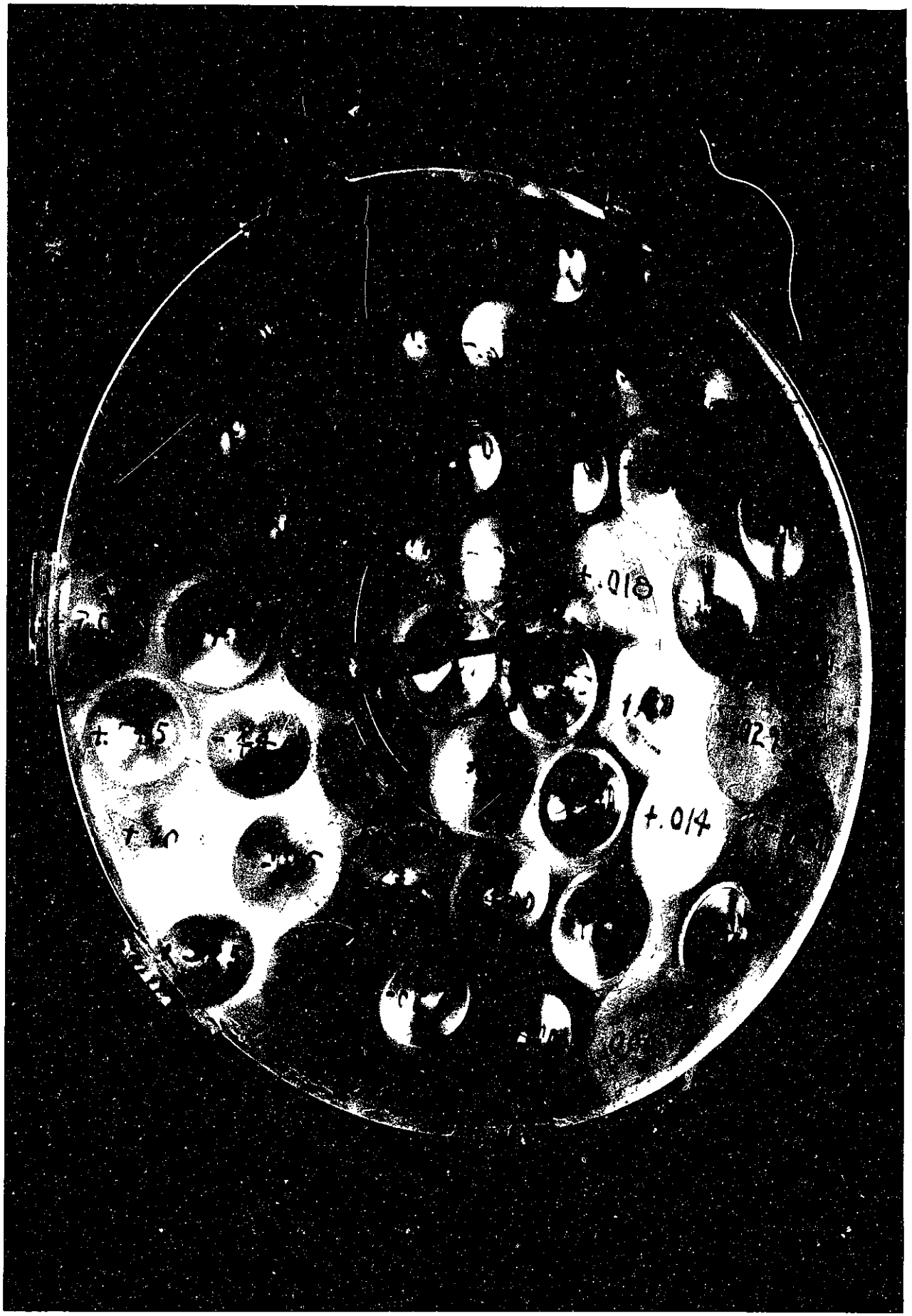
+.018
+.014

d) the individual indentations are independent, e) the phase errors come from a Gaussian population.

Before discussing the experimental results it should be pointed out that the shape of the mean square phase difference between two points a distance τ apart, eq. (103) which here resulted as we have chosen a Gaussian indentation would have occurred asymptotically for any shaped indentation, provided that the number of such indentations are large. This follows as we are actually interested in the phase difference averaged over the aperture and over a number of seemingly identical antennas and as this is an additive process, the Central Limit Theorem therefore applies. Hence considerable theoretical justification exists for the choice of the functional form eq. (73) (see also subsection on assumptions, 7(b)(3)).

To evaluate the theory, the gain of the battered dish was first compared with a "perfect" dish. Fig. No. 35 shows the comparative pattern, indicating a loss of gain of 2.5 db. As our statistics indicate that 68 percent of such distorted dishes should lie between 2.27 and 3.23 db our theoretical predictions are verified. This verification is all the more startling when photograph Fig. No. 34 is examined. In several places the reflector error is sufficient to cause an aperture phase error of almost a complete wavelength. This large error is permitted, in a few places, by our Gaussian distribution of indentations and in that we are interested only in the mean square error. As it is common in the industry to specify reflector tolerance to one thirty secondth of a wavelength the

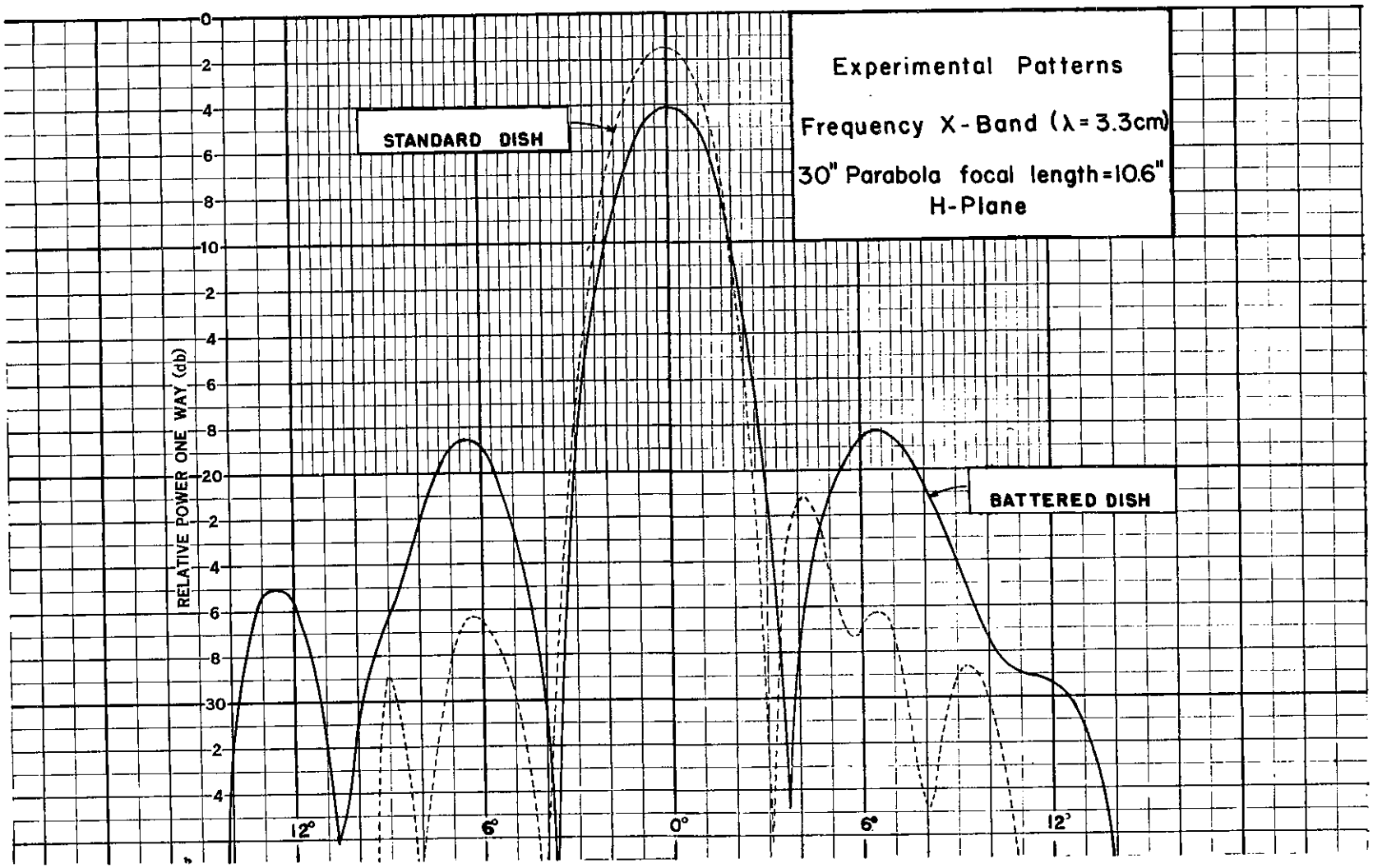
Experimental Patterns
Frequency X-Band (λ = 3.3cm)
30" Parabola focal length = 10.6"
H-Plane
STANDARD DISH
BATTERED DISH
RELATIVE POWER ONE WAY (db)
0
2
4
6
8
10
20
30
12°
6°
0°
6°
12°

Figure No. 35

performance of this excessively distorted reflector was suprising to antenna engineers.

Other characteristics of interest are: 1) the angular distribution of the side lobes, and 2) the distribution of magnitudes of the minor lobes. To check this with the theory a number of such battered dishes would have to be examined. To avoid this expense, patterns were taken only on a single dish. However, for each pattern the dish was rotated 15^{o} so that 11 different patterns were taken. These experimental patterns are superimposed in Fig. No. 36. In this figure, we also show the theoretical no-error pattern, the mean ensemble power pattern and the statistical patterns that indicate the probability that the experimental patterns lie 84 percent, 95 percent and 99 percent below these lines. The mean power pattern is equivalent to roughly a 60 percent probability line (see Fig. No. 12).

The data of Fig. No. 36 may be interpreted as follows:

(1) The angular distribution of the side lobe magnitudes follows the theoretical predictions rather well.

(2) Higher side lobes are present than would be indicated by the statistical theory - that is more patterns are found between the 99 percent and the 84 percent lines than 15 percent of the eleven polar diagrams recorded. This can be explained by the fact that we are basing our prediction on the theoretical antenna pattern. Even a "perfect" dish does not follow the theoretical pattern exactly, as Fig. No. 35 indicates. In general it is found that experimental side lobes

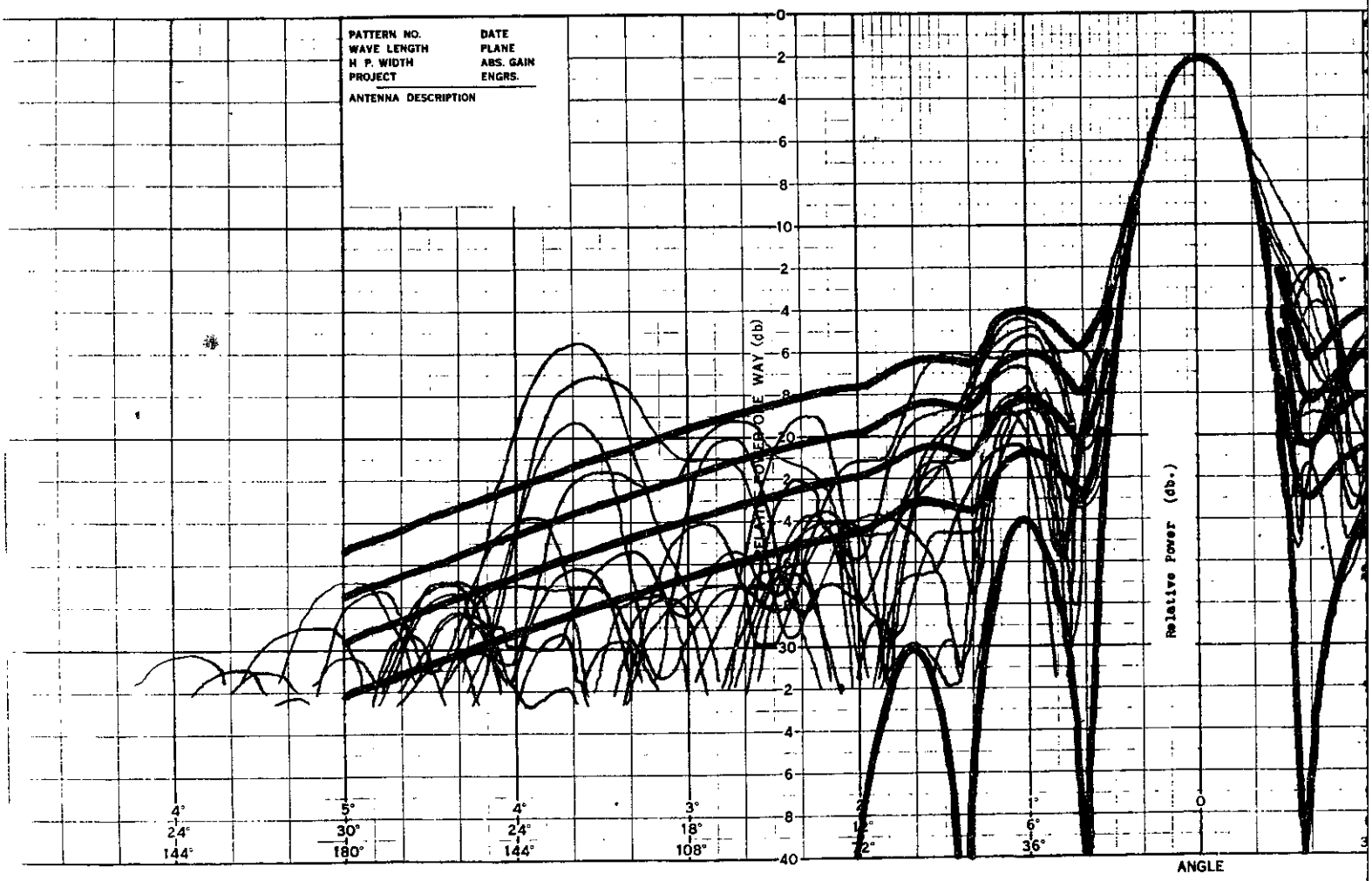
PATTERN NO.
WAVE LENGTH
H P. WIDTH
PROJECT
DATE
PLANE
ABS. GAIN
ENGRS.
ANTENNA DESCRIPTION
Relative Power (db.)
ANGLE
4°
24°
144°
5°
30°
180°
4°
24°
144°
3°
18°
108°
2°
12°
72°
1°
6°
36°
0

Fig. No. 36

Comparison of Experimental Patterns with Theoretical Predictions

of a

30" Parabolic Dish

focal length - 10.5" X - Band (3.2cm = λ)
double dipole feed H - Plane
r.m.s. reflector error - 0.39 radians (0.282")
correlation interval - one wavelength

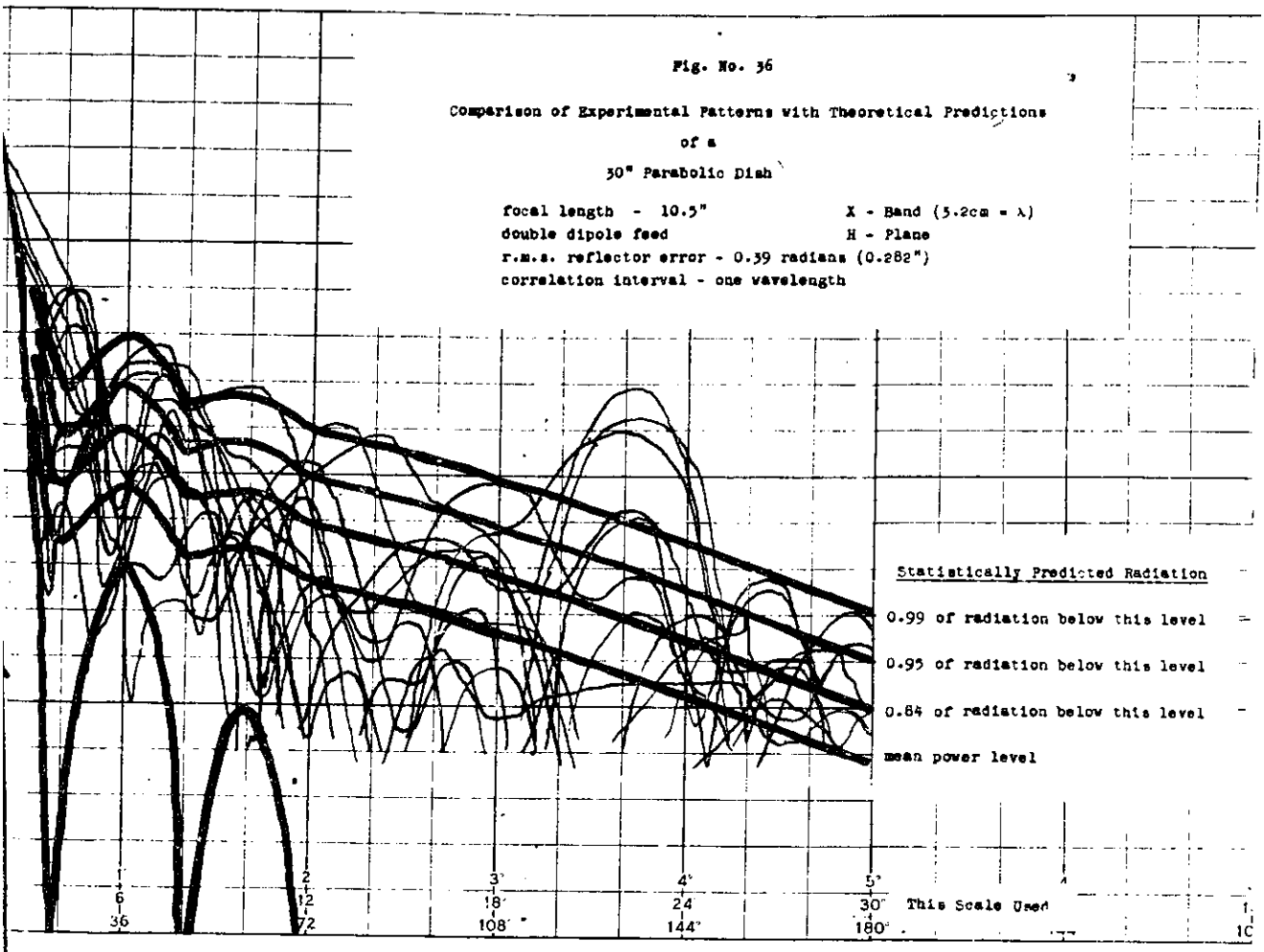

are unequal and higher than theoretical. By jockeying the feed, pattern symmetry frequently may be restored. This behavior of good dishes is due to a number of causes, such as: a) A non-spherical and an unsymmetrical primary pattern of the feed; b) Stray currents on the feed supporting structure; c) Field interaction between the feed and the dish; d) Secondary aperture blocking by the field structure; e) Direct radiation from the primary feed. In view of these neglected effects, it is not surprising that our distribution is shifted upward. However, we can say roughly that the agreement with our statistical theory, obtained with the battered dish, is as good as that normally obtained for so'called "good" dishes by the plane aperture calculations.

(3) In the vicinity of 22° off the major lobe, there exists a violent disagreement with statistical predictions in that spurious radiation is found, for some patterns, 6 db higher than expected by the 99 percent line. Actually 5 of the 11 patterns are in the region where only 1 percent is permitted. This at first appears as a violation of our statistical analysis. However, a little consideration reveals the cause of these lobes. Our battered reflector was constructed with indentations of random depth spaced 4 inches on centers. This introduced a periodic error whose fundamental period is 4 inches. This period will be in every member of the ensemble although its mean is zero. Referring to our subsection II. 3. on the effect of periodic errors, we note that such errors will generate lobes in the directions

$u = \pm n/d$. Converting our 4 inch period into wavelengths and computing this lobe position, we find that we would expect stronger radiation at 23°, 39° and 72°. This validates our statistical analysis and reveals the hidden periodicity we have invertently built into our battered dish.

9). Application of Similar Techniques to Other Fields

The statistical technique applied in this section to the antenna problem has been used for the investigation of the scattering of electromagnetic waves from randomly located scatterers such as a rough sea or a turbulent ionosphere. It has been mentioned that it also may be applied to the determination of the voltage standing wave ratio on a transmission line with randomly located discontinuities. Two other applications suggest themselves and are mentioned below.

a). Application to the Theory of Aberrations of Optical Instruments

The analysis which was presented relates the effect of the aperture distribution errors on the far field. This distribution and the far field are related by the Fourier Transform pair (eq. No. 9)

$$g(u) = \int_{-w}^{w} f(x)\, e^{j 2\pi u x}\, dx$$

$$f(x) = \int_{-\infty}^{\infty} g(u)\, e^{-j 2\pi u x}\, dx$$

The problem may be inverted and we inquire about the behavior of a converging wavefront (Fig. No. 37).

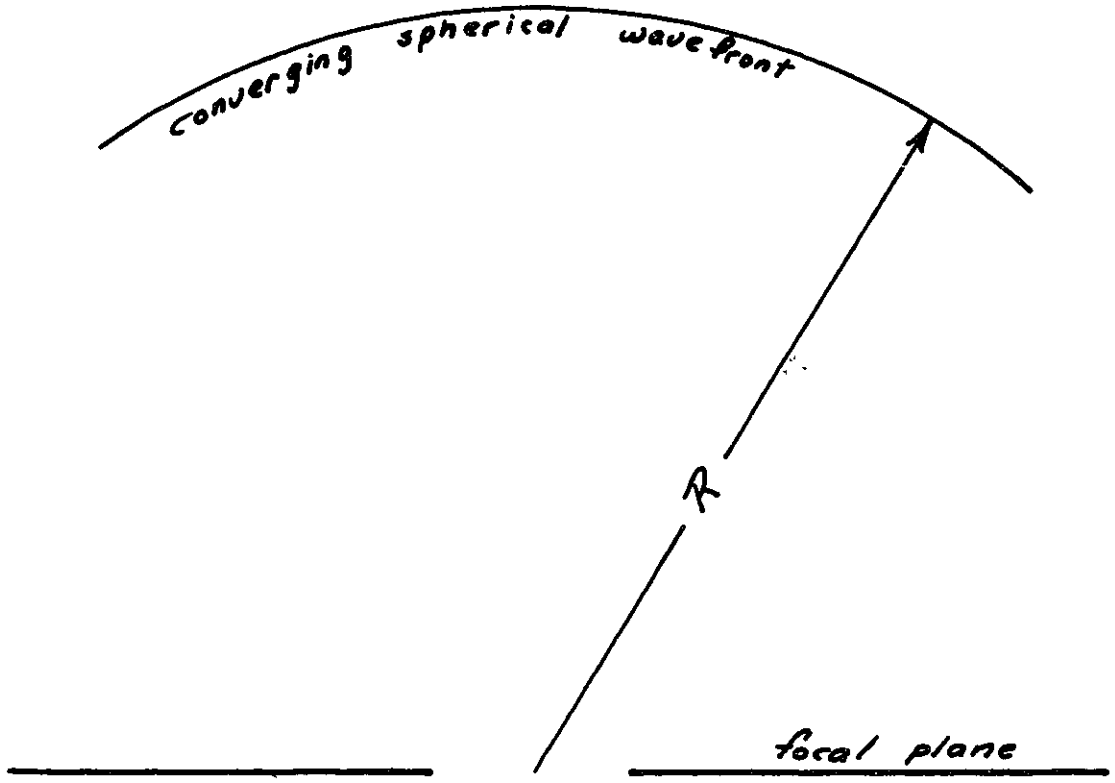

Fig. No. 37

Consider such a system of rays as would be formed by an optical instrument. It is well known in optical theory that a converging wavefront does not focus to a point but that the intensity distribution in the focal plane is given by the Fourier Transform pair above. In particular, if the converging wavefront is spherical and of uniform phase, the focal plane distribution is identical in functional form to the

polar diagram of a uniformly illuminated circular aperture, that is, roughly a (sin x)/x function or strictly a $J_1(x)/x$ relationship (Silver, pg. 194). This focal plane intensity distribution is termed an Airy disc (Born, pg. 195).

The converging wavefront is normally formed by a system of lenses. These lenses are subject to mechanical tolerances which lead to optical errors of a form that the phase front is not spherical but has phase errors. As we are dealing here with identical functional forms, the statistical analysis developed can be applied directly to the optical aberrations.

Unfortunately our analysis contributes little, except academic interest, to the optical problem; for there we are dealing with correlation intervals of many wavelengths where Spencer's Limiting Value applies and (Marechal's) theory of optical aberrations is sufficient.

b). Application to Electrical Filters

Electrical filters are generally designed for very low transmission in the attenuation band. The question arises as to what occurs to their performance when they are constructed, especially with inexpensive components. This again resolves itself into a statistical problem. The effect of circuit parameter deviations from the design value can be taken care of, to the first approximation, by the compensation theorem. At the filter output there will arise, in addition to the predicted output, a random and independent sum of voltages depending on the parameter tolerance and on the position

of the circuit element in question in the circuit.

The question arises, similarly, as in the antenna problem, as to what tolerances are required for a given attenuation and conversely for a prescribed attenuation how precise must our circuit components be? In addition, we query: "What types of circuits are least susceptible to component error"? It is believed that the type of analysis presented in this section may prove useful in this connection.

III. LIMITATIONS IMPOSED BY THE SYNTHESIS PROCEDURE

As stated in the introduction, the synthesis problem is one wherein we are given the shape of the polar diagram and we are required to find an aperture illumination of finite width, whose radiation pattern approximates the desired one, under some condition of optimization.

As we are primarily interested in synthesis methods and not in integration difficulties, we will restrict our discussion to antenna current distributions which are separable, that is, in eq. (1b) and (2b)

$$J_x(x,y) = J_x(x)\, J_x(y)$$

and to the principal planes, $\phi = 0$ or $\phi = 90^\circ$. Under these conditions, eq. (1b) or (2b), for a plane aperture, reduce to the form

$$g_1(u) = \int_{-W}^{W} f(x)\, e^{j 2\pi u x}\, dx \qquad (109).$$

and for a discrete array of $(2N + 1)$ equispaced elements we have

$$g_2(u) = \sum_{-N}^{N} I_n\, e^{j 2\pi n d u} \qquad (110).$$

where we have written $u = \sin\theta$ and "x" and "d" are measured in wavelengths; g(u) is the polar diagram and f(x) the continuous

and I_n is the discrete current distribution. We have made no assumption in neglecting any obliquity or screen factors as these can always be taken care of in our synthesis procedure by considering as the desired polar diagram the given pattern divided by any such obliquity factors.

In a practical problem we must deal with "restricted" apertures, that is, apertures of finite length. If further, we require that the antenna be a low "Q" device or one with a low ratio of reactive to radiated power, then certain restrictions are imposed upon the spatial variation of the current distribution. These restrictions will be made evident in Section IV of this thesis. As only certain functional forms of the current distribution will turn out to be permitted by our reactive power consideration, we can only approximate the desired polar diagram. The question discussed in this section is how to obtain this current distribution and what is the nature of the approximation.

We begin by introducing the two standard methods of antenna pattern synthesis, namely, 1) the Fourier-Series and Fourier-Integral method, and 2) the Woodyard-Levinson method. Then we discuss the nature of the approximation problem, particularly approximation in the Gaussian and the Tschbyscheff sense. Finally we introduce two methods of synthesis yielding an approximation optimum in an approximate Tschbyscheff manner.

1). Fourier Series and Fourier Integral Method

The Fourier Series synthesis procedure was probably first introduced into antenna array work by (Wolff). This method follows immediately upon recognition that the expression (110), for a discrete array, is a finite trigonometric series. As the function $g_2(u)$ is periodic in "u", the various current coefficients I_n can be obtained by Fourier decomposition, giving

$$I_n = \int_{1/d} g_2(u) e^{-2\pi d n u} du. \qquad (111)$$

where the integration is to be extended over the period "1/d". In eq. (110) we have dropped a constant factor. We shall neglect such constants in what follows as we are only interested in normalized polar diagrams and relative current distributions.

If now we are given an arbitrary function $g_0(u)$, specified in the interval $-1 < u < +1$, we can extend it periodically over the entire u-space. In general, for exact synthesis we would require an infinite trigonometric series. Since we are restricted to (2N+1) elements, we obtain only an approximation as we can only use (2N+1) terms. The excitation coefficients, however, are still given by

$$I_n = \int_{1/d} g_0(u) e^{-2\pi d n u} du \qquad (111a).$$

The approximating pattern $g_a(u)$ is given by (110) as

$$g_a(u) = \sum_{-N}^{N} \int_{1/d} g_o(u') e^{j2\pi d n (u-u')} du'$$

interchanging order of summation and integration

$$g_a(u) = \int g_o(u') \left[1 + 2 \sum_{1}^{N} \cos 2\pi n d (u-u') \right] du'$$

the bracketed term is equivalent to (Jackson, pg. 17)

$$1 + 2 \sum_{1}^{N} \cos 2\pi n d (u-u') = \frac{\sin (2N+1) d\pi (u-u')}{\sin \pi d (u-u')}$$

so that we can express the approximation pattern in terms of the desired pattern as

$$g_a(u) = \int_{1/d} g_o(u') \frac{\sin (2N+1) \pi d (u-u')}{(2N+1) \sin \pi d (u-u')} du'$$

If we had considered an even array instead of an odd array, we would have a similar expression so that we write for an array of any number of elements "M"

$$g_a(u) = \int_{1/d} g_o(u') \frac{\sin M \pi d (u-u')}{M \sin \pi d (u-u')} du' \qquad (112)$$

During the war years synthesis procedures were necessary for microwave aperture antennas. The discrete analysis of Wolff was extended to the continuous case (Ramsey) (Spencer, 3).

This extension follows from (109) as f(x) = 0 for $|x| > W$ and the integral can be extended to infinity. The Fourier Integral theorem may be applied and we obtain the Fourier Transform pair

$$\left.\begin{aligned} g(u) &= \int_{-\infty}^{\infty} f(x)\, e^{j 2\pi x u}\, dx \\ f(x) &= \int_{-\infty}^{\infty} g(u)\, e^{-j 2\pi x u}\, du \end{aligned}\right\} \quad (113)$$

so that given a required g(u) we can find the necessary f(x). However, this so determined f(x) will not, in general, be restricted to an aperture width of "2W". With this restricted aperture we will only obtain an approximation given by

$$g_a(u) = \int_{-W}^{W}\int_{-\infty}^{\infty} g_o(u')\, e^{j 2\pi x (u-u')}\, du'\, dx$$

The order of integration can be interchanged and that respective to the aperture performed. The result, similar to eq. (112) for the discrete case, is given by

$$g_a(u) = 2W \int_{-\infty}^{\infty} g_o(u') \frac{\sin 2\pi W(u-u')}{2\pi W(u-u')}\, du' \quad (114).$$

Results eqs. (112) and (114) are known as the Dirichlet formulation of the approximation.

As will be shown in subsection 3, the approximation indicated by eq. (112) or (114) is such that the squared error is minimized. It is therefore said to be optimum in the least square or Gaussian sense. As the number of terms is increased or as the aperture becomes larger the approximation becomes better. However, at every discontinuity or rapid change of the desired function there occurs in the approximating function an oscillating overshoot. This overshoot does not decrease in magnitude as the number of terms is increased, although the frequency of the oscillation is increased and it moves closer to the point of discontinuity. This overshoot has a limiting magnitude of about 9 percent of the total discontinuity. This behavior of the approximation is termed Gibb's phenomena (Guillemin, pg. 485).

The Fourier Series or Transform method therefore creates a side lobe intensity of about 21 db when it is applied to the synthesis of a square or cosecant beam. It approximates the desired function very well far from points of rapid change; however, at points of discontinuity it has its characteristic overshoot. The method is rather inflexible in that even though we may be willing to accept greater deviations at some points in return for a smaller overshoot, or a greater slope at points of rapid change, nothing can be done about this as the final result is given by eq. (112) or (114).

Figure No. 38 gives the approximation to a 90° square beam obtained by this method. (Fig. No. 38 on page 118.)

2). Woodyard-Levinson Method (Woodyard)

This method was introduced by Levinson at the Radiation Laboratory during the war years and has since appeared in the literature in a paper by Woodyard, who probably developed the method independently in England. Restricting our discussion to the continuous aperture, the method may best be introduced as follows:

Consider an arbitrary aperture distribution f(x) and its Transform g(u), illustrated in Fig. No. 39

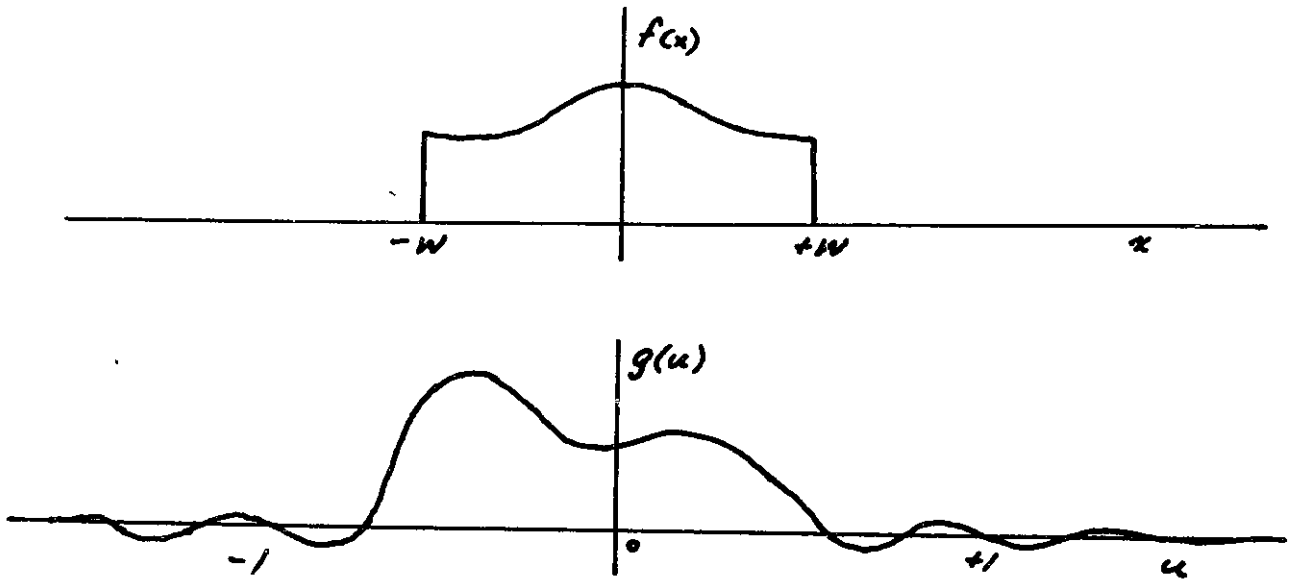

Fig. No. 39

The function f(x) may be expanded as a Fourier Series of fundamental period "2W", so that:

$$f(x) = \sum_{-\infty}^{\infty} C_n e^{-i\frac{2\pi n x}{2W}} \qquad |x| < W$$

$$f(x) = 0 \qquad |x| > W \qquad \Big\} \qquad (115)$$

The coefficients "C_n" are given by:

$$C_n = \int_{-W}^{W} f(x)\, e^{i\frac{2\pi n x}{2W}}\, dx \qquad (116)$$

Comparing eq. (109) and (116) we see that:

$$C_n = g\left(\frac{n}{2W}\right) \qquad (117)$$

Now f(x) is completely determined by its Fourier coefficients "C_n", or because of eq. (117) by the value of the polar diagram, g(u), at the infinite set of points u = n/2W. As f(x) is completely determined, so is g(u). We conclude that if a radiation pattern is due to an aperture of width "2W" then it and the corresponding aperture distribution is determined uniquely by the values g(n/2W). This is analogous to a theorem proved by Shannon for electric circuits (Shannon). The theorem as given by Shannon is: "If a function f(t) contains no frequencies higher than W cps., then it is completely determined by giving its ordinates at a series of points spaced 1/2W seconds apart."

The radiation pattern may be computed from the aperture Fourier series expansion, as:

$$g(u) = \int_{-W}^{W} f(x)\, e^{j\cdot 2\pi x u}\, dx$$

$$= \sum_{-\infty}^{\infty} \int_{-W}^{W} C_n\, e^{j\cdot 2\pi x\left(u - \frac{n}{2W}\right)}\, dx.$$

$$g(u) = \sum_{-\infty}^{\infty} C_n \frac{\sin 2\pi W\left(u - \frac{n}{2W}\right)}{2\pi W\left(u - \frac{n}{2W}\right)} \qquad (118).$$

The polar diagram is thereby expressed as a sum of functional forms which the aperture can generate. As any arbitrary function f(x) may be expanded in a Fourier series the expression (118) must include all possible patterns from the aperture of width "2W".

Sums of type (118) have been extensively treated in interpolation theory. The sum is called a cardinal series and the function (sin x)/x the cardinal function. (W. L. Ferrar) has proved an important property of this series and called by him its "consistency". Namely: if a function is constructed from n/2W equispaced ordinates in the form of a cardinal series and then if another set of displaced n/2W ordinates are chosen from this constructed curve and the corresponding cardinal series is formed, it will be found that the two series represent

the same function.

Our synthesis problem by means of this method reduces to choosing the arbitrary coefficients "C_n" so that the cardinal series fits as closely as possible to the desired pattern. The individual terms have an interesting property that at an ordinate "m/2W" all the terms except the "mth" are zero. Fig. No. 40 illustrates this phenomena.

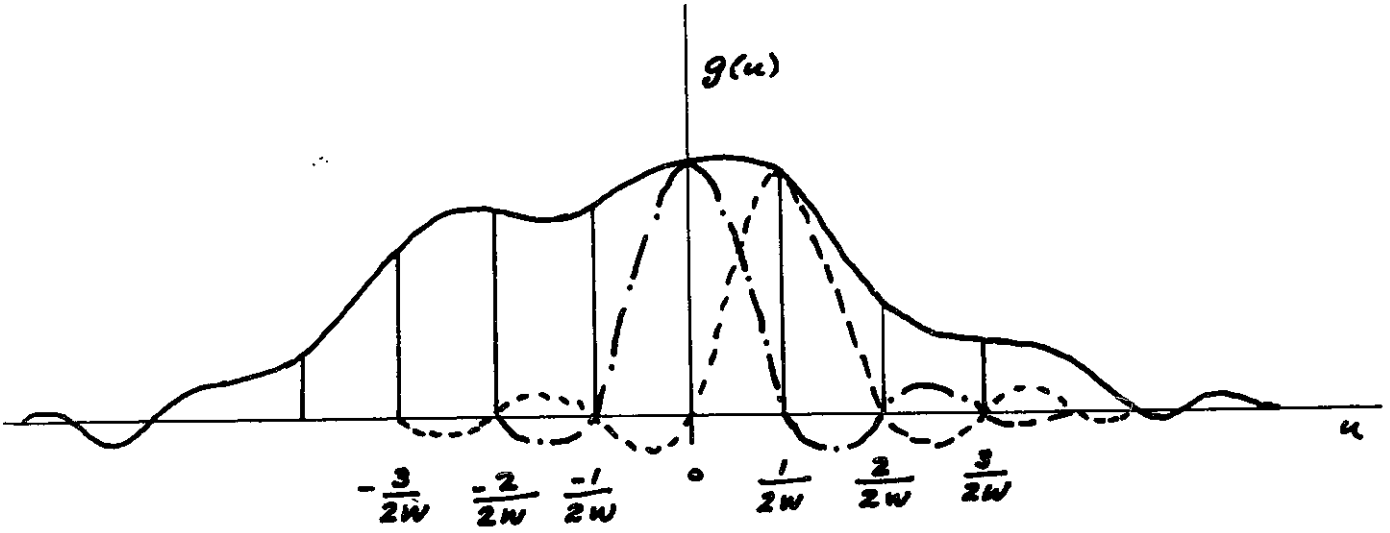

Fig. No. 40

This permits a very simple method of synthesis by choosing the C_m coefficient as equal to the desired pattern ordinate at the mth point. The approximating pattern then becomes:

$$g_a(u) = \sum_{-\infty}^{\infty} g_o\left(\frac{n}{2W}\right) \frac{\sin 2\pi W (u - n/2W)}{2\pi W (u - n/2W)} \qquad (119).$$

This approximating curve will pass exactly through the chosen ordinates, however in between it will deviate from the desired pattern by an unknown, but in a particular case a calculable, amount.

Actually the Woodyard method has considerable flexibility. We have at our disposal an infinite set of arbitrary constants and if we are interested in specifying g(u) in only a finite interval, say in the angular region of $-\frac{\pi}{2} < \theta < \frac{\pi}{2}$ or $-1 < u < +1$, and are not interested in its behavior outside this interval then a radiation pattern of any arbitrary shape or sharpness may be synthesized from an aperture of any specified width.

This striking statement brings us to the problem of "supergain". In order to obtain this arbitrary sharpness it is necessary to use contributions which have their maxima at the points $u = |\frac{n}{2W}| > 1$. Such contributions, due to the decreasing nature of the (sin x)/x functions, have little effect in the real angular region, so that terms of large magnitude must be used to be effective in fitting the function in the region of interest. It will be shown, in Section IV, that such terms contribute but little to the radiated power and represent reactive power flow through the radiating aperture. They therefore contribute to the reactive energy stored in the immediate vicinity of the antenna and raise its "Q". As we are primarily interested in physically realizable or low "Q" antennas, we must restrict the order of our coefficients to $|\frac{n}{2W}| < 1$. This condition eliminates those terms which contribute, in the large, to reactive

power. In f(x) they represent harmonics of spatial period smaller than a wavelength.

We still have available "4W" terms, where "W" is expressed in wavelengths, for fitting. We can, as we have done in eq.(119) choose equi-distant points, in which case the determination of the arbitrary coefficients becomes exceedingly simple being equal to the ordinates of the desired pattern at those points. We are also permitted to place our "4W" points at will, perhaps cluster them where we desire a closer fit. However, we then must solve a set of "4W" linear equations in the "4W" arbitrary constants. This latter method has the further disadvantage that terms which have their maximum value far from the cluster and are forced to form a better fit at this point will cause a large deviation from the desired pattern at their point of maximum value due to their weakness of control at the distant point.

It is of interest to compare the Fourier Integral approximation with that of the Levinson-Woodyard method using the ordinates at the equidistant points. At the n/2W points the Fourier Integral method yields for the ordinates (eq. 114):

$$g_i\left(\frac{n}{2W}\right) = 2W \int_{-\infty}^{\infty} g_0(u') \frac{\sin 2\pi W(u' - n/2W)}{2\pi W(u' - n/2W)}\, du' \qquad (114)$$

and the Levinson method

$$g_L\left(\frac{n}{2W}\right) = g_0\left(\frac{n}{2W}\right) \qquad (120)$$

If these were equal the two approximation patterns would be identical - as n/2W ordinates, for an aperture of width 2W, determine the pattern everywhere. The Levinson method yields ordinates that are equal to the desired pattern at these points and is dependent only on the value of the function at these ordinates, being independent of the value of the desired function in between. Whereas the Fourier Integral representation due to its integral formulation yields ordinates that depend on the value of the desired function everywhere. However, the ordinates as determined by the Fourier Integral method are heavily weighted at and near the point n/2W. This is due to the delta function nature of

$$2W \frac{\sin 2\pi W(u - n/2W)}{2\pi W(u - n/2W)}.$$

so that as W is made large or if $g_0(u)$ does not change appreciably in the vicinity of n/2W, we have

$$\lim_{W\to\infty} 2W \int_{-\infty}^{\infty} g_0(u') \frac{\sin 2\pi W(u' - n/2W)}{2\pi W(u' - n/2W)} du' \longrightarrow g_0\left(\frac{n}{2W}\right).$$

Hence, the two methods approach each other for large apertures, with the exception of the vicinity about the discontinuities of $g_0(u)$. As the ordinates of $g_0(u)$ correspond to the Fourier harmonics of f(x) the two methods yield similar aperture distributions with the exception of those harmonics corresponding

to ordinates near the discontinuities of $g_o(u)$.

Although both functional approximations approach the given function the behavior is different in the immediate neighborhood of discontinuities. Fig. No. 41 shows the result obtained by applying the Levinson procedure to a square beam. The overshoot has been substantially reduced to a value of 1.03, however, the average slope has decreased to 0.5(2W), a loss of 39 percent.

As the Levinson procedure differs from the Fourier Integral representation it is not a least square fit and therefore possesses a greater mean square error.

3). Some Remarks on Tschebyscheff and Gaussian Approximations

The approximation problem is one of fitting a given function $g_o(u)$, "as well as possible", by a finite sum of "n" terms of "suitable" functions. We have for our composition:

$$g_a(u) = \sum_{-n}^{+n} c_{n'} \rho_{n'}(u) \qquad (121)$$

The problem is the choice of the arbitrary coefficients "C_n" to achieve a "best fit". We inquire into the definition of the term "best fit". Until quite recently the definition of "best fit" has been taken, largely due to the investigations of Gauss, so that the integral of the squared error be a minimum. This condition may be expressed mathematically as:

$$\delta \int_{-\infty}^{\infty} [g_o(u) - g_a(u)]^2 du = 0 \qquad (122)$$

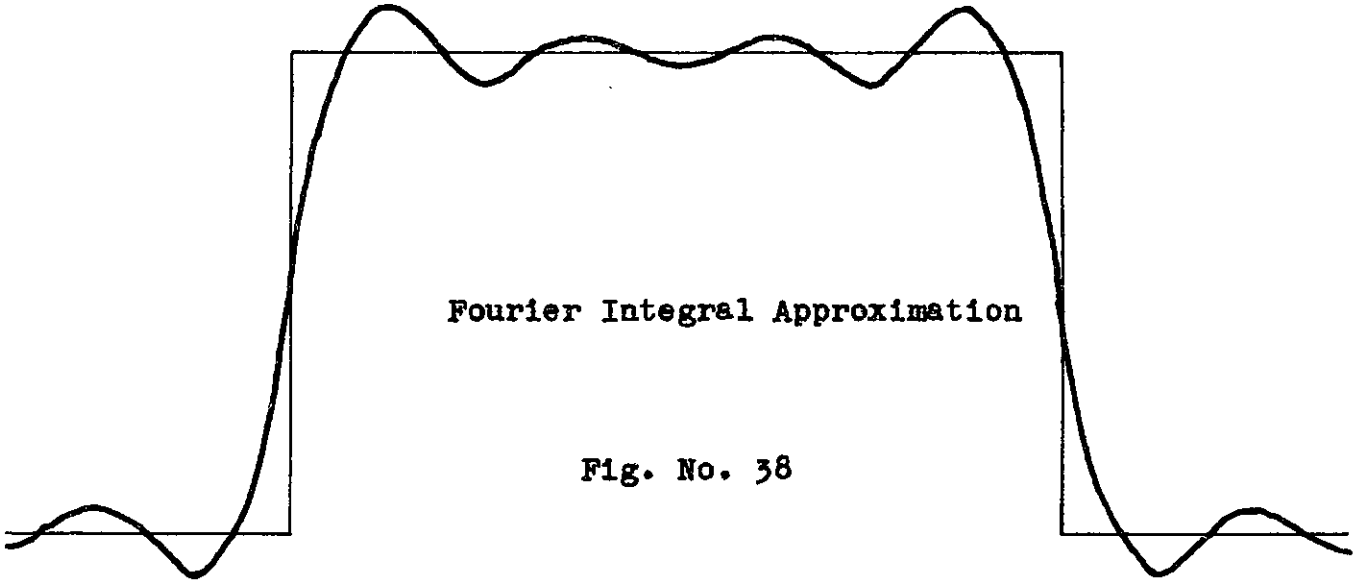

Fourier Integral Approximation

Fig. No. 38

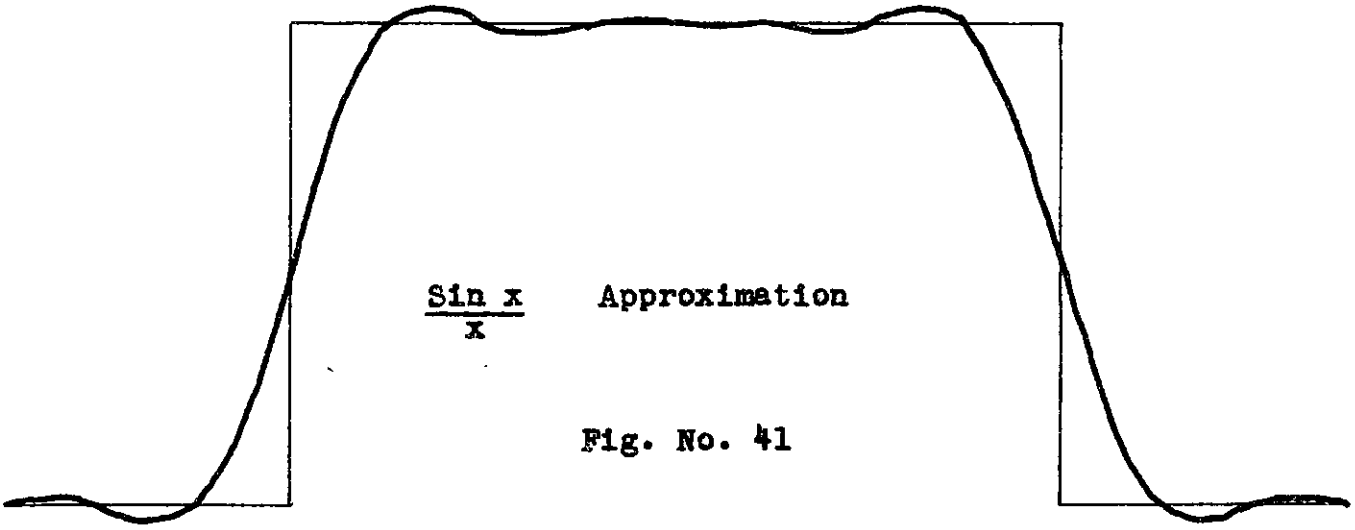

$\frac{\sin x}{x}$ Approximation

Fig. No. 41

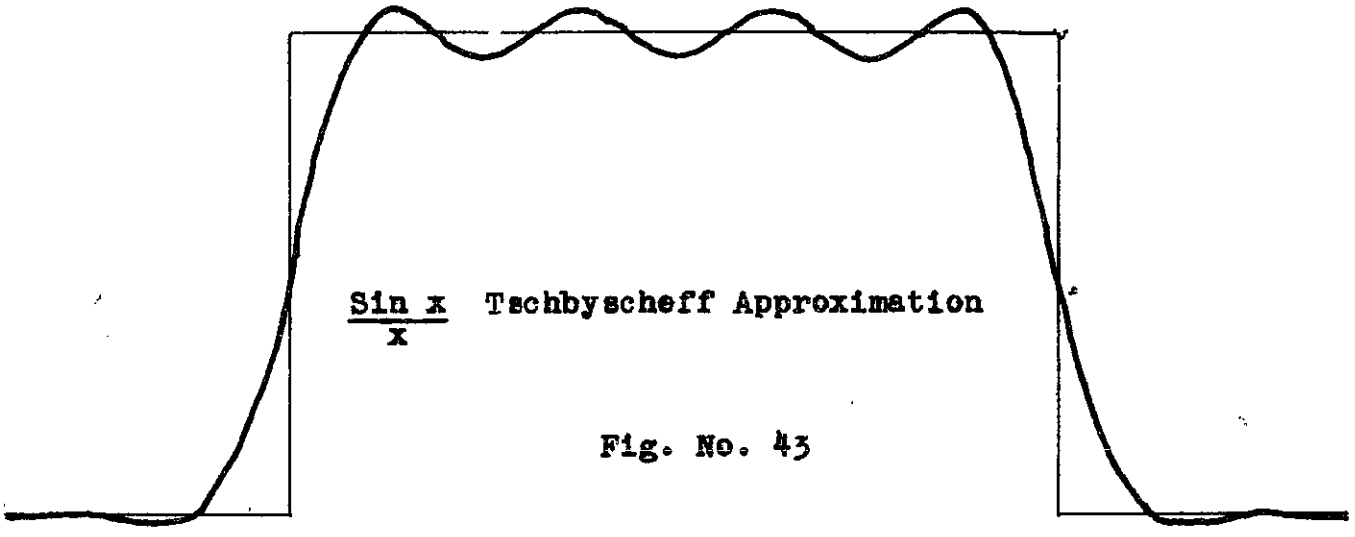

$\frac{\sin x}{x}$ Tschbyscheff Approximation

Fig. No. 43

The coefficients may be readily chosen to satisfy this condition for:

$$I = \int_{-\infty}^{\infty} [g_o(u) - g_a(u)]^2 du = \int_{-\infty}^{\infty} [g_o(u) - \Sigma C_k \rho_k(u)]^2 du.$$

$$= \int_{-\infty}^{\infty} g_o^2(u) du - 2\Sigma C_k \int_{-\infty}^{\infty} g_o(u) \rho_k(u) du$$

$$+ \sum_k \sum_\ell C_k C_\ell \int_{-\infty}^{\infty} \rho_k(u) \rho_\ell(u) du.$$

If the terms of our approximating function are ortho-normal or:

$$\int_{-\infty}^{\infty} \rho_k(u) \rho_\ell(u) du = \delta_{k\ell}$$

where

$$\delta_{k\ell} = 1 \qquad k = \ell$$

$$\delta_{k\ell} = 0 \qquad k \neq \ell$$

then the error integral becomes:

$$I = \int_{-\infty}^{\infty} g_o(u) du - 2\Sigma C_k \int_{-\infty}^{\infty} g_o(u) \rho_k(u) du + \Sigma C_k^2$$

We wish to determine the coefficients so that the error be a minimum or:

$$\frac{\partial I}{\partial C_k} = 0$$

Differentiating, we arrive at the condition for the coefficients:

$$C_k = \int_{-\infty}^{\infty} g_0(u)\, \rho_k(u)\, du \qquad (123).$$

As the members of the trigonometric series form such an ortho-normal set, the Fourier Series approximation or the limiting case of the Fourier Integral yield an approximation optimum in the least square sense. The cardinal functions also, as we shall show in the appendix, are ortho-normal and may be used to approximate the pattern in a least square sense. That is the arbitrary coefficients in

$$g(u) = C_n \frac{\sin 2\pi W(u - n/2W)}{2\pi W(u - n/2W)}.$$

may be chosen by the condition (123) so that:

$$C_n = 2W \int_{-\infty}^{\infty} g_0(u) \frac{\sin 2\pi W(u - n/2W)}{2\pi W(u - n/2W)}\, du.$$

but this is the same as the result obtained by the Fourier Integral method. We therefore obtain nothing new by using the cardinal functions as an ortho-normal set.

The definition of "best fit" could just as well have been taken so that we would determine the arbitrary coefficients from the condition that the integral of the mth power of the absolute error be a minimum; that is:

$$\delta \int_{-\infty}^{\infty} |g_a(u) - g_o(u)|^m du = 0 \qquad (124)$$

The advantage of the Gaussian approximation (m=2) is that it is amenable to a simple determination of the coefficients. It commands no preference on purely physical grounds. In fact its occurrence in nature is probably very rare. As an example, if a circuit is adjusted to generate what appears the best square wave on a cathod ray tube, a harmonic decomposition of the wave will generally not yield a Fourier decomposition.

Although mathematical methods do not exist for the determination of the coefficients except in the Gaussian sense, existence theorems are available that state that such decompositions exist for all integer values of the exponent and that such decompositions are unique (Jackson, 2, pg. 86).

As we increase the value of "m" in eq. (124) the larger errors are weighted more heavily, so that we would expect smaller overshoots in the vicinity of discontinuities and a more equal deviation distribution. In the limiting case when "m" becomes infinite, the maximum deviations become all equal in magnitude and we have an approximation in the Tschebyscheff sense or:

$$|g_o(u) - g_a(u)| \leq \epsilon \qquad (125)$$

A Tschebyscheff approximation is much more useful if we have to do with the design of equipment, such as electrical filters or antennas, as we can "guarantee" that the error will not exceed a prescribed value. Furthermore, in many applications we are interested in the maximum possible error and not its average squared value.

Even though the Tschebyscheff approximation has a larger mean square error than the Gaussian it would be more generally used if there were some simple mathematical technique of determining the coefficients of expansion. It would be of importance not only in antenna synthesis but also in the representation of periodic electric waveforms and electric transients. (Guillemin, pg. 506) indicates that such a method would be desirable and that this problem has received little attention to date. We shall present two such methods wherein we achieve approximation at least in an approximate Tschebyscheff sense. These methods will be presented in antenna terminology, however they may be readily converted for use for the representation of periodic and transient electrical signals.

4). <u>Pattern Synthesis in an Approximate Tschebyscheff Sense Using the Cardinal Functions</u>.

As the coefficients of the cardinal series are equal individually to the ordinates of the polar diagram at the n/2W points, this series forms a convenient means of approximating a desired pattern in the Tschebyscheff sense. We can even choose a different tolerance in different regions. Fig. No. 42

illustrates this procedure, where we require a tolerance of "h" in the pattern region and "e" in the remaining real region. It is evident from the nature of the (sin x)/x function that if alternate coefficients take on the permitted error with opposite sign then the rise time will be increased.

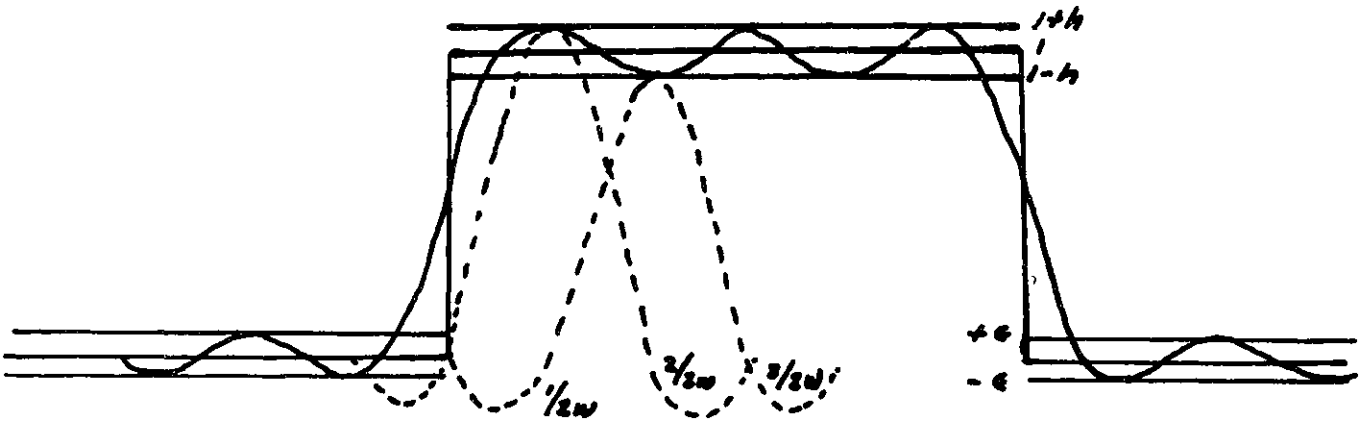

Fig. No. 42

We apply this procedure in Fig. No. 43 to our 90^{o} square pulse. In Fig. No. 43 we have permitted a 5 percent error in the radiation region and approximately zero tolerance in the side lobe part.

The procedure suggested above has only approximate Tschebyscheff behavior as at the points of discontinuity the error exceeds our tolerance. However, this cannot be helped if we attempt to approximate a discontinuous function with a finite sum. The choice of coefficients is also not rigorous as we do not know the extreme values of the approximation. Especially near

discontinuities and for small tolerances the extremes do not occur exactly at the equally spaced ordinates. However, as each component

$$\frac{\sin 2\pi W(u - n/2W)}{2\pi W(u - n/2W)}$$

function is largely effective only in the vicinity of the point n/2W and exercises only a small effect far from this point, the function may be fitted rather closely with a small amount of labor. A similar procedure with trigonometric functions would be impossible.

5). <u>Pattern Synthesis in an Approximate Tschebyscheff Sense by the Use of the Tschebyscheff Functions</u>

We recall eq. (114) giving the approximation pattern due to the Fourier Transform method:

$$g_a(u) = 2W \int_{-\infty}^{\infty} g_o(u') \frac{\sin 2\pi W(u-u')}{2\pi W(u-u')} du' \qquad (114)$$

or if we let

$$S(u-u') = 2W \frac{\sin 2\pi W(u-u')}{2\pi W(u-u')}$$

then

$$g_a(u) = \int_{-\infty}^{\infty} g_o(u') S(u-u') du' \qquad (126)$$

We can look upon this equation as physically representing a scanning operation. The approximation pattern is obtained by integrating the product of the desired pattern and a scanning function located at the general point "u". Fig. No. 44 indicates the operation:

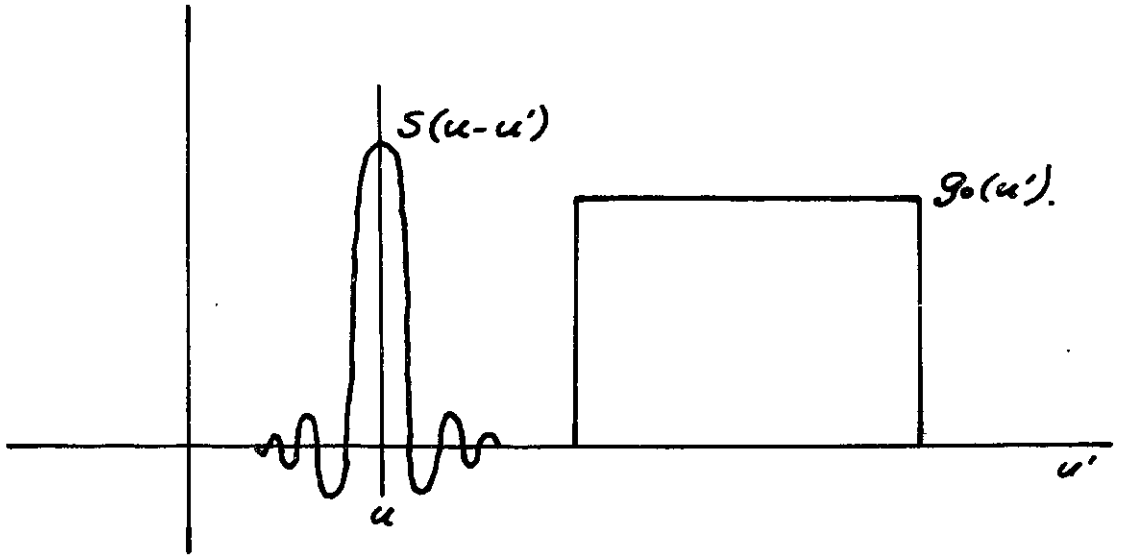

Fig. No. 44

The overshoot or Gibb's phenomena can now be seen to be a property of the scanning function, and its maximum value may be expressed as:

$$\frac{\int_{0}^{\infty} S(u)\,du + \int_{-\pi}^{0} S(u)\,du}{\int_{-\infty}^{\infty} S(u)\,du} \qquad (127).$$

$$\frac{1.57 + 1.86}{3.14} = \frac{3.43}{3.14} = 1.09$$

giving the accepted 9 percent overshoot.

The required aperture distribution can be written in terms of the scanning function, for:

$$f(x) = \int_{-\infty}^{\infty} g_a(u)\, e^{-j2\pi xu}\, du$$

$$f(x) = \int_{-\infty}^{\infty}\int_{-\infty}^{\infty} g_o(u')\, S(u-u')\, e^{j2\pi xu}\, du'\, du$$

letting

$$u - u' = y \qquad du = dy$$

$$f(x) = \int_{-\infty}^{\infty} g_o(u')\, e^{-j2\pi xu'}\, du' \int_{-\infty}^{\infty} S(y)\, e^{-j2\pi xy}\, dy$$

The second integral can be readily evaluated as it is merely the transform of the scanning function, or:

$$\int_{-\infty}^{\infty} S(y)\, e^{-j2\pi xy}\, dy = 2W \int_{-\infty}^{\infty} \frac{\sin 2\pi Wy}{2\pi Wy}\, e^{-j2\pi xy}\, dy = F(x)$$

where F(x) has the functional form

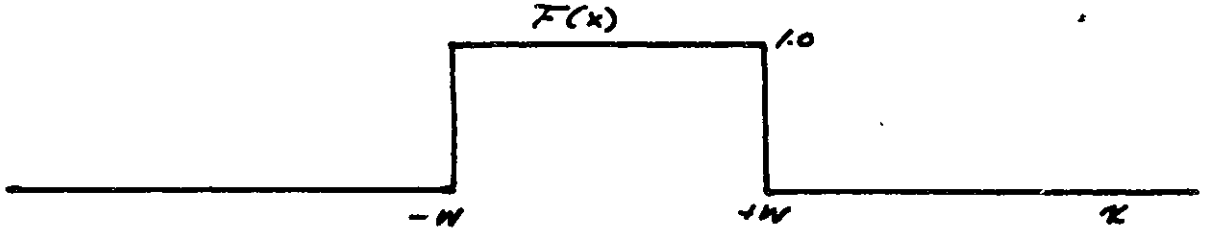

The required aperture distribution becomes:

$$f(x) = F(x) \int_{-\infty}^{\infty} g_0(u) e^{-j 2\pi x u} du. \qquad (128)$$

Although we have obtained no new results, our Fourier Integral example has served to introduce the concept of the scanning operation. We can also look upon this phenomena as a convolution of the desired pattern and the scanning function so that the final aperture distribution is given as the product of the transforms of the scanning function and the desired pattern, i.e.

$$f(x) = F(x) f_0(x) = \int_{-\infty}^{\infty} g_a(u) e^{-j 2\pi u x} du$$

where

$$g_a(u) = \int_{-\infty}^{\infty} g_0(u') S(u-u') du'$$

and

$$F(x) = \int_{-\infty}^{\infty} S(u) e^{-j 2\pi u x} dx$$

$$f_0(x) = \int_{-\infty}^{\infty} g_0(u) e^{-j 2\pi u x} dx.$$

We inquire whether it is possible to construct a scanning function which would be more useful than the previously introduced (sin x)/x function. Suppose we were to construct a function of the type

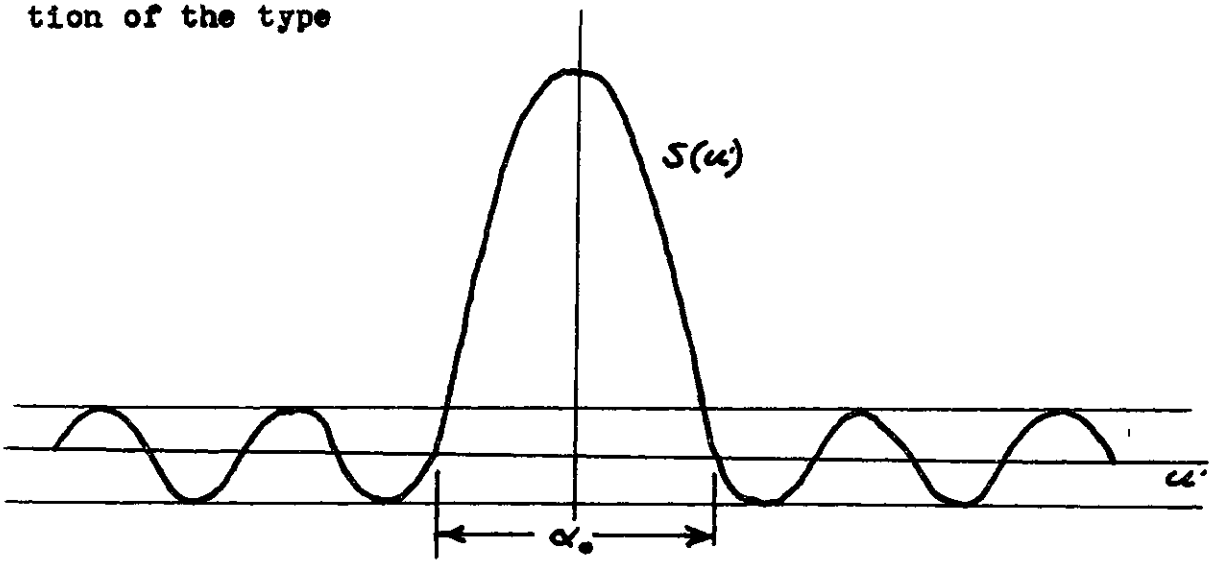

Then if we were to scan a unit step we would expect a result of the following type:

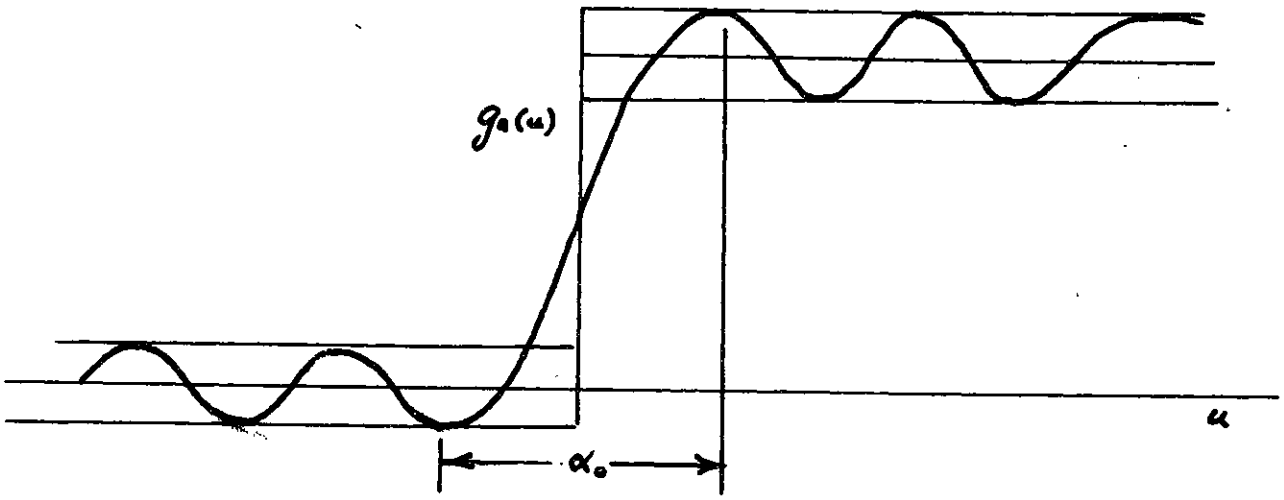

If our special scanning function had side lobes of equal area then the deviations in the approximating pattern would have equal value and could be expressed as a ratio of the side lobe

area to the main beam area of the scanning function. If, furthermore, we could arbitrarily set the value of the side lobe area by adjusting the side lobe magnitude and if we could show that for a given area the width of the main beam were a minimum, then we would have a quite useful function. At least in the case of approximating a unit step we would have the greatest average rate of rise for a prescribed deviation which we would not exceed.

When we approximate an arbitrary function with our special scanning function, we can no longer make definite statements about the deviations which will occur. The deviations will now no longer be equal and we cannot state definitely what they will be. However, for functionally smooth curves we would not expect any violent behavior.

Although we are not able to state anything with mathematical rigor as to the result of our approximation, it is felt that the procedure to be outlined can be useful in synthesizing antenna patterns or electric waveforms. This inability to judge the closeness of our approximations is not at all surprising if it is recalled that even in a finite Fourier approximation we cannot state with certitude the value of the deviation at any point. It is true that in the Fourier approximation we can say that the fit is optimum in the least square sense. However, this is of doubtful value as every approximation is optimum in some sense; that is there is a minimum value of the integral

$$\int w(u) \left| g_a(u) - g_o(u) \right|^m du \qquad (129).$$

where w(u) is some weighting function.

To be useful the scanning function should have the following properties:

1. It should be generatable by an aperture of width "2W".
2. The side lobe level should be capable of adjustment to any desired value.
3. The side lobe areas should be roughly equal.
4. It would be desirable to show that the scanning function used was the greatest rate of rise of all possible functions generatable by the specified aperture.

A scanning function fulfilling the above can be constructed based on the Tschebyscheff polynomials. These polynomials are defined by

$$T_n(x) = \cos(n \arccos x) \qquad x < 1$$

$$T_n(x) = \cosh(n \operatorname{arc\,cosh} x) \qquad x > 1 \qquad (130)$$

They are of degree "n" and have the graphical development shown in Fig. No. 45 for the special case of $n = 7$.

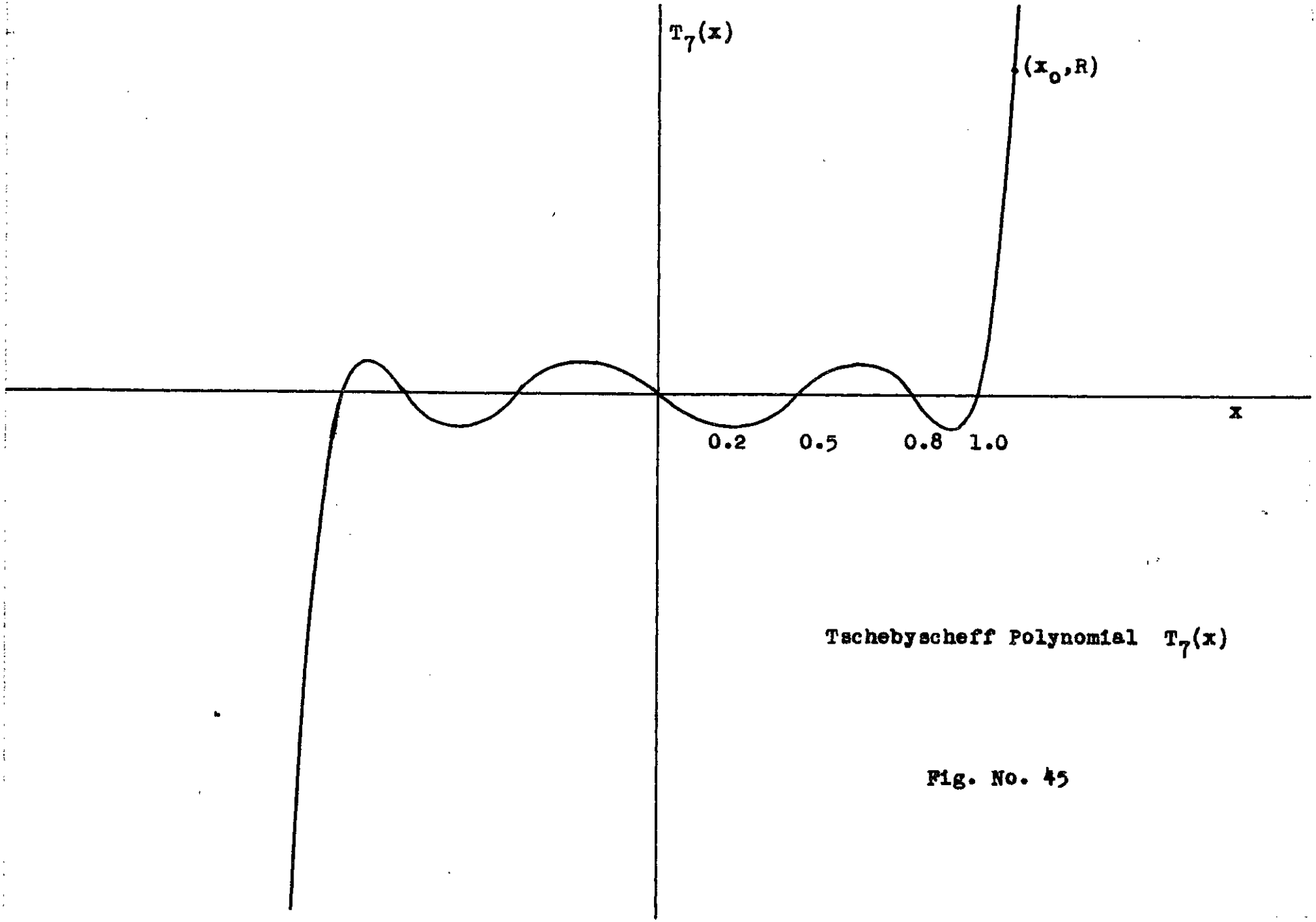

Tschebyscheff Polynomial $T_7(x)$

Fig. No. 45

6250-02C

If we make the transformation

$$x = x_0 \cos \frac{\pi}{2} u \tag{131}$$

we obtain the periodic function in "u", shown in Fig. No. 46, and of the mathematical form

$$T_n(u) = \cos [n \arccos (x_0 \cos \frac{\pi}{2} u)] \tag{132}$$

It is characterized by side lobes, all equal, and of relative magnitude 1/R. The zeros of this function are almost equally spaced being determined by

$$x_0 \cos \frac{\pi}{2} u_k = \cos \frac{(2k-1)}{n} \frac{\pi}{2} \tag{133}$$

where "x_0" is determined by the ratio 1/R and is a number slightly greater than unity.

Equation (132) is a polynomial in cos $\frac{\pi}{2}$ u of the nth order. As the powers of the cosine may be expanded into terms of multiple angle, (132) represents the pattern of an array of "n+1" elements spaced half wavelength apart. The excitation of the various elements are chosen according to the equation

$$\sum A_k \cos k \frac{\pi}{2} u = \cos [n \arccos (x_0 \cos \frac{\pi}{2} u)] \tag{134}$$

An array excited with the coefficient "A_k" will therefore yield a radiation pattern with all minor lobes equal and of the previously specified magnitude 1/R. The analysis presented is based on the work of (Dolph) who has shown in addition that

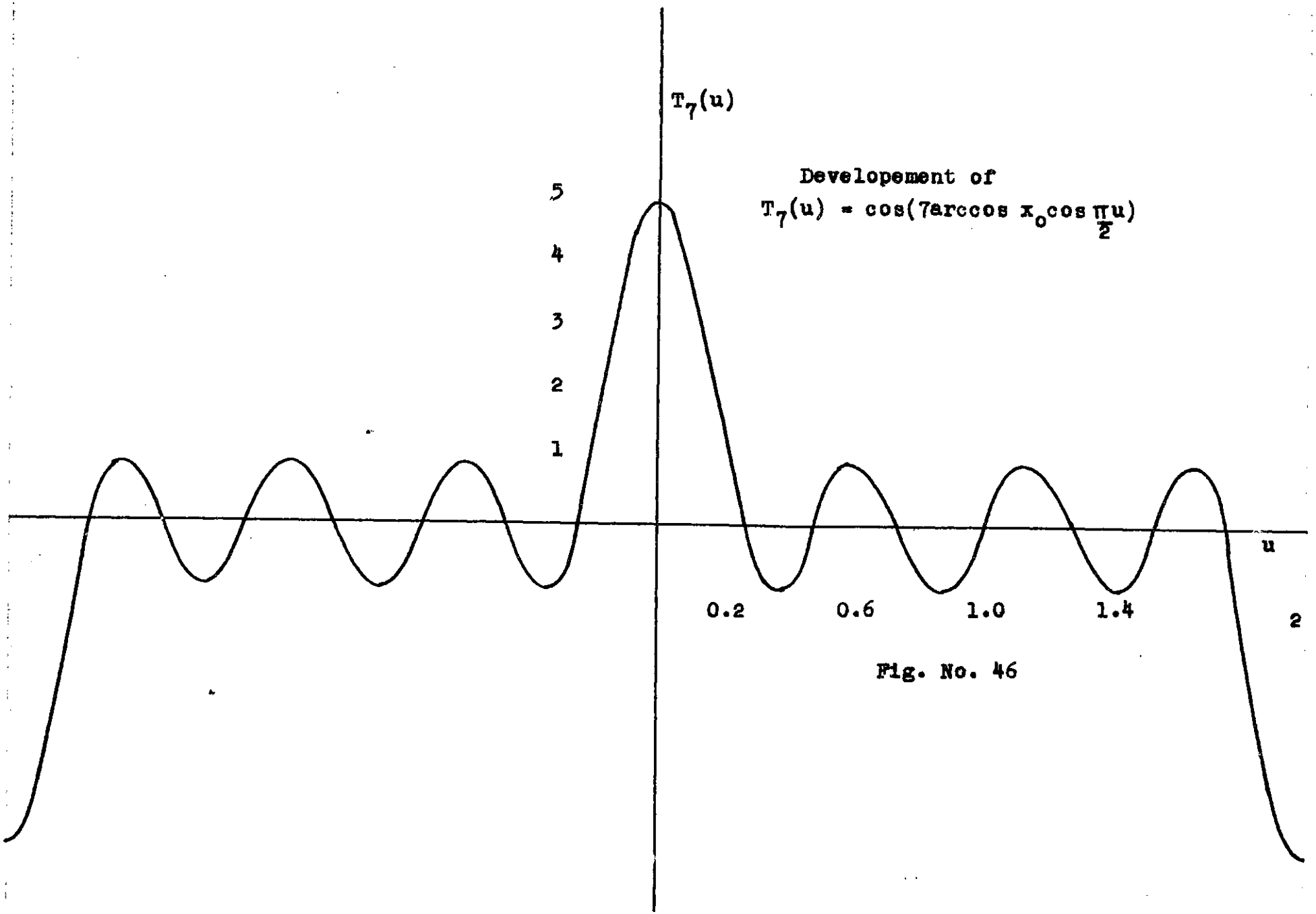

Developement of
$T_7(u) = \cos(7\arccos x_0 \cos \frac{\pi}{2} u)$

Fig. No. 46

6250-03 c

for a given side-lobe level the beam width (i.e., the number of degrees to the first null) is minimized.

We will use (132) as our scanning function in the approximation procedure for the discrete case. Although (132) is characterized as having minimum beam width, for a given minor lobe level and a given number of terms, it does not necessarily follow that the resulting approximation, to an arbitrary function, will have minimum rise time and possess exactly equal deviations in the Tschebyscheff sense. However, it is felt that this behavior will be approached and the procedure may prove quite useful. Let us apply it to some functional forms and examine the nature of the resulting approximations.

According to (128) the desired current distribution may be obtained by simply multiplying the coefficients as obtained by the Fourier Series method by the Tschebyscheff-Dolph coefficient A_k. It is convenient to have curves of A_k for various minor lobe levels or rise times. Figure Nos. 47 and 48 are plots of these values for an 8 and a 16 element array. The abscissa used is the rise time or beam width between first nulls relative to that obtained by the Fourier or least square fit. Figures 47 and 48 may just as readily be used for modifying the Fourier coefficients obtained in approximating electric wave forms.

The minor lobe level of our specially constructed scanning function can be obtained, for a specific relative beam width, from Figs. 47 and 48, with the aid of the equation

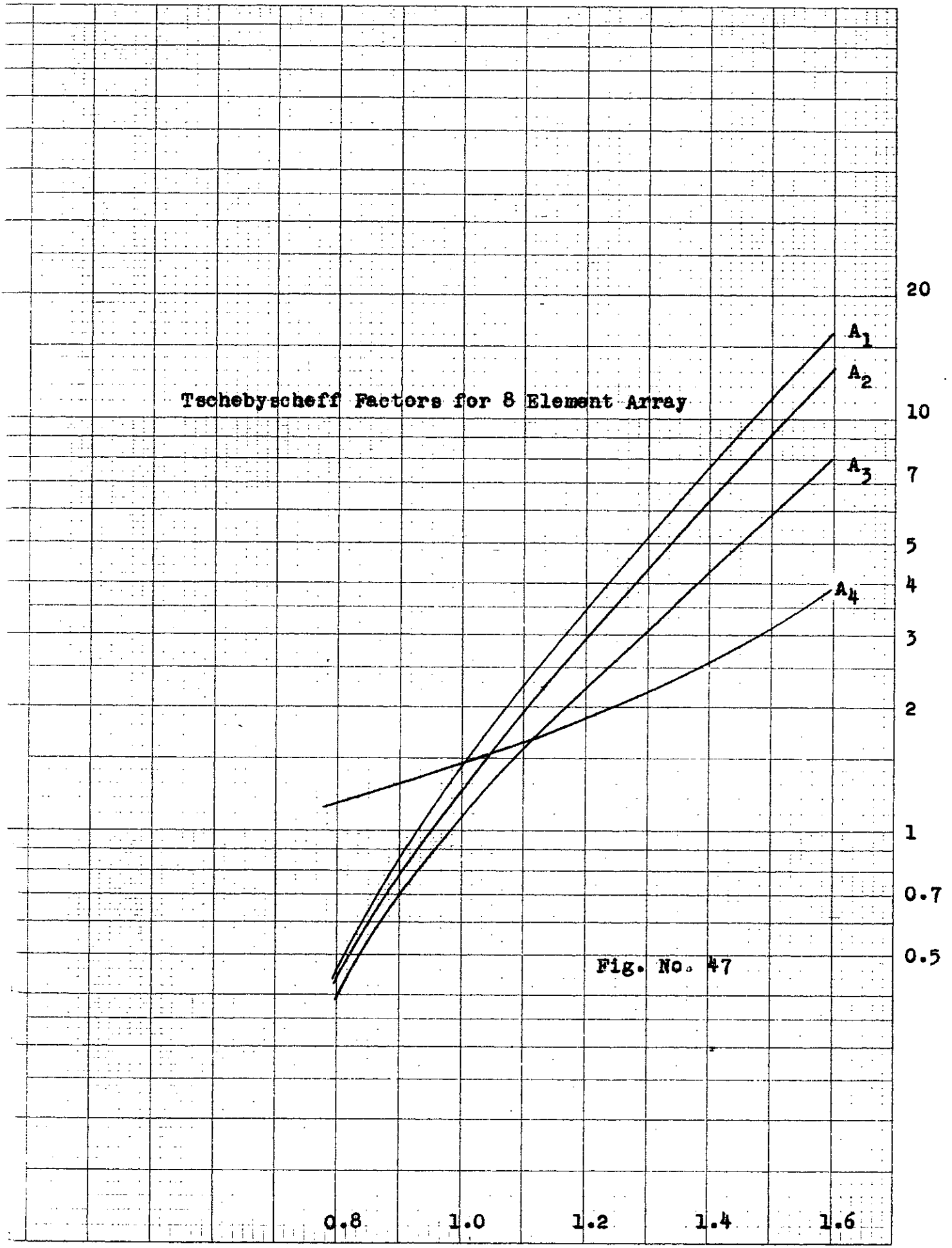

Fig. No. 47

6250-04C

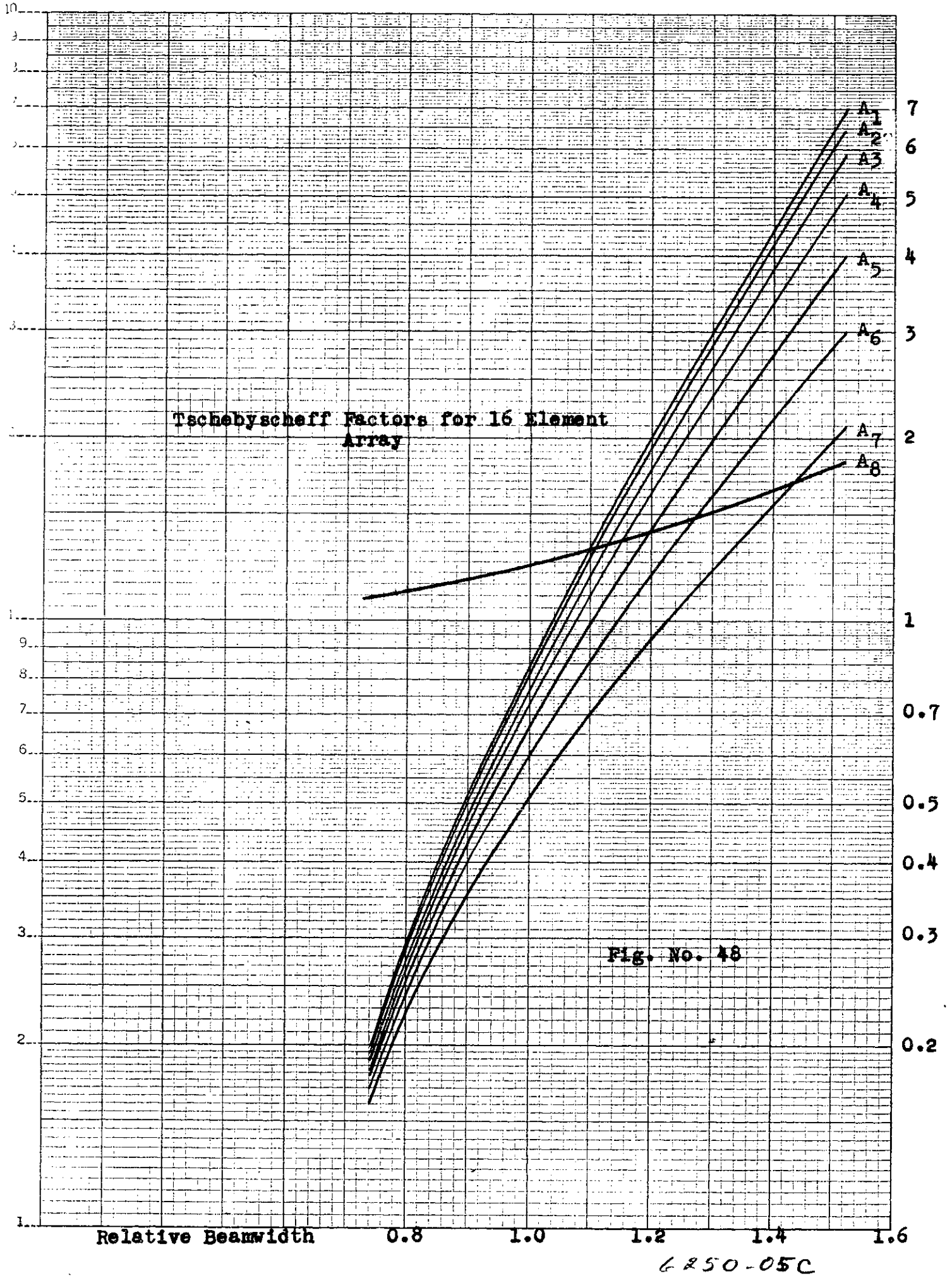

Fig. No. 48

6250-05C

$$\mathcal{R} = \sum^{N} A_k \qquad (135)$$

The coefficients as obtained cannot be used directly but must be normalized by multiplication with (for even array)

$$\frac{\sum^{N/2} 1/2K-1}{\sum^{N/2} A_k/2K-1} \qquad (136)$$

Figure No. 49 illustrates the result of applying this procedure to approximating a square beam by an array of eight elements spaced a half wavelength. The figure is equally valid for a periodic rectangular pulse with four harmonic frequencies. Figure No. 49a shows the Fourier Series or least square approximation with its characteristic Gibb's overshoot which amounts to 10 percent in this case (the 9 percent value quoted previously is only the limiting value for a unit step or very long pulse). Figure No. 49b shows the approximation obtained by the use of the suggested procedure with a scanning function rise time equal to the least square case. The deviation has become a uniform ripple of 6 percent. This is a reduction from the 10 percent overshoot; however the error is greater in the center of the pulse. Figures Nos. 49c and 49d give the approximations obtained with a 10 percent greater and a 10 percent smaller rise time respectively.

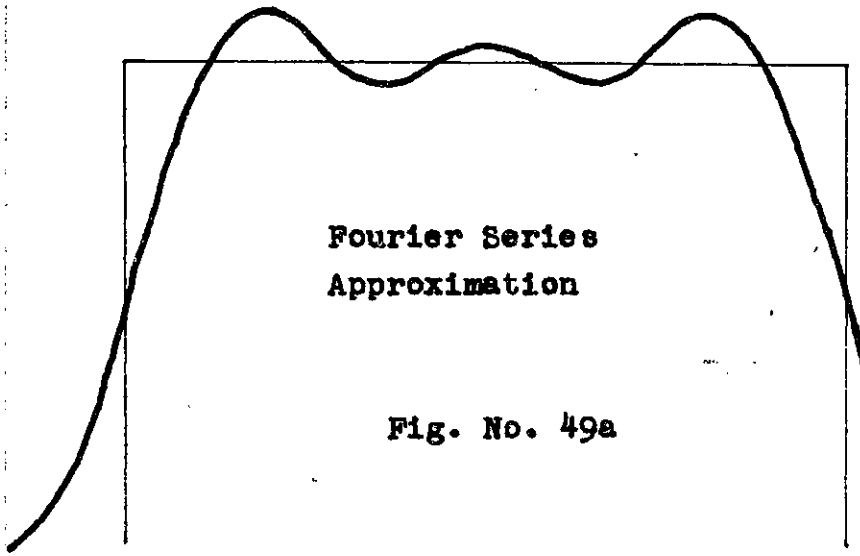

Fourier Series
Approximation

Fig. No. 49a

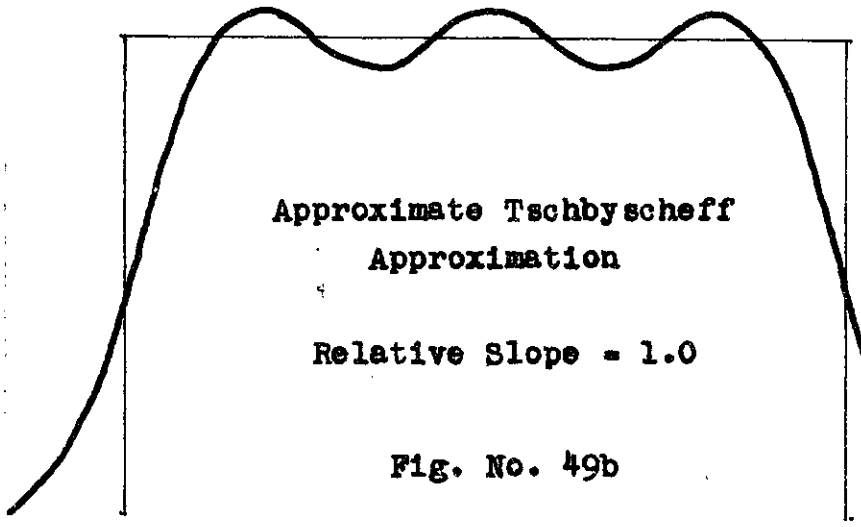

Approximate Tschbyscheff
Approximation

Relative Slope = 1.0

Fig. No. 49b

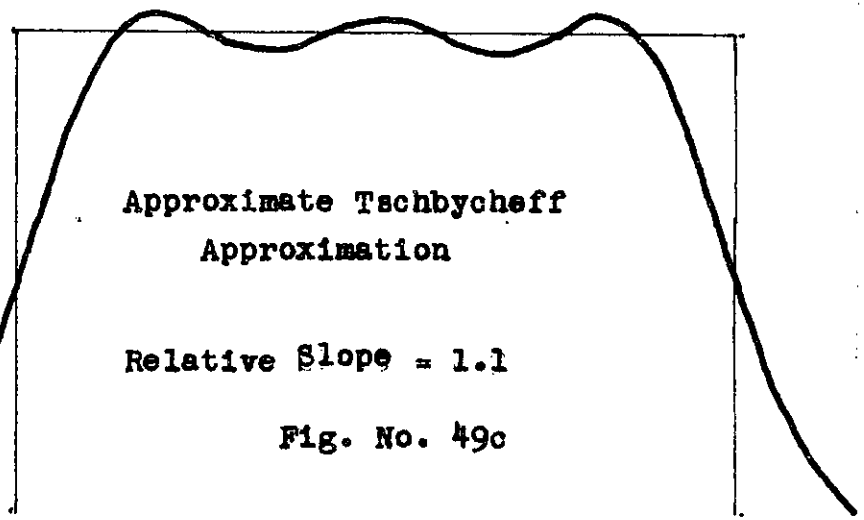

Approximate Tschbycheff
Approximation

Relative Slope = 1.1

Fig. No. 49c

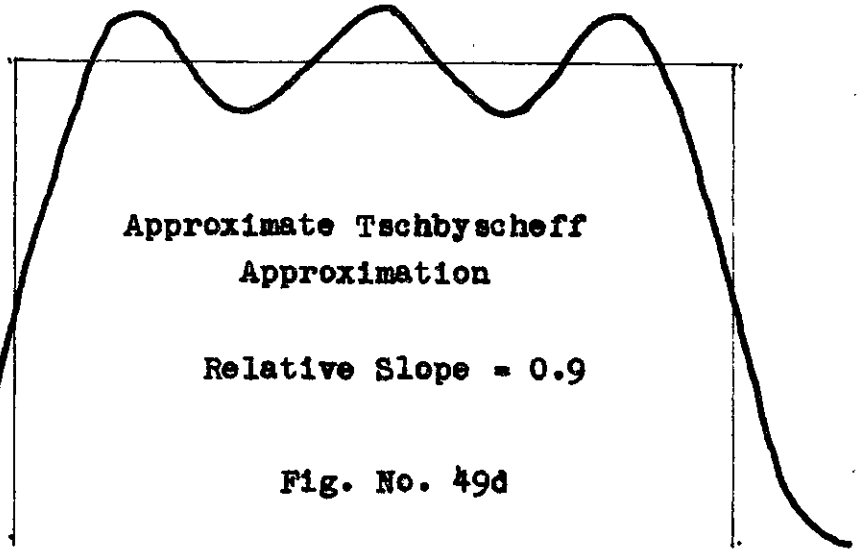

Approximate Tschbyscheff
Approximation

Relative Slope = 0.9

Fig. No. 49d

In examining Fig. No. 49 it is meaningless to ask which is the "best" approximation. "a" has the least square error; however if only a 4 percent overshoot is permitted and a continuing ripple of that magnitude is not objectionable, "c" is to be preferred. Similarly, if rise time is the consideration and a 10 percent ripple can be tolerated, "d" is preferable. The suggested procedure, however, provides a means of obtaining any desired ripple.

Let us apply our procedure to a more complex example. Consider the design of a cosecant squared antenna (Silver, pg. 465) with the following characteristics: beam to rise at zero degrees and continue at uniform intensity till six degrees, then the radiated power is to decrease in a cosecant squared manner until sixty-four degrees is reached, beyond which we desire no radiation.

Figure No. 50 shows the desired pattern with the Fourier Series approximation obtained by a 16 element array. Figure No. 51 gives the result of applying our procedure with equal rise time. Figures Nos. 52 and 53 present the approximations obtained with a 10 and a 20 percent reduction in rise time.

Above we have presented, for discrete arrays, a synthesis procedure which possesses approximate Tschebyscheff behavior. We inquire about its extension to a continuous aperture. If we were to take the convolution of our delta function current distribution and another function, the resulting radiation pattern would be the product of the patterns of the function and the array. A convenient function is

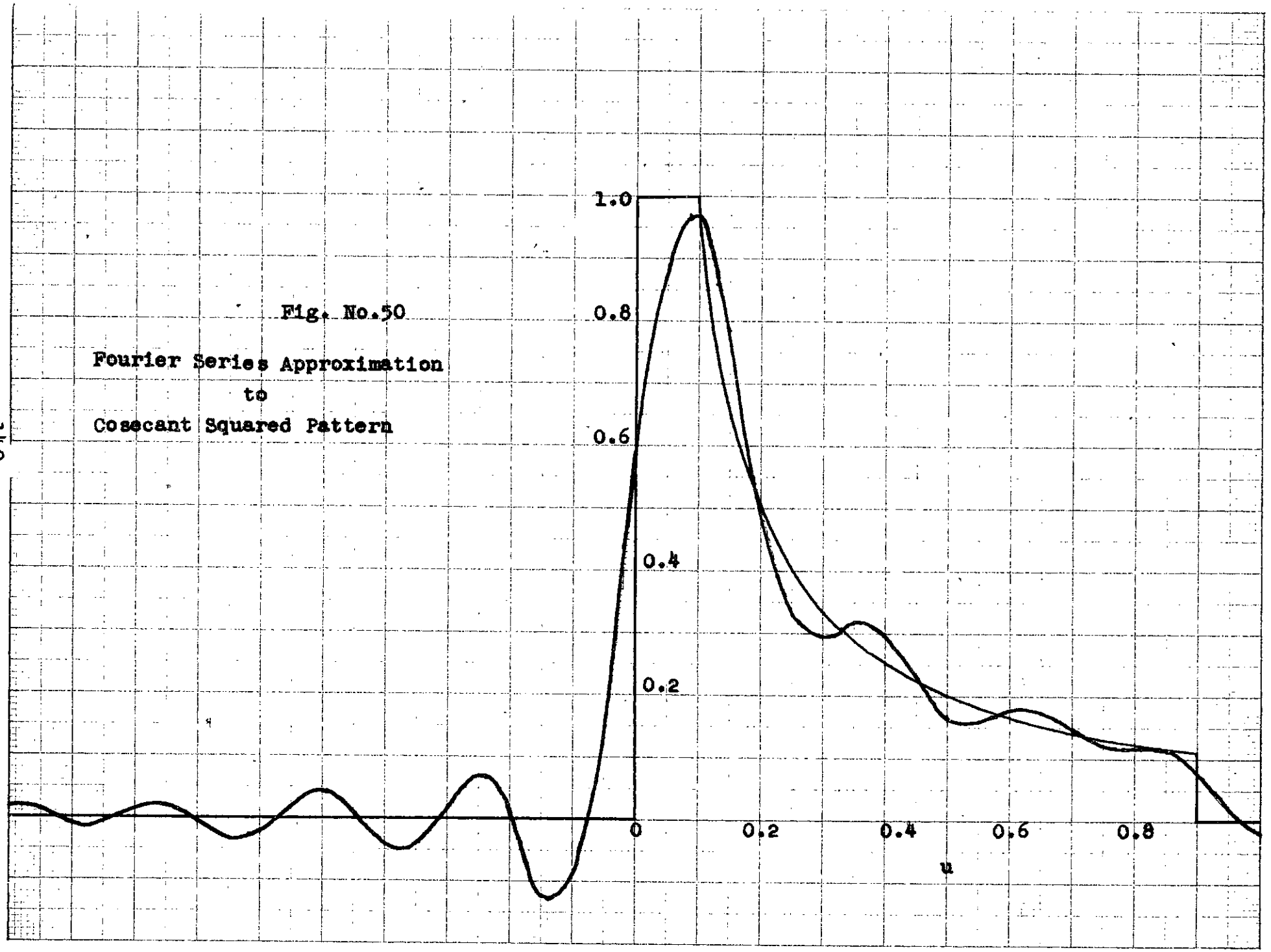

Fig. No.50

Fourier Series Approximation
to
Cosecant Squared Pattern

6250 - 07C

Fig. No. 51

Approximate Tschbyscheff Approximation

to

Cosecant Squared Pattern

Relative Slope = 1.0

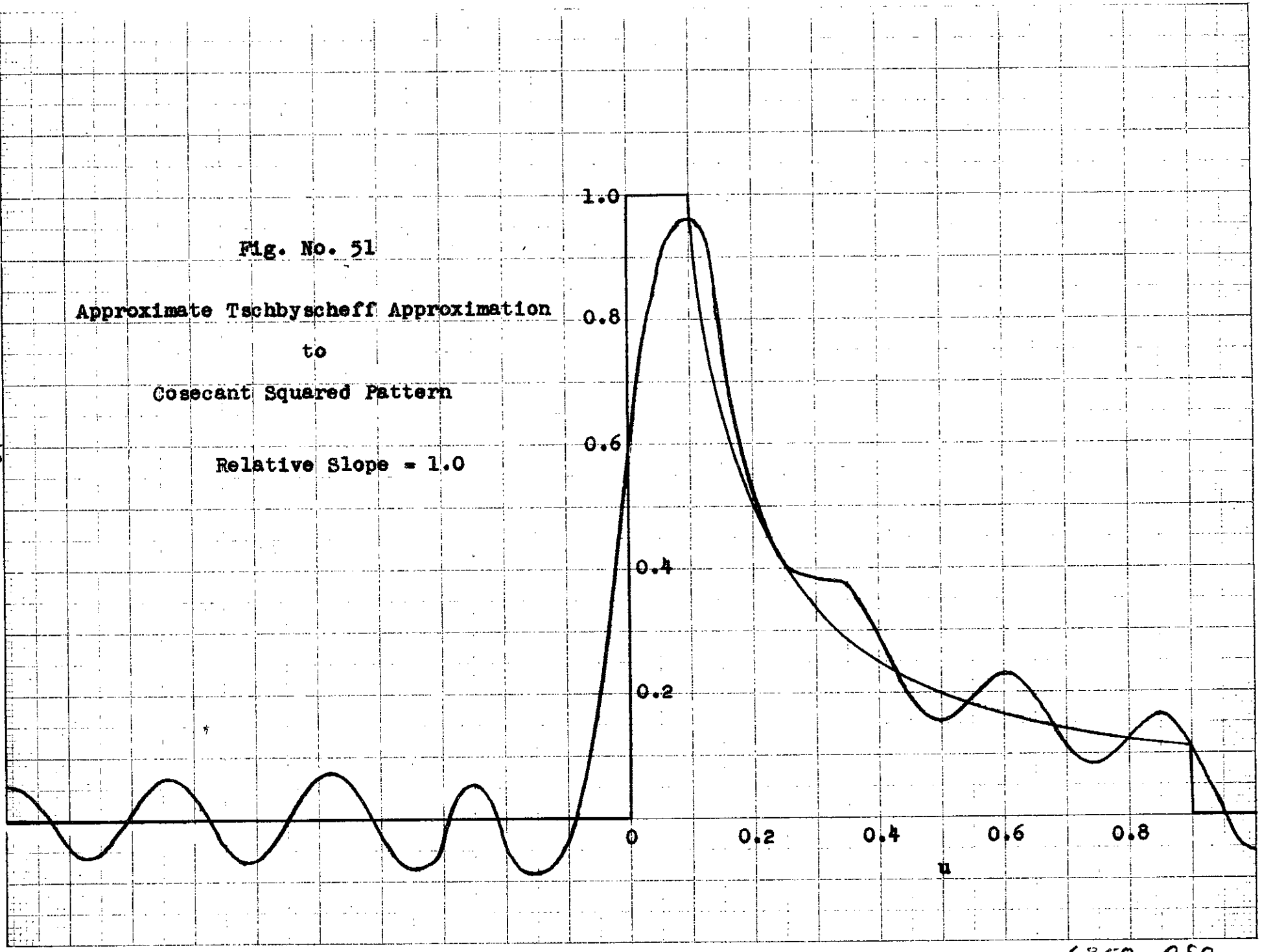

6250.08C

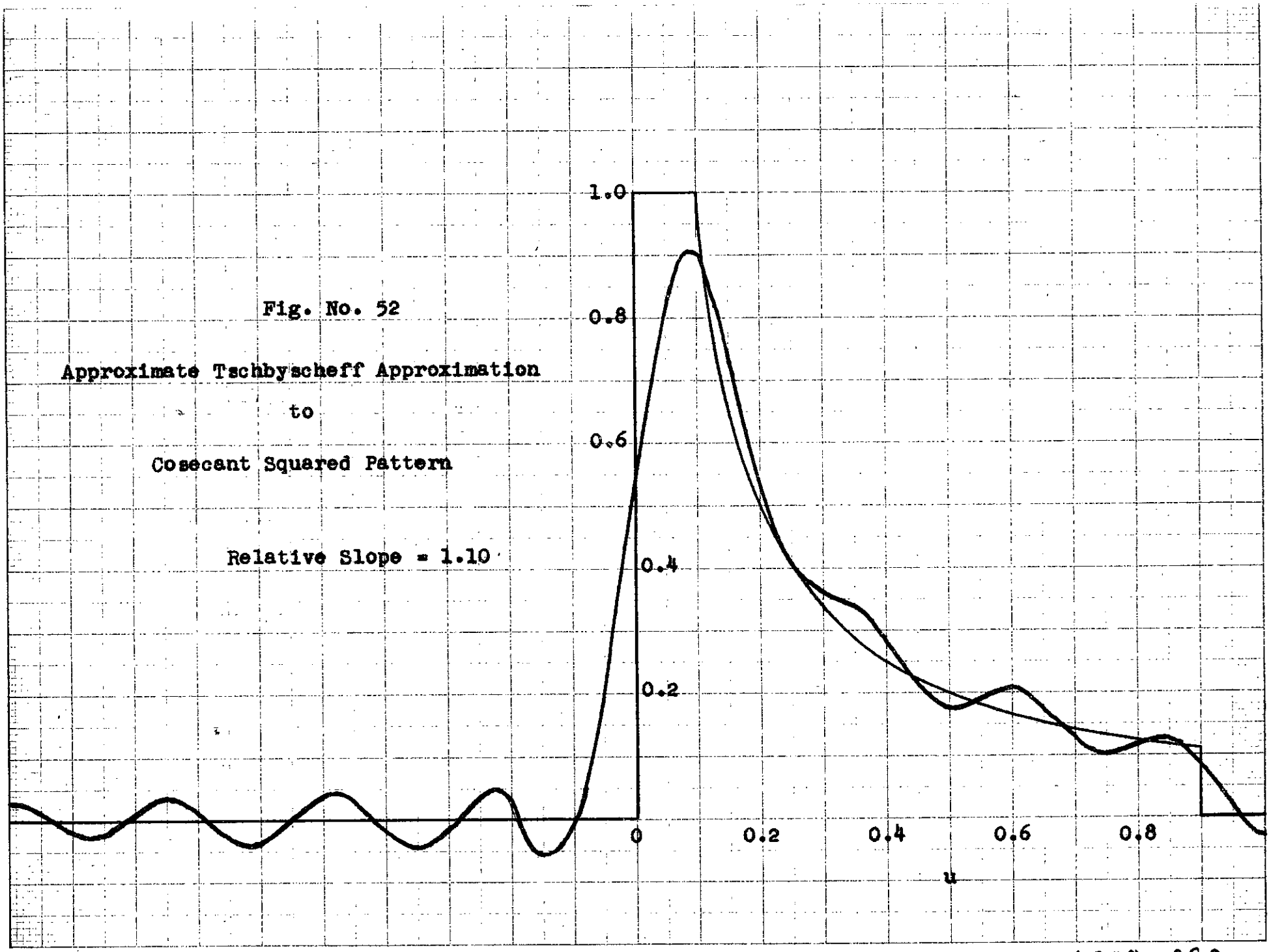

Fig. No. 52

Approximate Tschbyscheff Approximation

to

Cosecant Squared Pattern

Relative Slope = 1.10

6250-09C

Fig. No. 53

Approximate Tschbyscheff Approximation

to

Cosecant Squared Pattern

Relative Slope = 1.20

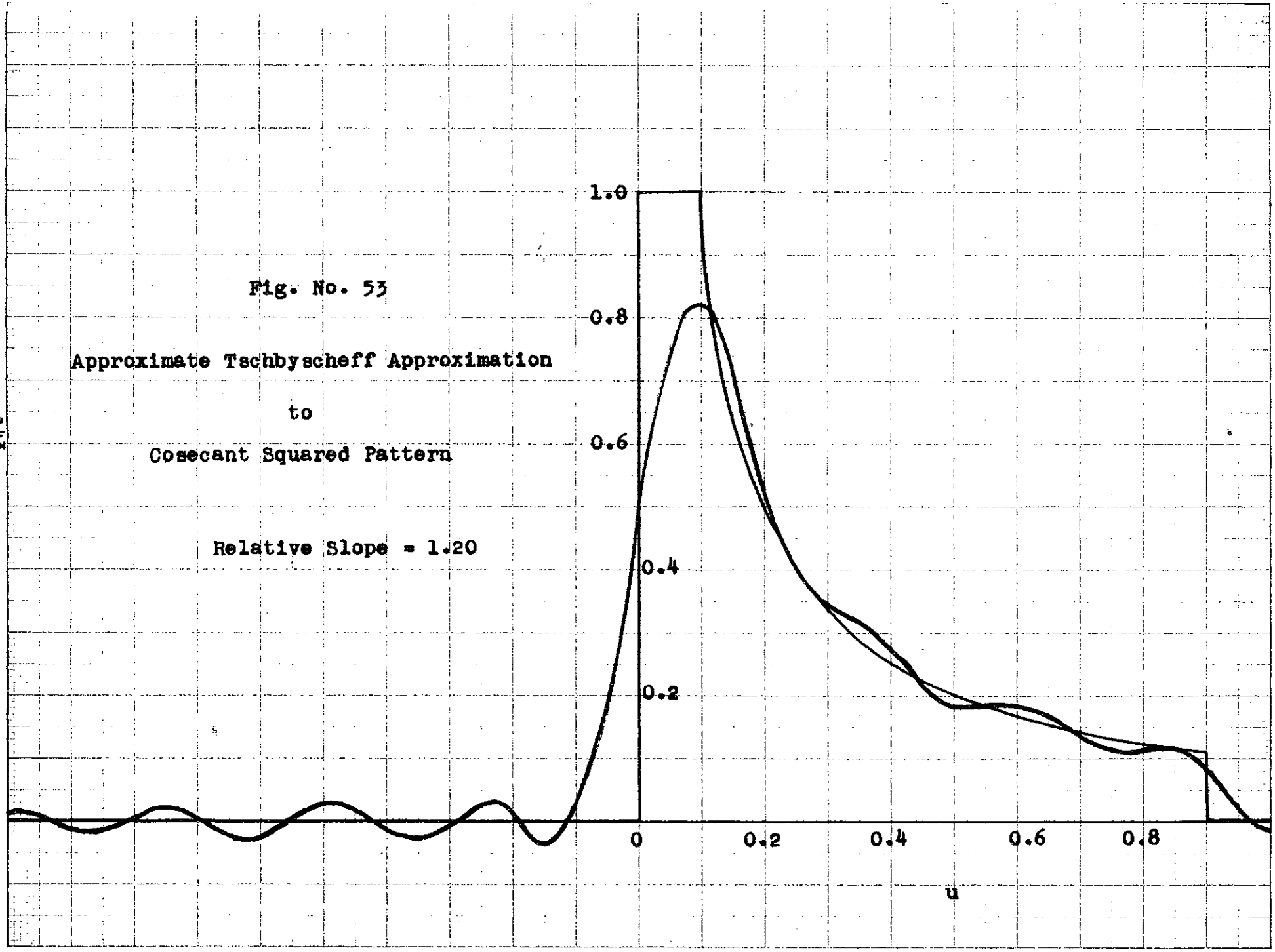

6250-010C

$$\cos^2 \pi \frac{x}{\lambda} \qquad \left(-\frac{\lambda}{2} < x < \frac{\lambda}{2}\right) \qquad (137)$$

as then we would have the correct value at the half wave points, the mean in between and a smooth interconnection. The pattern of (137) is

$$g(u) = \int_{-1/2}^{1/2} \cos^2 \frac{\pi x}{\lambda} e^{j \frac{2\pi}{\lambda} ux} dx$$

$$g(u) = \frac{\sin \pi u}{\pi u [1 - u^2]} \qquad (138)$$

If we were to divide the desired pattern by (138) before applying the synthesis procedure, the final pattern of the continuous aperture would approximate the original desired pattern.

IV. LIMITATIONS IMPOSED BY THE APERTURE "Q"

Throughout the thesis we have assumed that spatial current variations of rapidity greater than a wavelength were associated with reactive energy stored in the immediate vicinity of the aperture. This imposed a physical limitation on our synthesis method as it prohibited the use of those components in the cardinal series whose maxima occur in the region $|u| > 1$. This restriction to low Q structures prevented the realization of patterns of arbitrary sharpness from a given finite aperture or of "super gain" antennas.

The fact that the region of real angles, that is $|u| < 1$, is associated with real or radiated power is well known. However, the association of reactive or stored energy with the region $|u| > 1$ is only alluded to in the literature. As no investigation of the power flow through an arbitrarily illuminated aperture has been found, this section is devoted to an examination of this question. Such an examination is necessary to provide justification for the assumption made in previous sections of this thesis.

We restrict our discussion to the two dimension case. We first introduce the concept of an angular spectrum of plane waves (Woodyard and Lawson) (Booker and Clemmow).

1). Angular Spectrum of Plane Waves

Let a rectangular coordinate system be chosen such that x=0 represents the aperture plane. Let two semi-infinite conducting sheets be so placed as to form an infinite slot aperture of width "2W". Let us consider a two dimensional field independent of "z" in this system.

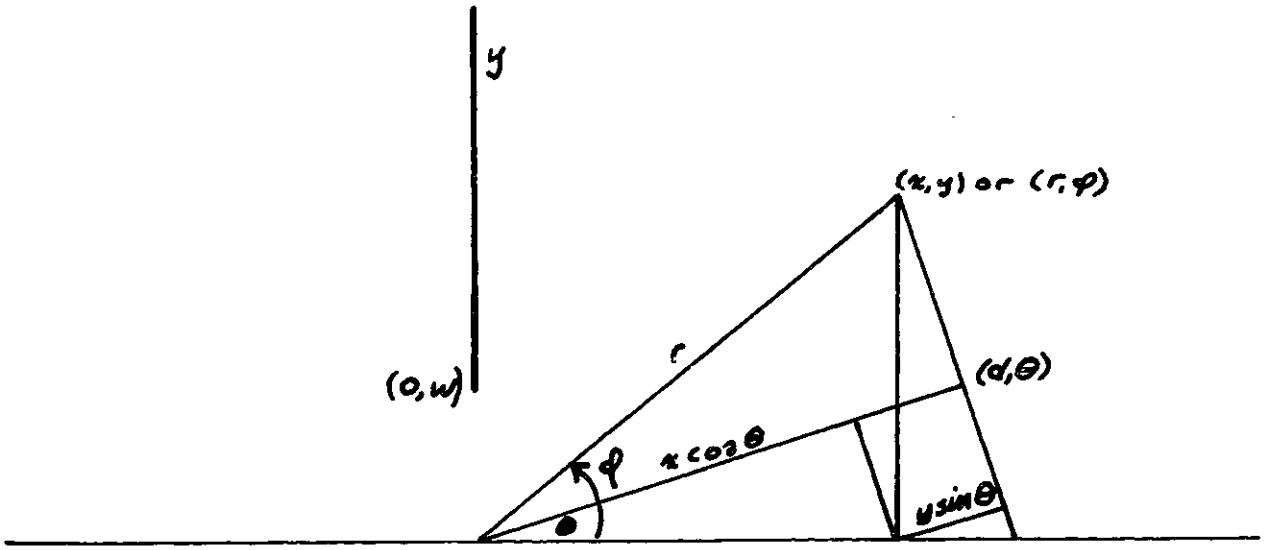

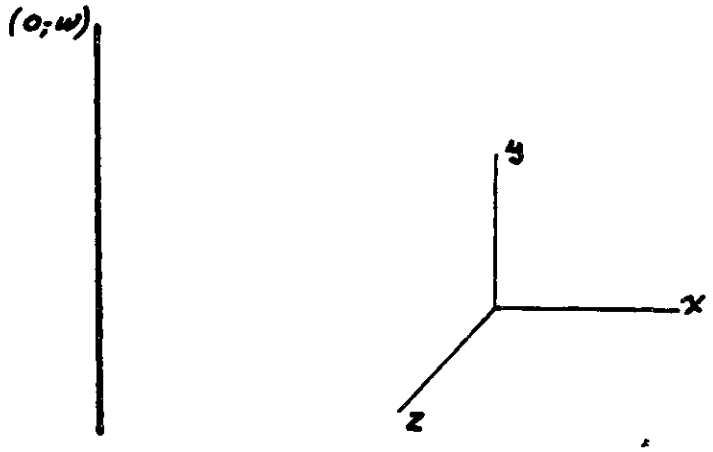

Next consider a plane wave propagating in the θ direction. For simplicity let one of the field vectors be parallel to the "z" axis. The electric vector will first be so chosen, although the analysis can be equally well carried out with the magnetic vector. A combination of them will yield the most general two dimensional field.

The electric component at the general point x,y may be expressed as

$$\mathcal{E}_z = \mathcal{E}_z e^{-j\alpha K} = \mathcal{E}_z e^{-jK(x\cos\theta + y\sin\theta)}$$

The corresponding magnetic field can be obtained from Maxwell's equation, namely:

$$\nabla \times \mathcal{E} = -\frac{\partial \mathcal{B}}{\partial t} = -j\omega\mu \mathcal{H}$$

and the plane wave components may be written,

$$\left.\begin{aligned} \mathcal{E}_z(x,y) &= \mathcal{E}_z e^{-jK(x\cos\theta + y\sin\theta)} \\ \mathcal{H}_x(x,y) &= \sin\theta \frac{\mathcal{E}_z}{Z_0} e^{-jK(x\cos\theta + y\sin\theta)} \\ \mathcal{H}_y(x,y) &= -\cos\theta \frac{E_z}{Z_0} e^{-jK(x\cos\theta + y\sin\theta)} \end{aligned}\right\} \quad (139).$$

Now all solutions of Maxwell's equation may be built up of a superposition or spectrum of such waves each propagating in a different "θ" direction and of arbitrary magnitude. The angle "θ", however, may accept all values including complex ones. We attempt to find that superposition which will satisfy the boundary conditions on the metal plates and at infinity.

As we are interested in waves radiating through the aperture into the right-half space all values of "θ" are not permitted. The exponent $-jk(x \cos\theta + y \sin\theta)$ determines the necessary values of "θ". The coefficient of "x" cannot have a positive real part nor can the coefficient of "y" have any real part. Otherwise the plane waves will grow exponentially as $x \to +\infty$ and/or $y \to \pm\infty$. We also exclude real values of "θ" confined to $\frac{3\pi}{2} < \theta < \frac{\pi}{2}$ as these waves represent plane waves travelling in from infinity.

The required range of "θ" or contour of integration can be obtained readily from the expansion

$$\cos\theta = \cos(\alpha + j\beta) = \cos\alpha \cosh\beta - j \sin\alpha \sinh\beta$$

$$\sin\theta = \sin(\alpha + j\beta) = \sin\alpha \cosh\beta + j \cos\alpha \sinh\beta.$$

It was shown by Woodyard and Lawson to be as indicated in the following figure:

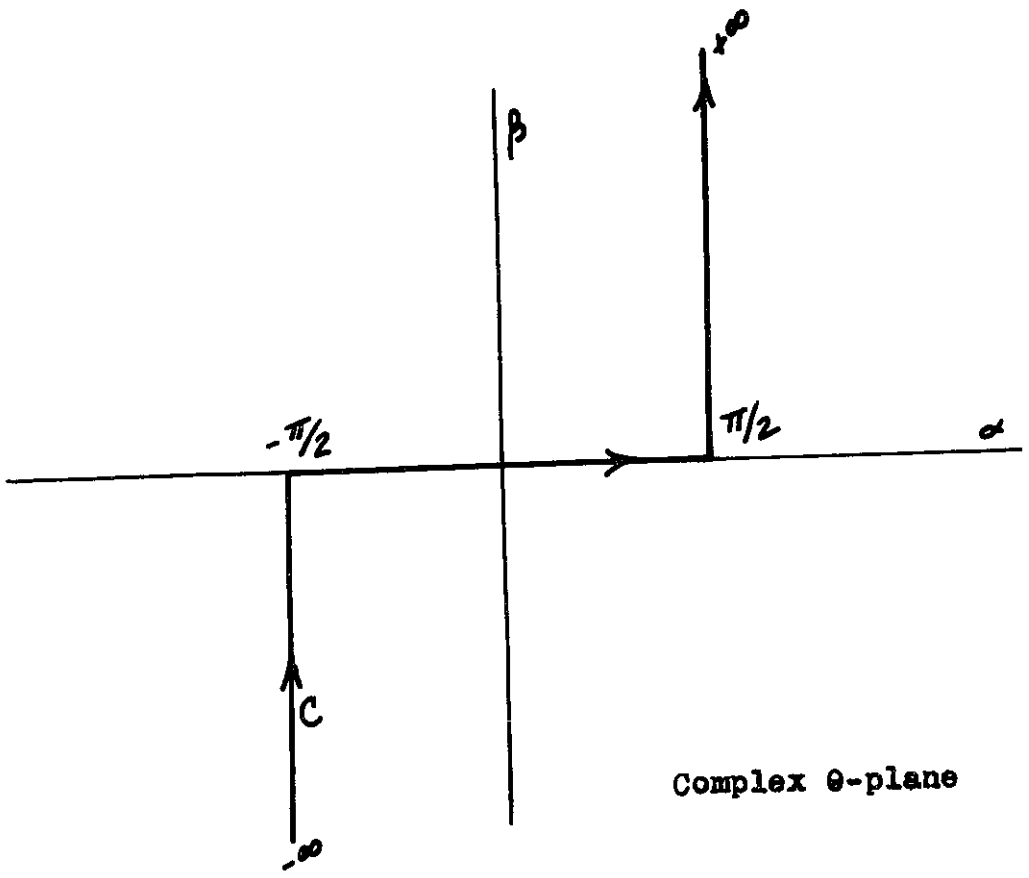

Complex θ-plane

The general two dimensional field which satisfies the conditions at infinity can be written:

$$\left.\begin{aligned} E_x(x,y) &= \int_C E_z(\theta)\, e^{-jk(x\cos\theta + y\sin\theta)}\, d\theta. \\ H_x(x,y) &= \frac{1}{Z_0}\int_C E_z(\theta)\sin\theta\, e^{-jk(x\cos\theta+y\sin\theta)}\, d\theta. \\ H_y(x,y) &= -\frac{1}{Z_0}\int_C E_z(\theta)\cos\theta\, e^{-jk(x\cos\theta+y\sin\theta)}\, d\theta. \end{aligned}\right\} \quad (140)$$

We next attempt to satisfy the boundary conditions on the metal plates. Here for $|"y"| > W$, $E_z(0,y) = 0$ and within the aperture the z-component of the electric vector has some arbitrary behavior.

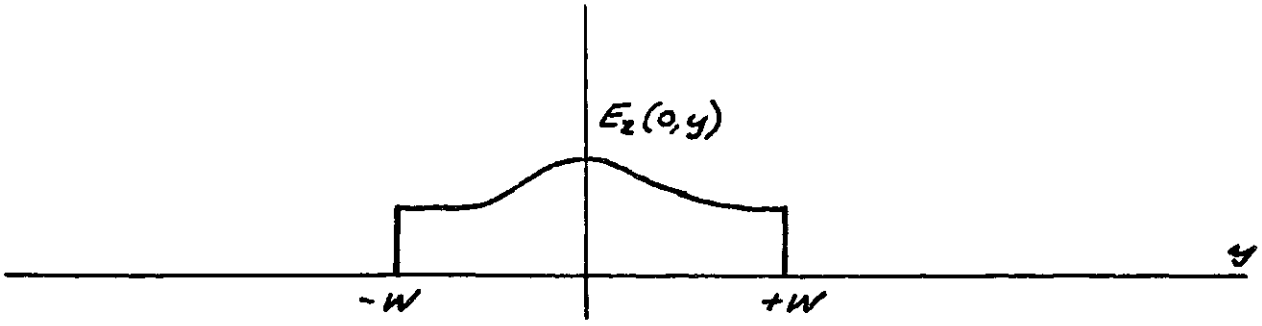

From (140) we can write the tangential components of the field in the plane of the aperture (x = 0)

$$\left.\begin{aligned} E_z(0,y) &= \int_C E_z(\theta)\, e^{-jky\sin\theta}\, d\theta \\ H_y(0,y) &= -\int_C \frac{E_z(\theta)}{Z_0}\cos\theta\, e^{-jky\sin\theta}\, d\theta \end{aligned}\right\} \qquad (141)$$

If we change variable and let $u = \sin\theta$, $du = \cos\theta\, d\theta$, then

$$d\theta = \frac{du}{\sqrt{1-u^2}}$$

The path of integration now runs over the entire real range of "u" and (141) becomes:

$$\left.\begin{aligned} E_z(0,y) &= \int_{-\infty}^{\infty} \frac{E_z(u)}{\sqrt{1-u^2}}\, e^{-j2\pi yu}\, du \\ H_y(0,y) &= -\frac{1}{Z_0}\int_{-\infty}^{\infty} E_z(u)\, e^{-j2\pi yu}\, du \end{aligned}\right\} \quad (142).$$

where "y" is measured in wavelengths.

The angular spectrum may be obtained from either equation by means of the Fourier Integral Theorem.

$$E_z(u) = \sqrt{1-u^2}\int_{-W}^{W} E_z(0,y)\, e^{+j2\pi yu}\, dy \qquad (143a)$$

$$E_z(u) = -Z_0\int_{-\infty}^{\infty} H_y(0,y)\, e^{j2\pi yu}\, dy \qquad (143b).$$

In the first integral we may restrict the range of integration to the aperture "2W" due to the boundary conditions. We are unable to do this in the second expression unless we assume the screen to be a perfect magnetic wall.

It should be noted that (140) expresses the field anywhere in the right-half space and that by inserting the expression for the angular spectrum given by (143) we satisfy the boundary

conditions on the metal plates and in the aperture. We have thus essentially solved a boundary value problem and our solution includes both the Fraunhofer and Fresnel solutions.

Let us now extend our consideration to a subject not covered in the literature, namely the complex power associated with our aperture. The complex power flow is given by the Poynting vector theorem as:

$$P = \int_{-W}^{W} (\mathbb{E} \times \mathbb{H}^*) \cdot dy = -\int_{-W}^{W} E_z(y)\, H_y^*(y)\, dy \qquad (144)$$

Substituting (142) we have

$$P = \frac{1}{Z_0} \int_{-W}^{W} \int_{-\infty}^{\infty} \int_{-\infty}^{\infty} \frac{E_z(u)\, E_z^*(u')}{\sqrt{1-u^2}}\, e^{j k y (u-u')}\, du\, du'\, dy$$

We may integrate over the aperture

$$P = \frac{2W}{Z_0} \int_{-\infty}^{\infty} \int_{-\infty}^{\infty} \frac{E_z(u) E_z^*(u')}{\sqrt{1-u^2}}\, \frac{\sin 2\pi W(u'-u)}{2\pi W(u'-u)}\, du\, du' \qquad (145)$$

Although (145) is a rigorous expression, it does not place in evidence the real and reactive components of the power. In

order to do this let us expand the arbitrary aperture distribution as a Fourier Series, that is we write

$$E_z(y) = \sum_{-\infty}^{\infty} C_n e^{-j\frac{2\pi n}{2W}y} \qquad \text{for } y < |W|$$

$$E_z(y) = 0 \qquad \text{for } y \geq |W|$$

As a general function, subject only to rather wide restrictions, may be so expanded we have lost little generality by means of this artifice. The angular spectrum now becomes from (143a)

$$E_z(u) = \sqrt{1-u^2} \sum_{-\infty}^{\infty} C_n \int_{-W}^{W} e^{j2\pi y\left(u - \frac{n}{2W}\right)} dy.$$

or

$$E_z(u) = 2W\sqrt{1-u^2} \sum_{-\infty}^{\infty} C_n \frac{\sin 2\pi W(u - n/2W)}{2\pi W(u - n/2W)} \qquad (146)$$

Substituting (146) into (145), we have for the complex power flow

$$P = (2W)^3 \sum_{-\infty}^{\infty}\sum_{-\infty}^{\infty} C_n C_m^* \frac{\sin 2\pi W(u - n/2W)}{2\pi W(u - \frac{n}{2W})} \frac{\sin 2\pi W(u' - \frac{m}{2W})}{2\pi W(u' - \frac{m}{2W})} \int_{-\infty}^{\infty}\int_{-\infty}^{\infty} \frac{\sin 2\pi W(u-u')}{2\pi W(u-u')} \times$$

$$\sqrt{1-u^2}\, du\, du'.$$

recalling that (proof is given in the appendix):

$$\int_{-\infty}^{\infty} \frac{\sin 2\pi W u'}{2\pi W u'} \frac{\sin 2\pi W(u'+\tau)}{2\pi W(u'+\tau)} du' = \frac{1}{2W} \frac{\sin 2\pi W \tau}{2\pi W \tau}$$

we may therefore perform our "u'" integration and obtain

$$P = \frac{4W^2}{Z_0} \sum_{-\infty}^{\infty} \sum_{-\infty}^{\infty} C_n C_m^* \int_{-\infty}^{\infty} \frac{*}{\sqrt{1-u^2}} \frac{\sin 2\pi W(u-\frac{n}{2W})}{2\pi W(u-\frac{n}{2W})} \frac{\sin 2\pi W(u-\frac{m}{2W})}{2\pi W(u-\frac{m}{2W})} du.$$

We can interchange our subscripts and obtain an identical expression

$$P = \frac{4W^2}{Z_0} \sum_{-\infty}^{\infty} \sum_{-\infty}^{\infty} C_m C_n^* \int_{-\infty}^{\infty} \frac{*}{\sqrt{1-u^2}} \frac{\sin 2\pi W(u-\frac{m}{2W})}{2\pi W(u-\frac{m}{2W})} \frac{\sin 2\pi W(u-\frac{n}{2W})}{2\pi W(u-\frac{n}{2W})} du.$$

Therefore we may write in symmetric form:

$$P = \frac{4W^2}{Z_0} \sum_{-\infty}^{\infty} \sum_{-\infty}^{\infty} \frac{C_n C_m^* + C_n^* C_m}{2} \int_{-\infty}^{\infty} \frac{*}{\sqrt{1-u^2}} \frac{\sin 2\pi W(u-\frac{m}{2W})}{2\pi W(u-\frac{m}{2W})} \frac{\sin 2\pi W(u-\frac{n}{2W})}{2\pi W(u-\frac{n}{2W})} du$$

Equation (147) places in evidence the real and reactive power as all factors with the exception of $*\sqrt{1 - u^2}$ are real. In the interval $-1 < u < +1$ this factor is real and that portion of the integral represents real power, whereas in the remaining region the factor is imaginary and we have reactive power.

It remains for us to show the connection between the angular spectrum of plane waves and the radiation pattern of the aerial. Further it should be possible to show the equality of the real power traversing the aperture and the radiated power as obtained by integration in the far-field of the aerial.

2). Radiation Pattern and Radiated Power

The complete field anywhere is given by (140). Let us introduce polar coordinates for the general field point $x = r \cos \phi$; $y = r \sin \phi$; then the electric field anywhere becomes:

$$E_z(r,\varphi) = \int_c E_z(\theta)\, e^{-j 2\pi r \cos(\theta - \varphi)}\, d\theta$$

In the far field or Fraunhofer region, "r" is large and the integral can be evaluated by the method of stationary phase (Jeffries). This yields

$$E_z(r,\varphi) \cong \frac{e^{-j(2\pi r + \frac{\pi}{4})}}{\sqrt{r}}\, E_z(\varphi) = f(r)\, E_z(\varphi) \qquad (148).$$

We see that the angular dependence of the far field is identical with the angular spectrum. This result was indicated by (Booker and Clemmow). Let us return to our power considerations. The total real power radiated is expressed as:

$$P = \int_{-\pi/2}^{\pi/2} \frac{E_z(r,\varphi)\, E_z^*(r,\varphi)}{Z_0}\, r\, d\varphi = \int_{-\pi/2}^{\pi/2} \frac{E_z(\varphi)\, E_z^*(\varphi)}{Z_0}\, d\varphi$$

Substituting from (146)

$$\frac{E_z(\varphi)\, E_z^*(\varphi)}{Z_0} = \frac{4W^2}{Z_0}\cos^2\varphi \sum_{-\infty}^{\infty}\sum_{-\infty}^{\infty} C_n C_m^* \frac{\sin 2\pi W(u-\frac{n}{2W})}{2\pi W(u-\frac{n}{2W})} \frac{\sin 2\pi W(u-\frac{m}{2W})}{2\pi W(u-\frac{m}{2W})}$$

we obtain:

$$P = \frac{4W^2}{Z_0} \sum_{-\infty}^{\infty}\sum_{-\infty}^{\infty} C_n C_m^* \int_{-1}^{1} \sqrt{1-u^2}\, \frac{\sin 2\pi W(u-\frac{n}{2W})}{2\pi W(u-\frac{n}{2W})} \frac{\sin 2\pi W(u-\frac{m}{2W})}{2\pi W(u-\frac{m}{2W})}\, du. \tag{149}$$

Now (149) for the radiated power, obtained by integrating the radiation pattern is identical to the real part of (147) giving the real power flow through the aperture as obtained by the Poynting vector theorem. We, of course, would expect to obtain this agreement. Equation (149) has physical

significance only for real angles. We can, however, extend our far field integral over our previously defined contour and, as now this extension of the integral is identical to the aperture integral yielding the reactive power, we can assign to the imaginary portion of the far-field integral the significance of reactive power stored in the neighborhood of the aperture. Hence we can write

$$\check{P} = P + jQ = \int_{-\infty}^{\infty} \frac{P(u)}{\sqrt{1-u^2}}\, du.$$

where the radiated power is:

$$P = \int_{-1}^{1} \frac{P(u)}{\sqrt{1-u^2}}\, du = \int_{-\pi/2}^{\pi/2} P(\varphi)\, d\varphi$$

3). "Q" of an Aperture

We may finally define the "Q" of an aperture as the ratio of reactive to dissipated power, that is:

$$"Q" = \frac{\int_{c} P(\varphi)\, d\varphi - \int_{-\pi/2}^{\pi/2} P(\varphi)\, d\varphi}{\int_{-\pi/2}^{\pi/2} P(\varphi)\, d\varphi} \qquad (150)$$

4). Complementary Case

In order to bring in some interesting connections, we wish to present briefly the corresponding formulas applicable to the case where the magnetic vector is taken parallel to the slot - however, the aperture plane is still an electric wall. The two cases are not complementary in the electromagnetic sense unless we replaced the electric wall with a magnetic one.

We have for the field anywhere (corresponding to (140)):

$$\left.\begin{aligned} H_z(x,y) &= \int_C H_z(\theta)\, e^{-j2\pi(x\cos\theta + y\sin\theta)}\, d\theta \\ E_z(x,y) &= -Z_0 \int_C H_z(\theta)\sin\theta\, e^{-j2\pi(x\cos\theta + y\sin\theta)}\, d\theta \\ E_y(x,y) &= Z_0 \int_C H_z(\theta)\cos\theta\, e^{-j2\pi(x\cos\theta + y\sin\theta)}\, d\theta \end{aligned}\right\} \quad (140c)$$

The field in the aperture plane becomes:

$$\left.\begin{aligned} H_z(0,y) &= \int_{-\infty}^{\infty} \frac{H_z(u)}{\sqrt{1-u^2}}\, e^{-j2\pi uy}\, du. \\ E_y(0,y) &= Z_0 \int_{-\infty}^{\infty} H_z(u)\, e^{-j2\pi uy}\, du \end{aligned}\right\} \quad (141c)$$

We still express the angular spectrum in terms of the tangential electric field in the aperture plane as the tangential component vanishes on the metal plates. The angular spectrum becomes

$$H_z(u) = \frac{1}{Z_0}\int_{-W}^{W} E_y(0,y)\, e^{j2\pi y u}\, dy \qquad (143ac)$$

The complex power flow through the aperture is

$$\check{P} = 2WZ_0 \int_{-\infty}^{\infty}\int_{-\infty}^{\infty} \frac{H_z(u)\, H_z^*(u')}{\sqrt{1-u^2}} \frac{\sin 2\pi W(u-u')}{2\pi W(u-u')}\, du\, du' \qquad (145c).$$

We can as previously expand the aperture distribution in a Fourier Series. Substituting this expansion in (143ac)

$$H_z(u) = \frac{2W}{Z_0}\sum_{-\infty}^{\infty} C_n \frac{\sin 2\pi W(u-\frac{n}{2W})}{2\pi W(u-\frac{n}{2W})}$$

Substituting this into (145c) and performing the evident integration we obtain for the complex power

$$\check{P} = \frac{4W^2}{Z_0}\sum_{-\infty}^{\infty}\sum_{-\infty}^{\infty} \frac{C_n C_m^* + C_m C_n^*}{2} \int_{-\infty}^{\infty} \frac{du.}{\sqrt{1-u^2}} \frac{\sin 2\pi W(u-\frac{n}{2W})}{2\pi W(u-\frac{n}{2W})} \frac{\sin 2\pi W(u-\frac{m}{2W})}{2\pi W(u-\frac{m}{2W})}$$

(147c)

The real part of this power can again be checked by far field integration of the radiation pattern.

Investigation of this alternate case has revealed that the sign of the reactive power has changed. As the root represents the cosine of the angle θ it must be taken as positive. The condition where the tangential electric vector lies across the slot is therefore capacitive whereas when it is parallel to the slot the reactive power is inductive. This agrees with waveguide theory as to the sign of an inductive or capacitive iris.

APPENDIX

On page ·· we assumed that the cardinal functions were ortho-normal and on page ·· we assumed the value of the integral

$$(2W)^2\int_{-\infty}^{\infty}\frac{\sin 2\pi Wu}{2\pi Wu}\,\frac{\sin 2\pi W(u+\tau)}{2\pi W(u+\tau)}\,du = \frac{\sin 2\pi W\tau}{2\pi W\tau}$$

As this integral form is not found in standard integral tables, it is evaluated in this appendix. This may be most readily accomplished by means of the convolution theorem. We proceed by noting the integral is of the auto-correlation form

$$\varphi(\tau)=\int_{-\infty}^{\infty}g(u)\,g(u+\tau)\,du.$$

since

$$g(u)=\int_{-\infty}^{\infty}f(x)\,e^{j2\pi ux}\,dx.$$

$$f(x)=\int_{-\infty}^{\infty}g(u)\,e^{-j2\pi ux}\,dx$$

then

$$\int_{-\infty}^{\infty}g(u)\,g(u+\tau)\,du=\int_{-\infty}^{\infty}g(u)\int_{-\infty}^{\infty}f(x)\,e^{j2\pi x(u+\tau)}\,dx\,du.$$

$$=\int_{-\infty}^{\infty}f(x)\,e^{j2\pi x\tau}\int_{-\infty}^{\infty}g(u)\,e^{j2\pi xu}\,du\,dx.$$

Therefore

$$\int_{-\infty}^{\infty} g(u)\, g(u+\tau)\, du = \int_{-\infty}^{\infty} f(x)\, f^{*}(x)\, e^{j2\pi x\tau}\, dx \qquad *$$

Applying this result to the case where

$$g(u) = \frac{2W \sin 2\pi W u}{2\pi W u}.$$

then f(x) will have the functional form

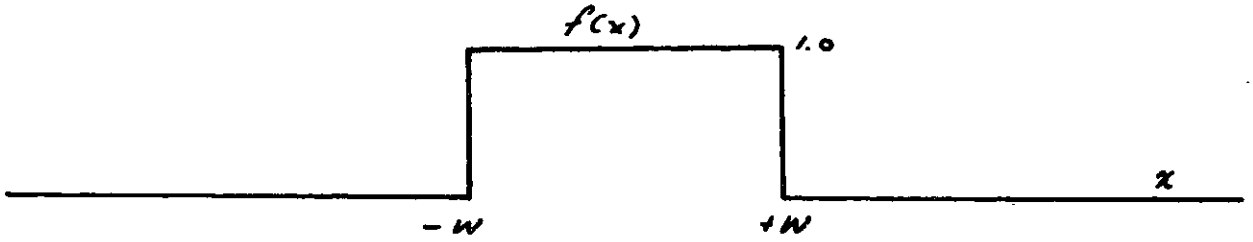

Therefore

$$(2W)^2 \int_{-\infty}^{\infty} \frac{\sin 2\pi W u}{2\pi W u} \frac{\sin 2\pi W(u+\tau)}{2\pi W(u+\tau)}\, du = \int_{-W}^{W} e^{j2\pi x\tau}\, dx$$

or

$$(2W)^2 \int_{-\infty}^{\infty} \frac{\sin 2\pi W u}{2\pi W u} \frac{\sin 2\pi W(u+\tau)}{2\pi W(u+\tau)}\, du = \frac{\sin 2\pi W\tau}{2\pi W\tau} \qquad *$$

by a change of variable the ortho-normal relation results,

$$(2W)^2 \int_{-\infty}^{\infty} \frac{\sin 2\pi W(u - \frac{n}{2W})}{2\pi W(u - \frac{n}{2W})} \frac{\sin 2\pi W(u - \frac{m}{2W})}{2\pi W(u - \frac{m}{2W})} du = \delta_{nm}$$

where $\delta_{nm} = 1$ for $n = m$

$\delta_{nm} = 0$ for $n \neq m$

BIBLIOGRAPHY

Bacon, G.E. - "Variable-Elevation Beam-Aerial Systems for 1½ Meters".

Proceedings at the Radio Location Convention, IEE Part III A. 1946

Bailin, L.L. and Ehrlich, M.J. - "Factors Affecting the Performance of Linear Arrays".

Transactions of the I.R.E. Publication of the Professional Group on Antennas and Propagation. February 1952.

Blake, L.V. - "Reflections of Radio Waves from a Rough Sea".

I.R.E. Vol. 38, pp. 301-304. March 1950.

Booker, H.G., Ratcliffe, J.A. and Shimi, D.H. - "Diffraction from an Irregular Screen with Applications to Ionospheric Problems."

Philosophical Transactions of the Royal Society of London. Series A. No. 856, Vol. 242, pp. 579-609. 12 September 1950

Booker, H.G. and Clemmow, P.C. - "The Concept of an Angular Spectrum of Plane Waves and Its Relation to That of the Polar Diagram and Aperture Distribution."

Proc. IEE, Part III. January 1950.

Born, M. - "Optik"

Julius Springer, Berlin. 1933

Brown, J. - "The Effect of a Periodic Variation in the Field Intensity Across a Radiating Aperture".

IEE, Part III, Vol. 97, pg. 419. 1950.

Chaudrasekhar - "Stochastic Problems in Physics and Astronomy."

Review of Modern Physics. January, 1943.

Copson, E.T. - "Theory of Functions of a Complex Variable."

Oxford University Press. 1944.

Cramer, H. - "Mathematical Methods of Statistics."

Princeton University Press. 1946.

Cutler, C. C. - "Parabolic Antenna Design for Microwaves".
IRE, Vol. 35, pp. 1284-1294. November 1947.

Dolph, C. L. - "A Current Distribution for Broadside Arrays Which Optimizes the Relationship between Beam-width and Side Lobe Level".
IRE, Vol. 34, June 1946.

Ferrar, W. L. - "On the Cardinal Function of Interpolation Theory".
Proc. Royal Soc. of Edinborough. pp. 323. 1925.

Friis, H.T. and Lewis, W.D. - "Radar Antennas"
B.S.T.J. April 1947.

Grobner, W. and Hofreiter - "Integraltafel. Part I and II".
Springer - Verlag. Wien. 1950.

Hiatt, R.E. - "Field Station for Antenna Measurements".
Rad. Lab. Report No. 632. February 1945.

Jackson, D. - "Fourier Series and Orthogonal Polynomials".
Carus Mathematical Monographs, No. 6.
Math. Assoc. of America.

Jackson, D. (2) - "The Theory of Approximation".
American Mathematical Society. Colloqium Publications Vol. XI.

Jeffreys, B.S. - "Mathematical Physics". pp. 503-507
Cambridge University Press.

Klein, W. - "Tschebyscheffe Funktionen".
Archiv fur Elektrotechnik. Vol. 39. pg. 647. 1950.

Kraus, John D. - "Antennas".
McGraw-Hill Book Co., New York.

Marechal, A. For English Summary see E. Wolf. "The Diffraction Theory of Aberrations". Reports on Progress in Physics. Vol. XIV (1951), pg. 106., published by The Physical Society. London. G.B.

McLachlan, N.W. - "Bessel Functions for Engineers".
Oxford University Press. 1934.

Morse, P.M. and Kimball, G.E. - "Methods of Operations Research".
The Technology Press. 1951.

Ramsey, J. F. - "Fourier Transforms in Aerial Theory".
Marconis Review. 1946.

Rayleigh, Lord - "On the Problem of Random Vibrations and of Random Flights in One, Two and Three Dimensions".
Scientific Papers. Vol. VI.

Sichak, W. - "Double Dipole Rectangular WaveGuide Antennas".
R.L. Report No. 54-25. June 26, 1943.

Silver, Samuel - "Microwave Antenna Theory and Design".
McGraw-Hill Book Co. 1949.

Spencer, R.C. and Austin, P.M. - "Tables and Methods of Calculation for Line Sources".
R.L. Report No. 762-2. March 30, 1946.

Spencer, R. C. (2) - "A Least Square Analysis of the Effect of Phase Errors on Antenna Gain".
Report No. E5025, Air Force Cambridge Research Center. January 1949.

Spencer, R.C. (3) - "Fourier Integral Methods of Pattern Analysis".
R.L. Report No. 762-1. January 1946.

Stevenson, A.F. - "Theory of Slots in Rectangular Wave Guides".
JAP. Vol. 19, pg. 24-38, 1948.

Stone, John - U.S. Patents No. 1,643,323 and No. 1,715,433.

Stratton, J. A. - "Electromagnetic Theory".
McGraw-Hill Book Co., New York. 1941.

Stratton, J.A. and Chu, L.J. - "Diffraction Theory of Electromagnetic Waves".
Physical Review, Vol. 56. pg. 99. 1939.

Uhlenbeck, G.E. and Lawson, J.L. - "Threshold Signals".
McGraw-Hill Book Co., New York.

Wolff, I. - "Determination of the Radiating System Which Will Produce a Specified Directional Characteristic".
Proc. IRE. Vol. 25, pg. 630. 1937.

Woodyard, P.M. and Lawson, J.D. - "The Theoretical Precision with Which an Arbitrary Radiation Pattern May Be Obtained with a Source of Finite Size."

Jour. IEE, Vol. 95, Part III. pp. 362-370. September, 1948.

BIOGRAPHICAL NOTE

John Ruze was born in New York, N.Y. on May 24, 1916. He received his B.S. degree in Electrical Engineering from the College of the City of New York in February 1938, and his Master's degree from Columbia University in June 1940.

In February 1939 he accepted employment in the Evans Signal Laboratory of the Signal Corps Engineering Laboratories at Red Bank, N.J. Here he worked on the design of some of the early radar equipment and finally gravitated into antenna design. During the war years he headed the Antenna Design Section at these Laboratories.

In the summer of 1946 he accepted a position with the Antenna Laboratory of the U.S. Air Force Cambridge Research Center and began his graduate work at the Massachusetts Institute of Technology on a part time basis. He was accepted as a full time doctoral candidate in the Dept. of Electrical Engineering in the summer of 1950.

Mr. Ruze is a member of Eta Kappa Nu, Tau Beta Pi, the American Physical Society, and the Institute of Radio Engineers.